ABSTRACT

Title of Dissertation:	THE EFFECT OF GLYCEMIC CONDITION ON SUBSTRATE STIFFNESS-MEDIATED MECHANOSENSITIVITY IN MACROPHAGES
	Courtney Dashawn Johnson, Doctor of Philosophy, 2023
Dissertation directed by:	Associate Professor, Assistant Department Chair & Graduate Director, Dr. Jose Helim Aranda-Espinoza, Fischell Department of Bioengineering
	Fischell Family Distinguished Professor & Department Chair, Dr. John P. Fisher, Fischell Department of Bioengineering

Diabetes is a disease that plagues over 463 million people globally. About 40 million of these patients have Type 1 diabetes, and the global incidence is increasing up to 5% per year. Type 1 diabetes is characterized by the body's immune system targeting the pancreas with antibodies, leading to a disruption in insulin production. While existing treatments, such as exogenous insulin injections, are both successful and popular, the exorbitant insulin costs and need for meticulous administration are driving factors for alternative long-term solutions to glucose dysregulation caused by diabetes. Encapsulated islet transplantation (EIT) is a tissue-engineered solution to address the challenges raised by diabetes. Donor islets are encapsulated in a semi-

permeable hydrogel, allowing the diffusion of oxygen, glucose, and insulin but preventing leukocyte infiltration. Despite its successes in small animal models, EIT is still far from commercialization due to the requirements of long-term systemic immunosuppressants and consistent immune rejection from the foreign body response. While most published research has focused on tailoring the characteristics of the capsule material to promote clinical viability, many studies have had a limited scope centered on biochemical changes. Current mechanobiology studies on the effect of substrate stiffness on the function of leukocytes, especially macrophages – primary foreign body response orchestrators, show promise in tailoring a favorable response to tissue-engineered therapies such as EIT. However, before successful integration into the EIT design, it is imperative to determine the impact of external glucose concentrations on substrate stiffness-mediated mechanosensitivity. Glucose plays a critical role in macrophage functionality, impairing or enhancing their function in certain situations. Immunometabolism literature demonstrates that decreasing or inhibiting the uptake of glucose via impairing glycolysis can result in a significant decline in functionality in macrophages. Patients suffering from diabetes experience dysregulation in glycemic maintenance, ranging from hypo-, normo-, and hyperglycemic conditions. As a result, it is imperative to assess whether these changes in external glucose conditions will affect macrophage mechanosensitivity in response to EIT biomaterials to use substrate stiffness as a design parameter for EIT effectively This project investigates the role of glycemic conditions on macrophage mechanosensitivity, considering substrate stiffness factors including morphology, phenotype, phagocytic and inflammatory functionality. These parameters aim to mimic the early stages of foreign body response, particularly the initiation and acute inflammation phases. This work demonstrates that glycemic condition significantly influences the severity of substrate stiffness-mediated mechanosensitivity in reference to macrophage phagocytosis and pro-inflammatory functionality. This study serves to advance the understanding of macrophage functionality, bridging the fields of mechanobiology and immunometabolism. Understanding the role of glycemic conditions on substrate stiffness-mediated mechanosensitivity will assist in EIT design to enhance the clinical viability of the therapy and prevent immune rejection by pericapsular fibrotic overgrowth.

THE EFFECT OF GLYCEMIC CONDITION ON SUBSTRATE STIFFNESS-MEDIATED MECHANOSENSITIVITY IN MACROPHAGES

by

Courtney Dashawn Johnson

Dissertation submitted to the Faculty of the Graduate School of the
University of Maryland, College Park, in partial fulfillment
of the requirements for the degree of
Doctor of Philosophy
2023

Advisory Committee:
Professor Jose Helim Aranda - Espinoza, Chair
Professor John P. Fisher, Co-Chair
Professor Xioming He
Professor Erika Moore
Professor David Mosser

Dedication

To my mother, Latayna Sewell, grandmother, Edna Ismay, and my late great-grandmother, Nora Tucker, this is for you. Thank you for being the matriarchs of my life. For the future Black scientists and engineers, know that you can do anything!

Acknowledgements

First, I want to thank my advisors, Helim and Dr. Fisher. Thank you for developing me into a researcher and keeping me curious and persistent even when I didn’t know if there was a light at the end of the tunnel. Your support was immense and kept me striving toward this goal. I wasn’t always the best pupil, but you remained patient and kept me on course. You two were the tag team duo of the world that always impressed and terrified me. I appreciate everything you have done and thank you for being a part of my journey.

To Helim, you met me at a crossroads, trying to figure out the best way to get into a doctoral program after being denied by everyone I applied to during my senior year of undergrad. You listened to my life story and took a chance on me to join the lab as your sole student. Along the way, you assisted me in getting into the program and finding additional support through Dr. Fisher. You challenged me to be better and think more. You kept me on my toes because I never knew what questions you would ask me. You helped mold me into a better researcher and to defend my work wholeheartedly, and I thank you!

To Dr. Fisher, your optimism is unmatched, and I’ve found it rubbed off on me. Now, when things aren’t going the best, I find myself saying, “Everything’s going to be fine,” even when I’m having trouble believing it. Thank you for being a complement to Helim in my PhD journey. You kept me pushing forward in my research. I look forward to joining the rest of the Fisher lab alum at the FDA soon.

To my family, my mother (Latayna Sewell), grandmother (Edna Ismay), sister (Aniyah Speight), brother (Antwone Speight Jr.), father (Fabian Johnson), uncle (Lascelles Sewell), aunt (Andrea Nicoleau), and father figures (Anthony Anderson and Richard Harris), thank you for loving me unconditionally and supporting me through this journey. I know academic life has been long, but we are finally at the end of a major milestone. It is time to truly begin my professional adult life.

To Chris Banks, thank you for your love and support during this process. You have been along for the ride since Boston, you kept me grounded, supported, and human outside of my studies. Thank you for the adventures. I love you!

To my core, Courtney Utsey, Brandon Berry, Aaliyah Johnson, and Christopher Taylor, thank you for your love and support. You all are my longest friends, my core, and I wouldn’t be the person I am without you.

To my undergrads, Colleen and Decklan, thank you for coming in when you did to support me in my work. While you didn't think it was much, it impacted me greatly, and this would have been a more arduous process without you. Colleen - you are an all-star, and I think you will be a phenomenal researcher and PhD student one day. I look forward to your continued work in the lab and next steps.

To my current labmates, Shannon, Robert, Pieper, Amal, and Ryan, I cherish you more than you know. I would not have been able to finish this degree successfully without you. You were a part of my sanity in the lab, my sounding board when I thought I had a dumb idea, and my support when experiments weren't working. I look forward to attending your dissertation defenses and being addressed as Doctor. I am always in your corner. Shannon, you're next!

To Ariana DeCastro, my best friend through this program, we did it! From classes, to quals, to COVID, to proposals, to defense. We've been with each other every step of the way. From the venting session after terrible meetings to the pep talks for long experiment days. You were the friend that I needed along this journey. Thank you so much for everything. I look forward to this next chapter of our lives. You had a head start, but I am on my way.

To Ian Smith, my academic nephew! You are amazing! I've learned so much from you these last few years. Thank you for all your assistance in and out of the lab. I look forward to your defense, future Professor.

To Henoss Taddesse, my brother! I love you to death! Thank you so much for your support during my academic journey. I truly admire the amount of effort and care that you display. You have a heart of gold, and I appreciate everything you do.

Lastly, to my NSBE and BESS family, thank you for elevating my leadership abilities as well as keeping me sane through my academic journey. To Nadjia Motley, Alaisha Alexander, Rukayah Balogun, Paula McCall, Josh Crittenden, Dario Boyce, James Tukpah, Destinee Batson, Alex Julien, Thurston Brevett, Dr. Sarah Brown, and Dr. Racheida Lewis, you all are lifelong friends, and I look forward to our next adventure.

Table of Contents

List of Tables

List of Figures

List of Abbreviations

2-DG: 2-deoxy-D-glucose
BMDM: bone-marrow-derived macrophage
BSA: bovine serum albumin
CD206: cluster of differentiation 206
CD80: cluster of differentiation 80
CD86: cluster of differentiation 86
DAMP: damage-associated molecular pattern
DC: dendritic cell
ECM: extracellular matrix
EIT: encapsulated islet transplantation
FAK: focal adhesion kinase
FBGC: foreign body giant cell
FBR: foreign body response
GAPDH: glyceraldehyde 3-phosphate dehydrogenase
GelMA: gelatin methacrylate
GLUT1: glucose transporter 1
IgG: immunoglobulin G
IL-10: interleukin-10
IL-6: interleukin-6
IL-8: interleukin-8
LAP: lithium phenyl-2,4,6-trimethylbenzoylphosphinate
LPS: lipopolysaccharides
NFκB: nuclear factor kappa-light-chain-enhancer of activated B cells
PBS: phosphate-buffered saline
PDGF: platelet-derived growth factor
PEG: polyethylene glycol
PFO: pericapsular fibrotic overgrowth
PVA: polyvinyl alcohol
ROS: reactive oxygen species
T1DM: type 1 diabetes metillus
TGF-β: transforming growth factor
TLR4: toll-like receptor 4
TNF-α: tumor necrosis factor-α
VEGF: vascular endothelial growth factor

Chapter 1: Introduction

Encapsulated islet transplantation (EIT) is a novel tissue-engineering approach to treat glucose dysregulation caused by Type 1 diabetes.[1] Donor islets are encapsulated in a semi-permeable polymeric membrane, commonly alginate, tasked to protect the cells from leukocyte invasion while providing transport of oxygen, glucose, insulin, and waste products. Though promising, the therapy has consistently faced one main challenge due to its inability to overcome the body's natural immune defenses long-term. For success, patients need harmful immunosuppressant drugs to systemically weaken the immune system and prevent rejection of the therapy, hindering long-term viability.[2] An effective strategy is required to prevent EIT rejection by the foreign body response.

Foreign body response (FBR) encompasses a cascade of signaled reactions in four main phases: ignition, acute inflammation, chronic inflammation, and fibrosis.[3,4] Macrophages, primary orchestrators of the foreign body response, adhere to the material surface and remain at the EIT site for the complete response. During this time, macrophages release reactive oxygen species and pro-inflammatory cytokines in an attempt to phagocytose the transplant while also promoting intercellular signal cascades. This results in complete encapsulation of the transplant with fibrous tissue, pericapsular fibrotic overgrowth (PFO), blocking the transplant from oxygen, leading to loss of function and apoptosis of the transplant islets.[5]

Strategies for improvement to the clinical viability of EIT have consistently relied on manipulating the biochemical properties of the capsule to promote integration of the therapy by the immune response utilizing immunomodulatory biomaterials, islet cell modifications with anti-inflammatory proteins, and the incorporation of immunomodulatory cells such as regulatory T-cells and mesenchymal stem cells.[6] However, this additions have still not overcome rejection through FBR without the use of systemic immunosuppressive drugs, a significant limitation to adaption of the therapy.

Mechanobiological studies, specifically on the immune system (immuno-mechanobiology), have shown that the mechanical properties of implanted materials can impact the extent of FBR providing a potential strategy for reduction and intergration.[7] Of which, it can be concluded that macrophages are mechanosensitive. Literature has demonstrated mechanical properties of the material and surrounding environment, such as substrate stiffness, can significantly affect macrophage characteristics and function.[8,9]

Though we can reasonably conclude macrophages are mechanosensitive, we do not understand the impact of changes in glycemic condition, experienced by patients with diabetes, on mechanosensitivity. It has been extensively reviewed that glucose metabolism regulates macrophage function.[10] During acute inflammation, proinflammatory macrophages utilize glycolysis primarily to support their inflammatory function of ROS and cytokine production.[11] Further to this point, Gonzalez et al. displayed that hyperglycemic conditions induced proinflammatory cytokine production in primary human monocytes, upregulating IL-6 and TNF-α.[12] Freemerman et al. demonstrated a similar conclusion by overexpressing GLUT1 in RAW264.7 macrophages to increase glucose uptake.[13] Work in the fields of immunometabolism and immuno-mechanobiology lead us to hypothesize that there is a link between the two and should be explored to improve implanted material-based therapies for diabetic patients such as EIT.

This dissertation will explore the effect of glycemic condition on the mechanosensitivity of macrophages to substrate stiffness focusing on normoglycemic (100 mg/dL glucose) and hyperglycemic (450 mg/dL glucose) conditions. These findings will act as a case for the inclusion of substrate stiffness as a parameter to improve the clinical viability of encapsulated islet transplantation design for diabetic therapy. Throughout this work, we will assess the effect of glycemic condition on various characteristics and functions of the macrophage tied to the ignition (unstimulated morphology, phenotype, and frustrated phagocytic capability) and acute inflammation (proinflammatory phenotype, gene, and protein secretion) stages of the foreign body response.

Recently, microcapsule stiffness has been investigated to improve functionality in insulin-secreting cells.[14,15] As microcapsules used for EIT can range in stiffness depending on crosslinker density[16], we will use a polyacrylamide model of 2-order of magnitude in stiffness (2 – 274 kPa) to explore changes to macrophage characteristics and functionality in hyper- and normoglycemic conditions. Chapter 3 and 4 will explore the role of glycemic conditions and substrate stiffness-mediated mechanosensitivity in unstimulated and LPS-stimulated macrophages on a 2D polyacrylamide gel. Chapter 5 expounds on proinflammatory findings by developing a 3D model with the addition of gelatin methacrylate (GelMA) as an ECM representative, discussed in detail later in the dissertation. Overall, this work successfully showcases the synergistic effect of glucose and mechanosensitivity in macrophage function and builds a case for the inclusion of substrate stiffness as a parameter of interest in tissue-engineered therapies for patients experiencing diabetes such as EIT.

Chapter 2: A Case for Material Stiffness as a Design Parameter in Encapsulated Islet Transplantation[1]

[1]Adapted from Johnson C. D., Aranda-Espinoza H., and Fisher J. P. (2023). A Case for Material Stiffness as a Design Parameter in Encapsulated Islet Transplantation. *Tissue Engineering Part B: Reviews, 29*(4), 334-346. https://doi.org/10.1089/ten.teb.2022.0.157

2.1. Introduction

Diabetes is a leading cause of death and affects more than 463 million people globally.[17] Categorized into two main types, Type 1 and Type 2, diabetes is the loss of function in pancreatic islets to produce insulin and regulate blood glucose levels. While Type 2, the most common of the two, refers to the body's ineffective use of produced insulin[18], Type 1 (T1DM) is an autoimmune disease associated with immune cells, leukocytes, attacking pancreatic islets, specifically the insulin-secreting β-cell component, due to a misrecognition of self-antigens.[19] Treatment of diabetes consists of a routine schedule of exogenous insulin injected into the patient to regulate their blood glucose levels. However, as the prevalence of people with diabetes expands, estimated to be over 578 million people by 2035, the financial burden on healthcare institutions will exponentially grow.[17,20] Global spending on diabetes treatment was estimated at $673 billion in 2015, with a projection of $802 billion in 2040.[21] Individuals are also negatively impacted financially. According to the American Diabetes Association, patients diagnosed with diabetes, on average, have medical expenses 2.3 times higher than patients without the disease.[22] Financial costs of insulin have also hindered accessibility to treatment long term.[23] This burden has increased the demand for therapies that provide long-term solutions to exogenous insulin dependence.

To address exogenous insulin dependence, particularly by people with T1DM, tissue engineers have developed encapsulated islet transplantation (EIT).[1] This tissue engineering-based therapy consists of donor islets being encapsulated in a semipermeable polymeric membrane. The capsule protects the cells from the leukocytes of the patient's immune system while promoting islet function and viability.[24] The permeability of the capsule allows the transport of oxygen, glucose, insulin, and waste products while blocking leukocyte migration into the capsule. Structurally, ideal pore size is needed for maximum diffusion of oxygen (~300 pm in diameter), glucose (~1 nm), and insulin (2.7 nm)[25] but restrictive to antibody (10 nm) and leukocyte invasion (~0.67 µm).[26–29] Larger pore sizes allow leukocytes to traverse entirely through the material, interacting with the transplanted cells and increasing the chances of rejection. Moreover, poor diffusion of oxygen and nutrients can hinder insulin production by the islets and cell death.

Encapsulation can range in size and geometry, categorized by its islet capacity and transplantation site in connection to the bloodstream. Macroencapsulation specifies the ability to encapsulate a large mass of islets within the capsule. Macrocapsules are usually tubular or planar in geometry, with a lower surface area/volume ratio than the smaller capsules. Developed to enhance oxygen diffusion to the encapsulated islets, microcapsules are typically spherical with a lower islet capacity and higher surface area/volume ratio compared to macrocapsules. Nanoencapsulation, also known as conformal coating or layer-by-layer coating, drastically minimizes the thickness of the capsule, creating a polymeric layer on the surface of the islet to maximize the diffusion of oxygen and nutrients from the host to the islet. Once constructed, capsules will be transplanted intravascularly, attached directly to an artery[30], or extravascularly, in locations such as peritoneal cavity[31,32], subcutaneous space[33,34], omentum[35], and striated muscle.[36] Each EIT technique has its advantages and disadvantages for islet vitality and functionality and has been extensively reviewed by Wu et al.[6] While achieving results in autoimmune diabetic animal models, EIT therapies are not a long-term solution to insulin dependence. They have consistently encountered the major challenge of overcoming the body's natural defenses long-term. For the continued success of EIT procedures, patients must continuously ingest harmful immunosuppressant drugs to weaken the immune system and prevent immune rejection systemically.[2] Furthermore, EIT therapies do not remain clinically viable long-term, even with consistent immunosuppressant usage. Patients often still need exogenous insulin due to loss of function by the transplanted islets over time.[37] As a result, a more effective strategy for sustained localized immune suppression is necessary to prevent EIT rejection by foreign body response.

Methods to tailor the immune system's response have become increasingly sought in islet transplantation. EIT strategies have generally emphasized the use of biochemical changes to the capsule's design by using various ligand incorporations[38,39], material changes[35,40,41], and cellular additions[5,42] to increase the viability of the therapy. However, recent literature has shown that a strong case can be made to include mechanical parameters in capsule design due to advancements in immune cell mechanobiology. Mechanobiology can be described as the study of the essential roles physical factors, such as force[43], geometry[44], and matrix viscoelasticity[45], play on cell and tissue function and morphology, human physiology, and pathology.[46] This form of immune engineering focuses on changing the material's mechanical properties to promote a more favorable response to the therapy.

Substrate stiffness has not been a parameter of focus in EIT design. However, there has been a multitude of evidence displaying the effect of ECM stiffness on cellular function. Examples from literature include ECM stiffness's ability to induce stem cell differentiation into osteoblasts,[47] assist in stem cell differentiation into insulin-secreting β cells,[15,48] influence motility and migration,[49] actin cytoskeletal reorganization,[50] as well as regulate T cell activation and proliferation.[51] Recent findings on the effect of substrate stiffness on the function of the immune system, particularly macrophages, could be promising for encapsulated islet technology. Macrophages attach to the material using integrins and focal adhesion proteins, discussed further in this chapter. Through these adhesion proteins, the macrophages sense the stiffness of the substrate leading to the functional changes that could be utilized to improve EIT design against immune rejection. Through this chapter, we will detail current strategies to increase the clinical viability of EIT with an argument to add substrate stiffness as a parameter of interest. We will briefly overview the foreign body response concerning EIT, discuss material changes to promote EIT viability, and provide substrate stiffness findings that would prove advantageous to include in capsule design. To focus the argument better, stiffness findings will be discussed primarily on macrophages, a significant contributor to the foreign body response and immune rejection.

2.2. Foreign Body Response to EIT

As stated previously, the goal of EIT is to transplant viable insulin-secreting cells with minimal invasiveness into a vascularized area of a patient's body. A successful transplant should promote glycemic control without using long-term exogenous insulin or destruction from the patient's immune system (**Figure 2.1**). Foreign body response (FBR) toward EIT spans the innate and adaptive immune systems as the phagocytes, primarily macrophages, cannot fully degrade the transplanted biomaterial. However, specific response and severity depend on the material's physical and biochemical composition and its effect on the activation of immune cells. As severity is variable based on a myriad of parameters, the timeframe of FBR can span from months to years.[31] FBR can be organized into four phases: ignition, acute inflammation, chronic inflammation, and fibrosis.[3,52]

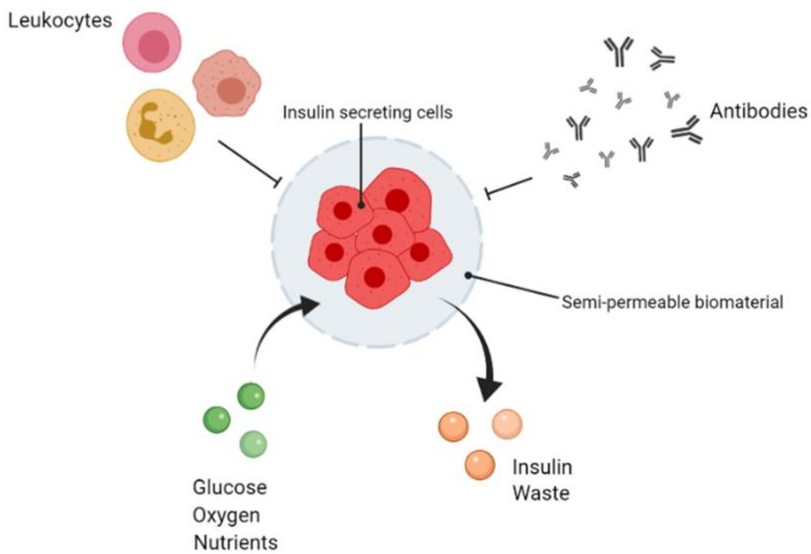

Figure 2.1: A Schematic of the Overall Goal of Encapsulated Islet Therapy. Insulin-secreting cells – islets, beta cells, or differentiated stem cells – are encapsulated in a semi-permeable biomaterial intended to block leukocyte interaction and their secreted antibodies. The biomaterial also allows the diffusion of glucose, oxygen, nutrients, insulin, and waste to maintain cellular function.

2.2.1. Ignition

FBR is initiated at the transplantation site, similar to other biomaterial implants. Due to tissue injury and material-blood interactions, complement proteins from endothelial cells and blood coagulants are adsorbed to the capsule surface within seconds in an unrecognizable conformation through the Vroman Effect.[53,54] This non-specific protein adsorption forms a 2-5 nm thick transient provisional matrix coated at the interface between the material and the native tissue.[55,56] These proteins can include fibrinogen[57], albumin, fibronectin[58], gamma globulins, thrombospondin, and vitronectin.[59] While fibrinogen, gamma globulins, and albumin modulate the immune response, fibronectin and vitronectin enhance cellular adhesion and play a role in the later chronic stage of FBR.[60–62] Simultaneously, cell membrane disruption of neighboring cells and injured tissue results in the release of chemokines CXCL1, CXCL2, CXCL8, and CCL2, as well as a diverse pool of endogenous proteins known as damage-associated molecular pattern (DAMP) molecules.[63,64] These proteins induce chemotaxis of neutrophils, monocytes, and immature dendritic cells (DCs) from the bloodstream and surrounding tissue to the transplantation site to elicit an immune response.[65,66]

2.2.2. Acute Inflammation

As neutrophils and monocytes infiltrate the transplantation site through ignition, proinflammatory cytokines, IL-1 and IL-8, among others, are released at the site, beginning acute inflammation.[65,67,68] Monocytes differentiate into macrophages accompanied by the attraction and stimulation of other innate immune cells. These cells are essential in the initiation, duration, and outcome of the response against the biomaterial.[69,70] Using integrins, macrophages attach to the provisional matrix and differentiate into their inflammatory M1 phenotype through pattern recognition receptors.[71] Integrins are transmembrane glycoproteins that initiate cytoskeletal changes by actin polymerization and mechanotransduction of the focal adhesion kinase (FAK) pathway.[72,73] Substrate stiffness is essential in this integrin engagement as it alters actin distribution in macrophages leading to cell morphology changes. On soft stiffnesses, macrophages tend to be more circular in morphology. However, as substrate stiffness becomes more rigid, F-actin expands, creating more structural protrusions that grow the cell area and reduce circularity into a more spindle morphology.[8,74,75] Morphological changes have been linked to macrophage functional changes. Rounder cell morphology has been associated with pro-inflammatory functionality characteristic of M1 macrophages with the ability to secrete proinflammatory cytokines such as tumor necrosis factor (TNF-α), IL-1, and IL-6, as well as degrading enzymes.[76] In contrast, spindle-shaped cell morphology has corresponded to anti-inflammatory behavior associated with M2 macrophages.[77]

M1 macrophages increase inflammation at the EIT site releasing reactive oxygen species (ROS), cytokines, and lysosomal enzymes, such as nitric oxide synthase (iNOS), to phagocytose and dispose of the transplant.[71] Substrate stiffness has also been demonstrated to affect pro-inflammatory gene expression in macrophages. Using lipopolysaccharides (LPS), a bacterial endotoxin, as a stimulant, substrate stiffness was investigated on the expression of genes along the LPS/TLR4 (toll-like receptor 4) pathway[78] leading to proinflammatory cytokine secretion. Soft (0.2 kPa) stiffness polyacrylamide gels were shown to upregulate downstream TNF-α, IL-6, and IL-1β pro-inflammatory cytokine genes compared to more rigid (33.1 kPa) gels, illustrating stiffness can be used to reduce inflammation by macrophages.[79] Furthermore, cytokine and degradation enzyme secretion can be regulated by stiffness. Markov et al. displayed acute inflammation increased with hardness, Young's modulus, and compressive strength *in vivo*.[7] Soft pectin (14 kPa) hydrogel scaffolds implanted in Wistar albino rats held a lower proinflammatory potential. In contrast, hard (106 kPa) pectin was overpopulated with collagen fibers and contributed to the formation of new connective tissue.[7] Interestingly, this outcome was the opposite of findings described *in vitro*, where soft stiffnesses promoted increased proinflammatory cytokine production.[79–81] However, this alternative result *in vivo* could be attributed to the biodegradable nature of pectin. Soft pectin degraded more rapidly *in vivo* than hard pectin, unquantifiable by day three compared to day 11. Using a 2D polyacrylamide model, Chen et al.[82] determined that TNF-α and IL-1β secretion was reduced as substrate stiffness increased. These findings align with previous studies by Irwin et al.[83], Patel et al.[81], and Gruber et al.[74] using a 2D polyacrylamide-PEG model and similar polyacrylamide models, suggesting a linear trend in key proinflammatory markers based on stiffness which can assist in acute inflammation reduction.

2.2.3. Chronic Inflammation

After 1-2 weeks of frustrated phagocytosis, the adaptive immune system begins the chronic inflammation phase due to the EIT being too large to internalize. This phase should last no more than a couple of weeks as more extended periods can indicate infection.[84] DCs, now mature through activation at the transplantation site, migrate through the lymphatic vessels to the lymph nodes to activate and recruit T cells.[85] Once at the transplant site, T cells assist in prompting integration or exacerbating the destruction of EIT during this process, essentially moving the process along in returning to homeostasis. These cells secrete anti-inflammatory cytokines, IL-4 and IL-13, to begin tissue remodeling, inducing fibroblast migration and proliferation. While this occurs, macrophages begin shifting between M1 and their anti-inflammatory M2 phenotype. Simultaneously, to increase their phagocytic capability and response to the presence of IL-4, adhered macrophages fuse to form foreign body giant cells (FBGCs) - a signature of chronic inflammation.[86] Recently, there has been evidence that the mechanosensitive cation channel transient receptor potential vanilloid 4 (TRPV4) is crucial in the formation of the FBGCs, which increases the role of substrate stiffness in chronic inflammation implanted materials.[87–89] FBGCs form a barrier around the implant, working to deteriorate it and participate in tissue regeneration around the implant.[86] Pro-fibrogenic factors, such as vascular endothelial growth factor (VEGF), transforming growth factor (TGF-β), platelet-derived growth factor (PDGF), collagenase and matrix metalloproteinases, are released as a result of both innate and adaptive immune cells to begin the recruitment of myofibroblasts.[90,91]

2.2.4. Fibrosis

The fibrosis step orchestrates the regeneration of damaged tissues and is the final step in FBR. M2 macrophages contribute significantly to the regeneration process through crosstalk with T cells, stimulation of fibroblasts and angiogenesis, and direct the production and remodeling of extracellular matrix (ECM).[92,93] Recruited fibroblasts secrete collagen I and III, further encapsulating the EIT, compromising its function due to lack of protein diffusion. This secludes the implant from the body's vasculature, leading to hypoxic stress and apoptosis as the encapsulated cells cannot receive oxygen and nutrients from the patient’s blood supply. The duration of chronic inflammation and the anti-inflammatory response of the leukocytes in the area are critical determinants of implant integration with restored functional tissue or its seclusion by forming fibrotic tissue around the implant. The construction of fibrotic tissue depends on the ratio of collagen I to collagen III.[94] Greater collagen I to collagen III results in elevated fibrotic tissue formation. In the case of EIT, the fibrotic tissue formation results in pericapsular fibrotic overgrowth (PFO), a significant signal of rejection. PFO further leads to hypoxia of encapsulated islets.[1]

This is currently an expected outcome of the therapy where most patients receiving EIT clinically return to insulin dependence over time (**Figure 2.2**).[31]

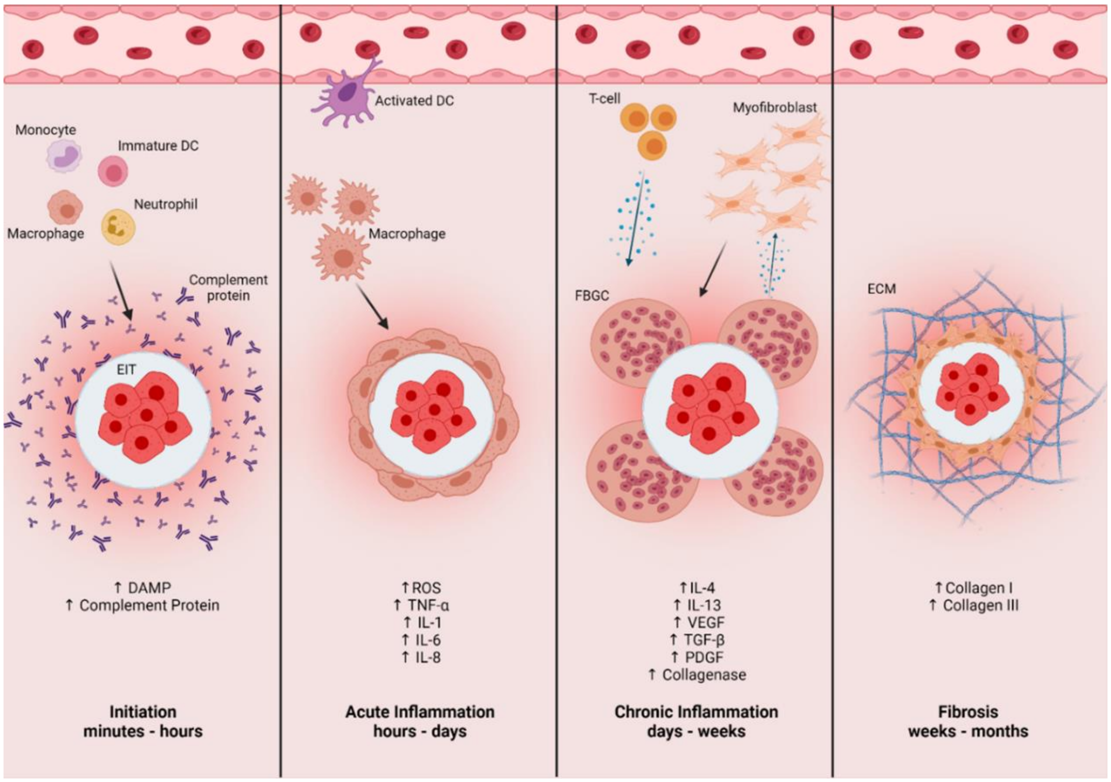

Figure 2.2: A Time Course of Foreign Body Response to Encapsulated Islet Transplantation. When encapsulated islets are transplanted into the body, instantaneously complement proteins adsorb to the material interface. Simultaneously, damaged endothelial cells release DAMP signals and chemokines to recruit innate leukocytes to the transplant site to restore homeostasis, initiating the foreign body response. Macrophages adhere to the material surface, secreting ROS and pro-inflammatory cytokines to degrade and phagocytose the encapsulated islets signaling acute inflammation. Dendritic cells, activated from pro-inflammatory antigens, navigate to the lymph nodes to activate and recruit T cells to the site for assistance in the response. After several days to a couple of weeks, frustrated macrophages, due to ineffective phagocytosis, merge to form foreign body giant cells (FBGCs), a hallmark of chronic inflammation. Through the secretion of anti-inflammatory cytokines and pro-fibrogenic factors, myofibroblasts are recruited to begin fibrosis surrounding the EIT. The foreign body response concludes with increased collagen production and fibrotic tissue secluding the EIT from receiving oxygen, glucose, and nutrients.

Substrate stiffness has been shown to reduce PFO *in vivo*. Acellularly, Ibrahim et al. studied FBR by subcutaneously implanting in mice five commonly used biomaterials: polyvinyl alcohol (PVA), silicone, expanded PTFE (ePTFE), polypropylene, and cotton.[95] Over 180 days, silicone held the thinnest fibrotic capsule. In contrast, the thickest fibrotic capsule varied per time point and material though PVA had the thickest fibrotic capsule from day 60 onward, indicating a need to consider the biomaterial carefully. While the study did not quantify the stiffness of each material used, it can be inferred that Young's modulus varied between materials. There was also a geometric difference between the samples with PVA, silicone, and cotton constructed into 8 mm diameter disks and ePTFE and the polypropylene sectioned in 2 cm long tubes. However, this physical difference can be ruled out as a factor for FBR changes in this study as this did not prove significant in changing fibrotic capsule thickness or leukocyte population. Elucidating the effect of stiffness on fibrotic capsule formation, Blakney et al. implanted PEG-based hydrogels of different stiffnesses in C57BL/6 mice for 28 days, showing a decrease in fibrous capsule thickness in soft stiffnesses.[80] More studies need to be conducted to determine which moduli would be most appropriate for EIT.

2.3. EIT Biomaterial Approaches

There is promising evidence to support using other mechanical properties, such as substrate stiffness, as another parameter to explore to increase EIT viability. Physiologically, Young's modulus of the human body ranges vastly and is tissue-dependent (**Figure 2.3**). Common physiological stiffness values relevant to EIT include the liver (2 – 8 kPa),[96,97] kidney capsule (5 – 10 kPa),[98] and hypodermis, referred to as the subcutaneous cavity, (15 – 34 kPa)[99,100] as standard locations for islet transplantation. Hydrogels are commonly used materials for encapsulation. Due to their hydrophilic nature, high water content, tailorable three-dimensional structure, and transparency, hydrogels provide a robust, highly biocompatible material that prevents damage to surrounding tissues and easily visualizes encapsulated cells. As natural and synthetic polymers, the elastic moduli of hydrogels can be tuned to mimic the entire physiological range by increasing crosslinker concentration or co-polymerization with other materials during synthesis (**Figure 2.3**). Several natural and synthetic polymers have been investigated to improve efficacy and clinical viability since the inception of encapsulated islet transplants. This includes alginate[101], agarose[102], chitosan[103,104], polyethylene glycol (PEG)[38,105], and polyurethane.[106,107]

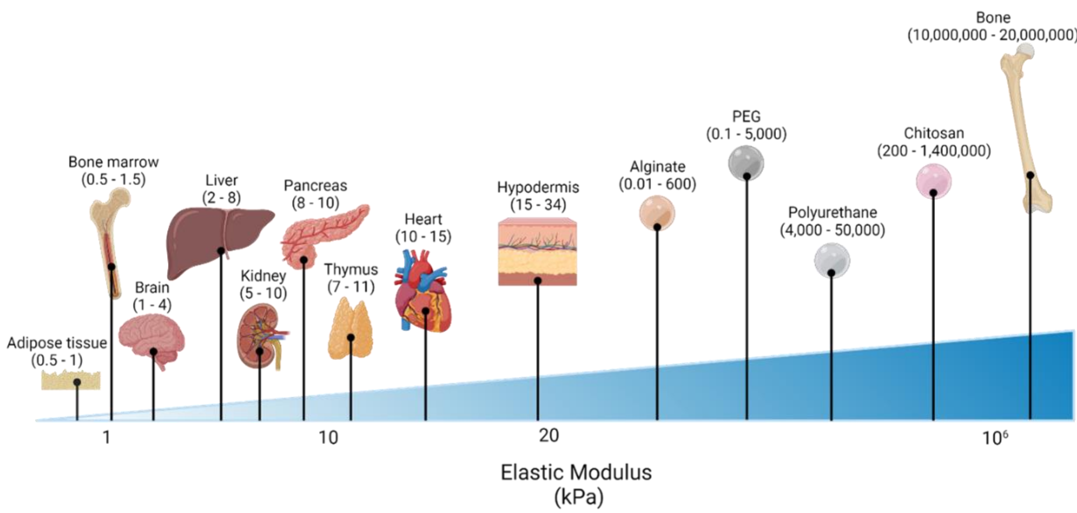

Figure 2.3: Physiological and Material Elastic Moduli Range Relevant to EIT. Adapted from Handorf et al.[108], Young's modulus has been measured for commonly known organs, such as adipose tissue[109], brain[110,111], heart[112], and bone.[113,114] Also, organ stiffnesses relevant to macrophages and EIT including the bone marrow[115], thymus[116], liver[96,97], pancreas[14,117], kidney[98], and subcutaneous cavity (hypodermis).[99,100] Though substrate stiffness is not a primary parameter in EIT capsule design, Young's moduli of materials used, such as alginate[15,16,118], agarose[119], chitosan[120–122], PEG[123–125], and

polyurethane[126,127] are included. While transplantation sites for EIT are secluded to the liver portal vein, kidney capsule, or subcutaneous cavity, it is essential to note macrophages engage with the entire physiological and material stiffness range as tissue-resident and migratory cells.

2.3.1. Alginate

The most widely used and studied hydrogel for microencapsulation-based therapies is alginate. For a more detailed review, see Vaithilingam et al.[1] Characteristically, alginate is robust, topographically smooth, non-biodegradable over prolonged periods, hydrophilic, readily available, and generally inert. The versatility of alginate has been displayed through various methods of microcapsule development to promote increased biocompatibility and islet viability.[128] To make microcapsules for EIT, alginate is typically crosslinked with Ca^{2+} or Ba^{2+} with concentrations ranging from 10 mM to 100 mM.[15] The stiffness of these concentrations range from 1 – 100 kPa. However, the stiffness of alginate microcapsules can be increased to ~600 kPa with changes in alginate and crosslinking concentrations.[16] Permeability can also be manipulated to vary diffusion in and out of the capsule.[129] These tailorable and beneficial features led alginate to be used clinically for EIT therapy.[130] However, although widely used, alginate has several drawbacks that prevent commercial success. Alginate composition varies from sample to sample.[131] This variability makes it challenging to reproduce previous studies for comparable results. Also, due to environmental factors, alginate can contain various impurities, such as heavy metals, proteins, and endotoxins.[132] These contaminants are significant factors leading to fibrotic overgrowth and EIT failure. Though purification methods have been developed to remove these impurities, these methods are costly. They have a limited scope, purifying mainly endotoxins such as lipopolysaccharide (LPS), the most common endotoxin.[133] Even commercially sold 'ultra-pure' alginate has been shown to induce a pro-inflammatory response by macrophages, promoting a thick fibrotic layer around the microcapsule, which must be considered for long-term transplantation.[134] However, due to its chemical structure, alginate can bind with other polymers such as poly-l-lysine, poly-l-ornithine, and PEG to overcome challenges.

Though researchers have begun to study the effect of alginate microcapsule stiffness on EIT, the literature has been limited to islet functionality and capsule stability, not FBR.[14,15] For example, Richardson et al.[15] investigated the effect of Ba^{2+} crosslinked alginate microcapsule stiffness ranging from 1 – 100 kPa, on human embryonic stem cell (hESC) differentiation and growth to pancreatic progenitor cells. The stiffness range of 4 – 7 kPa was more favorable for differentiating hESCs to pancreatic progenitor cells. Low stiffness also promotes cell growth which was stunted at higher stiffnesses. Moreover, Enck et al.[14] found that the incorporation of pancreatic ECM fragments into the alginate matrix will significantly improve the durability of the capsule while slightly improving islet functionality at 7 days. The scalability of alginate-based microencapsulation techniques needs to be investigated in more extensive studies with larger animals. Still, alginate will remain an attractive material for EIT due to its versatility.

2.3.2. Agarose

Similar to alginate, agarose is a seaweed-derived polysaccharide used for cell encapsulation. Agarose gel is temperature-dependent, curing at a temperature under

25°C and being able to withstand temperatures up to 60°C before degradation begins. This robust temperature range makes the hydrogel a promising candidate for islet encapsulation and has been in consideration since the 1980s.[135,136] Islets encapsulated in alginate were demonstrated to maintain comparable gene expression of insulin signaling pathways compared to free islets after eight weeks of culture.[137] Also, through incorporating a coculture of regulatory T cells, agarose encapsulated islets maintained viability and functionality *in vivo* for up to 100 days.[138] The Young's modulus of agarose can range from 1.5 – 2600 kPa correlating with agarose weight percentage.[119] This increase in agarose weight percentage leads to smaller pore sizes as well to assist with permeability.[139] Holdcraft et al.[102] investigated the effect of varying agarose type and concentration on islet viability and insulin production. Using 1.5% SeaKem Gold (SG) agarose, 0.8% SG agarose, and 0.8% Litex agarose, insulin production was significantly improved by the islets encapsulated in 0.8% agarose compared to 1.5% agarose. Though the team did not measure the modulus of the investigated agarose concentrations, it can be inferred that insulin production by islets are impacted by substrate stiffness and should be investigated further.

2.3.3. Chitosan

As an alternative to alginate microcapsules, chitosan has been proposed to increase the clinical viability of EIT.[140] Chitosan is a cationic polysaccharide synthesized from chitin shells of crustaceans with a stiffer and more robust modulus range than alginate ranging from 200 kPa – 1.4 GPa.[103,104] Chitosan has been demonstrated to reduce the production of inflammatory cytokines, IL-6 and TNF-α, and inhibit T cell proliferation.[141] It has been suggested to improve the mechanical stability of alginate long-term. Chitosan-alginate microcapsules have decreased PFO, leading to a more biocompatible implant long term.[40,140,142] Yang et al.'s xenogeneic and allogeneic transplanted chitosan-coated alginate capsules demonstrated significantly reduced cell adhesion compared to alginate capsule control up to a year post-transplantation.[140] Though stiffness was not measured, we can infer the stiffness to be ~5 kPa due to the use of 10 mM barium crosslinked alginate, characterized by Richardson et al.[15] and findings by Williams et al.[143] demonstrating chitosan coatings slightly stiffens alginate microcapsules. Despite promising results, a low pH of at least four is needed to dissolve the polymer, which can be detrimental in islet applications. However, several groups are modifying chitosan for microcapsule development under physiological pH conditions to promote a more viable encapsulation method. For example, Kim et al. used chitosan in conjunction with dexamethasone 21-phosphate and alginate to produce microcapsules for EIT.[40] While stiffness was not characterized, similar to the previous study, the inclusion of dexa-chitosan in the alginate microcapsule synthesis can be inferred to increase the stiffness of the microcapsule. Moreover, the permeability remained comparable among the dexa-chitosan and alginate microcapsules. Dexa-chitosan microencapsulated islets promoted better glucose control and reduced PFO and inflammatory cell infiltration after 231 days *in vivo* compared to alginate controls.

2.3.4. PEG

A synthetic polymer, PEG, can be used with alginate-based microcapsules to increase mechanical stability by hindering swelling and rupture.[144,145] PEG hydrogels are nanoporous, preventing the infiltration of leukocytes into the material but allowing the transport or diffusion of oxygen, nutrients, and insulin. Also, PEG removes the immunogenic variability seen with alginate by being synthetic, promoting immunoprotective properties, bio-inertness, and exceptional biocompatibility.[146,147] PEG can also be tailored through functionalization to assist with the engraftment of the implant.[148] Due to these factors, many labs have used PEG as a material of interest in EIT.[145,149,150] Weaver et al. demonstrated that RGD-functionalized PEG gels produced smaller diameter capsules (310 ± 14 µm) compared to alginate (≥ 500 µm), resulting in increased insulin responsiveness and islet viability.[150] Though the stiffness of the microcapsules was not characterized by this study; it can be estimated using the concentrations provided. The PEG microcapsules were synthesized using 5% PEG crosslinked with 30 mg/mL dithiothreitol; it can be inferred that the stiffness of the capsule would be ~10 kPa.[151] While the alginate microcapsules were synthesized using 1.6% alginate and 50 mM Ba^{2+}; the stiffness can be estimated at ~20 kPa.[15] This reduction in stiffness may also be associated with improved insulin responsiveness seen in the PEG microcapsules as it is closer to the native stiffness of the pancreas. Haque et al. developed a layer-by-layer hyperbranched PEG and heparin (hb-PEG/Heparin) nanoencapsulation for EIT.[149] Nonhuman primate islets were encapsulated and transplanted into the subcapsular kidney space of diabetic C57BL/6 mice. Compared to non-encapsulated islets, the approach allowed the transplanted islet protection from leukocytes while promoting engraftment and better function over four weeks. However, an immunosuppressive drug protocol was needed to achieve the intended results. Current limitations of PEG include the elicitation of inflammation due to complement activation. Minimally invasive methods have been introduced as a prevention strategy against complement activation. One of which demonstrated the ability of an injectable PEG hydrogel as a minimally invasive way to transplant islets to a secure location subcutaneously and retrieve them if adverse events occur.[152] The team showed PEG encapsulated islet injections promoted reduced blood glucose levels two days after transplantation into a B6D2F1 mouse model compared to a non-encapsulated islet control. While the work did not completely alleviate diabetes in the model compared to the tubular alginate implant under the same timeframe, the approach demonstrated some feasibility and warrants future investigations.

2.3.3. Polyurethane

Since the early 1990s, polyurethane has been a material of interest in EIT.[106] As polyurethane held wide success in other implant therapies, its biocompatibility and versatility provided great promise for EIT. This biocompatibility was tested in early EIT studies by Zondervan et al. [106] and Ward et al.;[153] however, it held limited success due to permeability constraints. More recent studies showed that altering the chemical structure and scaffold development process of polyurethane could assist in overcoming these constraints.[107,154,155] As a proof-of-concept study, Liu et al. recently developed a zwitterionic polyurethane implant for EIT.[155] This electrospun implant provides tunable nanoporous structures that prevent cell escape while allowing the diffusion of insulin and nutrients. When implanted intraperitoneally in C57BL/6 mice for six months, lower FBR and fibrotic overgrowth were induced compared to unmodified polyurethane implants. Polyurethane has also been demonstrated to promote localized immunosuppression by adding rapamycin.

Francis et al. loaded 8mm x 2mm polyurethane disks for EIT with 2nM of rapamycin.[107] The disks exhibited a sustained release of rapamycin over seven days with no adverse effects on the viability of murine and human islets. T cell proliferation was also suppressed during *in vitro* studies. When implanted subcutaneously in mice, signs of engraftment could be detected from blood vessel formation. Though promising, more work is needed to strengthen the mechanical properties and reduce hydrogel swelling for clinical success.[156,157]

Conclusion

Encapsulated islet therapy is a novel and minimally invasive strategy to treat T1DM. While EIT has successfully cured most small animals of diabetes, returning hosts to normoglycemic conditions for extended periods without the use of injected insulin, it has been challenging to replicate this success with humans and non-human primates without systemic immunosuppressive drug assistance. A long-lasting functioning therapy must utilize biochemical and mechanical approaches to tailor the immune system to integrate the transplant.

This chapter detailed current methods to increase EIT viability and made a case for using substrate stiffness to assist in EIT success based on macrophage findings. While these findings suggest stiffness could be a beneficial factor in immune rejection prevention, it is fair to note these studies have not incorporated glycemic condition as a parameter of study to mimic the mechanosensitivity of macrophages in healthy patients versus diabetic patients. Nor do these studies mimic the glucose dysregulation seen in diabetic patients alone as it varies from hypoglycemia (<70 mg/dL glucose), normoglycemia (70 – 120 mg/dL), and hyperglycemia (>120 mg/dL). As macrophages are glycolytic cells, changes in glycemic conditions have been shown to alter the function of macrophages.[10] It is currently unknown how changes in glucose will alter mechanosensitivity in macrophages and will be explored in the chapters moving forward.

Chapter 3: Investigation of Glycemic Condition Effect on Stiffness-Mediated Mechanosensitivity of Unstimulated Macrophages

3.1. Introduction

Macrophage adherence is crucial for effective response to foreign pathogens and biomaterials. As one of the first leukocytes to interact with implanted tissue-engineered therapies and the central orchestrator of the foreign body response (FBR), macrophages adhere to surface-adsorbed proteins on the biomaterial by the use of integrins. These transmembrane glycoproteins initiate cytoskeletal changes by F-actin polymerization.[158,159] This physical cell-biomaterial interaction promotes morphological and functional changes, which can dictate the extent of foreign body response (FBR) to tissue-engineered therapies, such as encapsulated islet transplantation (EIT) for patients with diabetes.[160]

During FBR, macrophages engage with the implanted material in an effort to phagocytose it. It is a key objective for macrophages and other phagocytes to clear foreign objects from the body. This actin-based process is promoted through numerous mechanisms.[161] One such process is Fc-mediated phagocytosis, an essential component of FBR. Fc receptors on the surface of the macrophage recognize and bind to opsonin on the surface of the biomaterial. This junction causes actin to polymerize and protrude out to envelope the material. During FBR to EIT, macrophages undergo frustrated phagocytosis as the biomaterial is too large (>5μm) for the macrophage to digest efficiently.[44] Because of this, it is critical to understand how macrophages interact with the physical properties of implanted biomaterials to dictate their function.

Currently, the substrate stiffness of the biomaterial has been demonstrated to alter cytoskeletal construction, leading to morphological and functional changes in macrophages.[8] Our lab has identified that as macrophages adhere to a substrate, over time these cells grow drastically with reduced circularity on stiffer substrates compared to soft substrates.[8] Macrophage morphology is a key indicator of phenotype and functionality.[77,162] Furthermore, substrate stiffness has also been shown to modify phagocytic capabilities in macrophages.[163,164] Increased substrate stiffness causes a significant rise in the percentage of frustrated phagocytes and mechanical stress generated by macrophages.

While the effect of glycemic condition on the cytoskeletal structure leading to morphology changes is not fully understood, literature has shown that glucose can affect mitochondrial shape internally causing changes to functionality in the various eukaryotic cells.[165–167] External glucose levels have been shown to affect macrophage function, including those requiring cytoskeletal change, such as phagocytosis.[168] However, the role of glucose, through glycolysis, has not been revealed in the substrate stiffness-mediated mechanosensitivity of focal adhesion dictated morphology and functional changes. This relationship will be elucidated in this chapter.

In this chapter, the effect of external glucose concentrations on substrate stiffness-mediated mechanosensitivity in macrophages. This investigation will correlate the relationship between glycemic condition and substrate stiffness in unstimulated macrophage morphology identified by cell area and circularity, phenotype, and phagocytic capacity indicated through Fc-mediated frustrated phagocytosis to mimic foreign body response in patients with glucose dysregulation. We hypothesize that hyperglycemic conditions will promote enhanced substrate stiffness-mediated mechanosensitivity effects in macrophage function through frustrated phagocytosis. However, we anticipate that morphological alterations will primarily be attributed to substrate stiffness and remain independent of glycemic condition. This study will expand knowledge in the fields of mechanobiology and immunometabolism to improve tissue-engineered therapy design for patients with diabetes.

3.2. Methods

3.2.1. Cell Culture

RAW264.7 and J774.1 macrophages (ATCC, Manassas, VA, USA) were cultured separately based on cell line and glucose conditions. Macrophages cultured under hyperglycemic conditions were cultured in 450 mg/dL Dulbecco's Modified Eagle's Media (DMEM) (ATCC, Manassas, VA, USA). In contrast, cells in normoglycemic conditions were cultured in 100 mg/dL DMEM (Thermo Fisher Scientific, Waltham, MA, USA). 10% heat-inactivated fetal bovine serum (FBS) and 1% penicillin/streptavidin were added to all culture media.

3.2.2. Polyacrylamide Synthesis and Characterization

Polyacrylamide gels were synthesized according to previously established methods.[8,169] Concentrations for each stiffness were as follows: 2 kPa – 3% acryl and 0.1% bis, 15 kPa – 8% acryl and 0.2% bis, 55 kPa – 10% acryl and 0.4% bis, 110 kPa – 12% acryl and 0.6% bis, and 274 kPa – 15% acryl and 1.2% bis (Bio-Rad laboratories, Hercules, CA, USA). Ammonium persulfate (APS) (Thermo Fisher Scientific, Waltham, MA, USA) and N, N, N', N' – tetramethylethylenediamine (TEMED) (Bio-Rad Laboratories, Hercules, CA, USA) were added to the acrylamide mixture. Gel substrates about 80 µm thick were synthesized by dispensing 30 µL of polyacrylamide on amine-activated glass coverslips (22 x 22 mm, Fisher Scientific, Pittsburg, PA, USA) and sandwiching between a sterilized glass slide. Gels were cured at room temperature for 30 mins and then pried from the glass slide using a sterile razor blade. For morphology studies, gels were coated with 0.1 mg/mL human fibronectin (Sigma-Aldrich, St. Louis, MO, USA) after activating with 0.5 mg/mL sulfo-SANPAH (Sigma-Aldrich, St. Louis, MO, USA) according to previously published methodology.[169] For frustrated phagocytosis studies, gels were coated with 1 mg/mL human IgG.[163,164] Gels were sterilized by exposure to ultraviolet light for 15 mins and rinsed with sterile phosphate-buffered saline (Thermo Fisher Scientific, Waltham, MA, USA) before cells were seeded for experimentation. To validate the stiffness of each gel, bulk polyacrylamide was synthesized using the same formulations previously outlined. Gels were sectioned into cylindrical columns using a 2:1 ratio of height to the diameter as outlined by the ASTM standard for compressive testing of hydrogels.[170,171] Bulk compression tests on the Instron confirmed Young's modulus of each gel (**Table 1.1**).

Table 1.1: Young's Modulus measurements through bulk gel compression tests based on acrylamide and bis concentrations.

Acrylamide and Bis Concentration	Young's Modulus (kPa)
3% acrylamide + 0.1% bis	2.34 ± 0.66
8% acrylamide + 0.2% bis	14.88 ± 3.30
10% acrylamide + 0.4% bis	54.24 ± 10.62
12% acrylamide + 0.6% bis	109.62 ± 14.56
15% acrylamide + 1.2% bis	273.86 ± 23.30

3.2.3. Cellular Area and Circularity

10^5 macrophages were seeded onto fibronectin-coated polyacrylamide gels in a 6-well dish and allowed to adhere for 1hr or 18hr at 37°C, 5% CO_2 in their respective media condition. Samples were then washed with 1X PBS and fixed with 4% PFA for 30 mins at room temperature. Samples further undergo three 1X PBS washes for 5 mins each at room temperature on a shaker. Cells are permeabilized with 0.25% Triton X-100 for 5 mins. After three more 1X PBS washes, cells are stained for F-actin using ActinRed 555 Ready Probes Reagent (Thermo Fisher Scientific, Waltham, MA, USA) using manufacturers procedures. Briefly, reagent was added to 1% BSA at a 2 drops/mL concentration. Samples are incubated in solution for 30 mins at room temperature. After 20 mins, DAPI 1:1000 is added to samples for the remaining 10 min incubation. Samples undergo three additional PBS washes and then imaged by fluorescent microscopy at 20X magnification. Images are analyzed using ImageJ where cell area and perimeter are measured. The circularity of each cell is calculated by **Equation 1.1**.

$$\boldsymbol{Equation\ 1.1}: Circularity = \frac{4\pi A}{P^2}$$

3.2.4. Macrophage Phenotype Imaging and Quantification

After culturing RAW264.7 macrophages for 18hr, samples were fixed with 4% PFA followed by 1X PBS washes before blocking with 2% BSA/PBS for 1 hour. The primary antibodies CD80 (5 µg/mL; goat anti-mouse; R&D Systems), CD86 (rat anti-mouse; Thermo Fisher Scientific, Waltham, MA, USA), and CD206 (rabbit anti-mouse; Thermo Fisher Scientific, Waltham, MA, USA) incubated overnight at 4°C. Samples were then washed with 1X PBS. Secondary antibodies, FITC (donkey anti-goat; 1:500; Thermo Fisher Scientific, Waltham, MA, USA), TRITC (donkey anti-rat; 1:500; Thermo Fisher Scientific, Waltham, MA, USA), and Cy5 (donkey anti-rabbit; 1:500; Thermo Fisher Scientific, Waltham, MA, USA) in 1% BSA/PBS was added to samples for 1hr incubation at room temperature in the dark. DAPI (1:1000) was used to counterstain the cell nucleus and added at the 50 min mark for the remaining 10 mins of incubation. Samples were washed three times with 1X PBS for 5 mins each at room temperature before imaging. Images were taken at 20X magnification with five images take per gel. N = 5 biological replicates were conducted for each sample condition. NIS-Elements AR software (Nikon Instruments, Melville, New York, USA) was used to determine the mean fluorescence intensity of each channel for each sample, thresholding each channel to only capture the fluorescence of the cells and remove background noise from data.

3.2.5. Frustrated Phagocytosis Assay

Polyacrylamide gels are opsonized with 1 mg/mL human-IgG (Rockland Immunochemicals, Pottstown, PA, USA) after activating with 0.5 mg/mL sulfo-SANPAH (Sigma-Aldrich, St. Louis, MO, USA) for 1 hour at room temperature. IgG coating was confirmed using immunofluorescence with rabbit anti-human FITC secondary antibody (1:500; Thermo Fisher Scientific, Waltham, MA, USA). Gels are then rinsed with 1X PBS three times before sterilizing in a UV chamber for 15 mins. 10^5 RAW264.7 macrophages are added to each gel with their respective glycemic conditioned media. Cells were incubated for 1 hour at 37°C, 5% CO_2 in their respective media condition. Samples were then washed with 1X PBS and fixed with 4% PFA for 30 mins at room temperature. Samples further undergo three 1X PBS washes for 5 mins each at room temperature on a shaker. Cells are permeabilized with 0.25% Triton X-100 for 5 mins. After three more 1X PBS washes, cells are stained for F-actin using ActinRed 555 Ready Probes Reagent (Thermo Fisher Scientific, Waltham, MA, USA) using manufacturers procedures described earlier. Cells were then imaged at 20X magnification. Macrophages experiencing frustrated phagocytosis were identified as cells with lamella extending in a radially symmetric fashion (**Figure 3.6A**). Percentage of cells experiencing frustrated phagocytosis were calculated by the ratio of positive cells to total cells in the image.

3.2.6. Statistical Analysis

Statistical tests were conducted using GraphPad Prism 9 (GraphPad, San Diego, CA). Normality was verified for data groups using Shapiro-Wilks tests with $n = 5$ biological replicates and $n = 5$ technical replicates for all images. Once completed, data groups were analyzed using ANOVA and between pairs using Tukey tests. Statistical significance was indicated by $p < 0.05$.

3.3. Results

3.3.1. Substrate stiffness-mediated macrophage morphology changes are unaffected by glycemic condition.

To assess the effect of glycemic condition on macrophage stiffness-driven mechanosensitivity, RAW264.7 macrophages we added to polyacrylamide gels of 2, 15, and 274 kPa under hyperglycemic (450 mg/dL glucose) and normoglycemic (100 mg/dL glucose) conditions. Cells were preconditioned in their respective media in cell culture before experimentation. At 1hr and 18hr, cell area and circularity were quantified for each sample condition. Macrophages cultured under hyperglycemic conditions began to demonstrate significant changes in cell area based on substrate stiffness at 1hr ranging from 129.80 ± 7.2 μm^2 on 2 kPa to 163.60 ± 16.9 μm^2 on 274 kPa (**Figure 3.1**). This substrate stiffness-mediated mechanosensitivity was not exhibited in normoglycemic conditions with cell area of 155.10 ± 8.3 μm^2 on 2 kPa, 160.90 ± 8.1 μm^2 on 15 kPa, and 154.20 ± 6.2 μm^2 on 274 kPa. Macrophages were also significantly rounder on normoglycemic conditions than hyperglycemic conditions on the same substrate stiffness at 1hr of adhesion; 2 kPa: 0.89 ± 0.01 (normoglycemic) to 0.84 ± 0.04 (hyperglycemic); 15 kPa: 0.92 ± 0.01 (normoglycemic) to 0.86 ± 0.01 (hyperglycemic); 274 kPa: 0.93 ± 0.01 (normoglycemic) to 0.85 ± 0.01 (hyperglycemic).

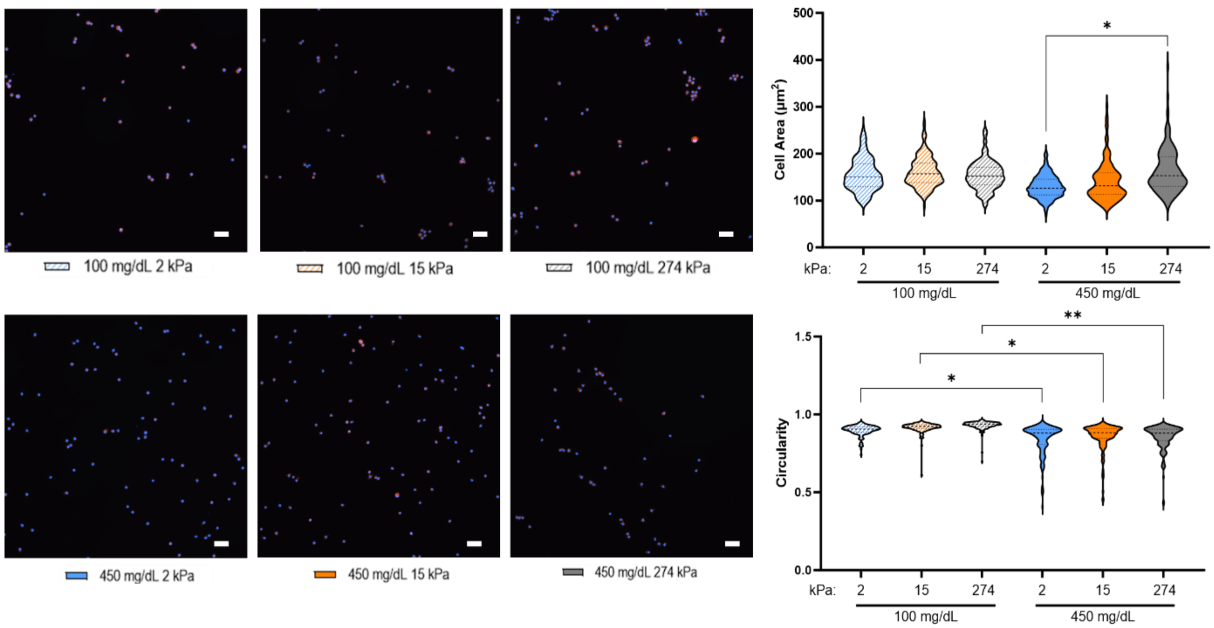

Figure 3.1: Hyperglycemic conditions promoted stiffness-based cell area growth and reduced circularity of RAW264.7 macrophages compared to normoglycemic conditions at 1hr. Macrophages were seeded on fibronectin-coated polyacrylamide gels of 2, 15, and 274 kPa under normoglycemic and hyperglycemic media conditions. Cells were incubated for 1hr at 37°C. Cells were then fixed and stained for F-actin (TRITC) and DAPI. *n* = 150 biological replicates across *n* = 3 polyacrylamide gels were conducted for all samples. Cell size and circularity were calculated using ImageJ. Statistical analysis was conducted using ANOVA and Tukey tests of mean values per gel, where $p < 0.05$ indicated statistical significance. Scale bar: 100 μm

At 18hr of adhesion, macrophages exhibited substrate stiffness-mediated mechanosensitivity trends in both cell area and circularity independent of glycemic condition (**Figure 3.2**). As stiffness increased from 2 to 274 kPa, cell area grew from 221.40 ± 9.5 μm^2 to 658.10 ± 21.6 μm^2 in hyperglycemic conditions and 248.60 ±

16.4 µm^2 to 611.90 ± 16.8 µm^2 in normoglycemic conditions. Circularity was also reduced in stiffer substrates independent of glycemic condition: 0.81 ± 0.03 to 0.37 ± 0.02 in hyperglycemic conditions and 0.82 ± 0.01 to 0.45 ± 0.08 in normoglycemic conditions. This same phenomenon was also demonstrated in J774.1 macrophages, an additional murine cell line (**Figure 3.3**). J774.1 macrophages grew from 264.10 ± 35.11 µm^2 to 469.60 ± 27.17 µm^2 in normoglycemic conditioned macrophages and 303.70 ± 14.19 µm^2 to 509.90 ± 43.76 µm^2 in hyperglycemic conditions. With the circularity of the J774.1 macrophages diminished significantly from 2 to 274 kPa ranging from 0.73 ± 0.03 to 0.64 ± 0.03 in normoglycemic conditions and 0.74 ± 0.03 to 0.56 ± 0.04 in hyperglycemic conditions. These results suggest that substrate stiffness is a driver in adhesion and morphology changes.

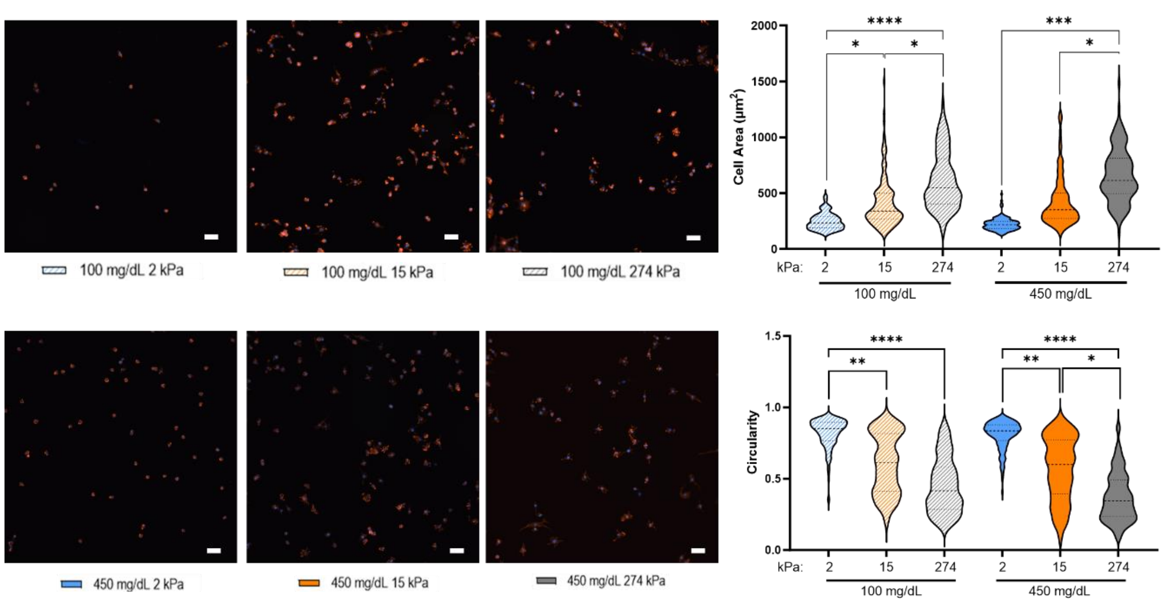

Figure 3.2: Increased substrate stiffness drove cell area and circularity changes in RAW264.7 macrophages at 18hr. Macrophages were seeded on fibronectin-coated polyacrylamide gels of 2, 15, and 274 kPa under normoglycemic and hyperglycemic media conditions. Cells were incubated for 1hr at 37°C. Cells were then fixed and stained for F-actin (TRITC) and DAPI. Cell size and circularity

were calculated using ImageJ. n = 150 biological replicates across n = 3 polyacrylamide were conducted for all samples. Statistical analysis was conducted using ANOVA and Tukey tests of mean values per gel, where $p < 0.05$ indicated statistical significance. Scale bar: 100 µm

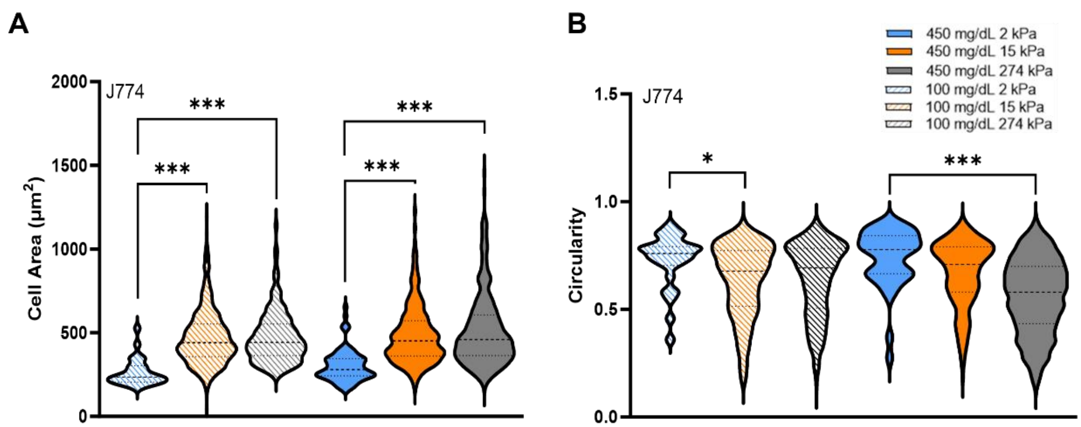

Figure 3.3: Confirmation of increased substrate stiffness driving morphology changes independent of glycemic conditions in J774 macrophages at 18hr. Macrophages were seeded on fibronectin-coated polyacrylamide gels of 2, 15, and 274 kPa under normoglycemic and hyperglycemic media conditions. Cells were incubated for 1hr at 37°C. Cells were then fixed and stained for F-actin (TRITC) and DAPI. Cell size and circularity were calculated using ImageJ. n = 3 polyacrylamide gels were conducted for all samples. Statistical analysis was conducted using ANOVA and Tukey tests of mean values per gel, where $p < 0.05$ indicated statistical significance.

3.3.2. Unstimulated macrophage phenotype remained comparable across substrate stiffness and glycemic condition after 18hr adherence.

As significant morphology changes occurred due to substrate stiffness at18hr of adherence, macrophage phenotype was assessed using immunofluorescent imaging at 18hr to further characterize the effect of glycemic condition and substrate stiffness on unstimulated macrophages. At 18hr, RAW264.7 macrophages were stained for the pro-inflammatory surface marker, CD86, anti-inflammatory surface marker, CD206, and the co-stimulatory marker, CD80. The mean fluorescent intensity was quantified and compared for each marker. Though morphology changes occurred based on stiffness, phenotypic markers remained comparable across all glycemic conditions and substrate stiffnesses (**Figure 3.4**).

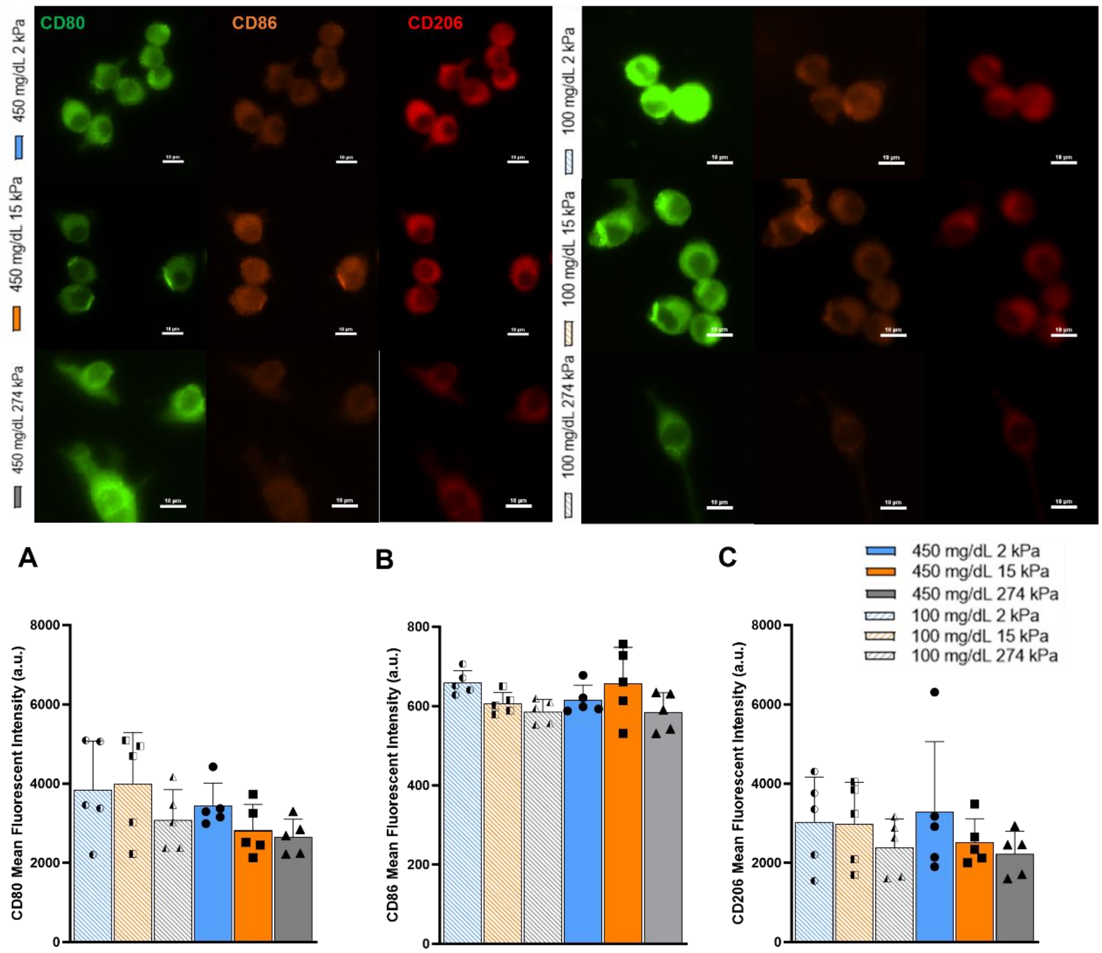

Figure 3.4: Phenotypic markers of unstimulated macrophages remained comparable under stiffness and glucose changes. Phenotype changes of unstimulated macrophages at 18 hr on 2, 15, and 274 kPa. Macrophages stained for **A.** co-stimulatory surface marker CD80, **B.** pro-inflammatory surface marker CD86, and **C.** anti-inflammatory CD206. Mean fluorescent intensity was quantified and compared using NIS-Elements AR. n = 5 biological replicates were conducted for all samples. n = 5 technical replicates conducted for each biological replicate. FITC: CD80, TRITC: CD86, Cy5: CD206. Statistical analysis was conducted using ANOVA and Tukey tests, where $p < 0.05$ indicated statistical significance. ***$p < 0.0005$; ****$p < 0.0001$. Scale bar = 10 µm.

3.3.3. Hyperglycemic conditions enhance substrate stiffness-derived mechanosensitivity of Fc-mediated phagocytosis indicated through F-actin extension.

To address the role of glycemic condition in phagocytotic substrate stiffness-mediated mechanosensitivity, polyacrylamide gels were opsonized with human IgG (**Figure 3.5**) to promote Fc-receptor-mediated phagocytosis by the macrophages. As the macrophages undergoes the process of phagocytosis, the lamella of the macrophage begins to extend to engulf the subject. However, when an opsonized particle is >5 μm in diameter, it cannot be fully ingested by the cells. This phenomenon is referenced as frustrated phagocytosis and can be demonstrated by the lamella extending in a radially symmetrical fashion from the nucleus to engulf the substrate. This can be visualized through phalloidin staining after 1hr of incubation on IgG-coated substrates (**Figure 3.6A**).[163,164] Macrophages that did not extend in this fashion with no lamella extension, the nucleus offset to one side of the cell, or multi-nucleic were counted as negative (**Figure 3.6B**). Macrophages undergoing frustrated phagocytosis indicated by actin extension described previously were individually identified and a percentage of frustrated phagocytes to total cells (**Figure 3.7**).

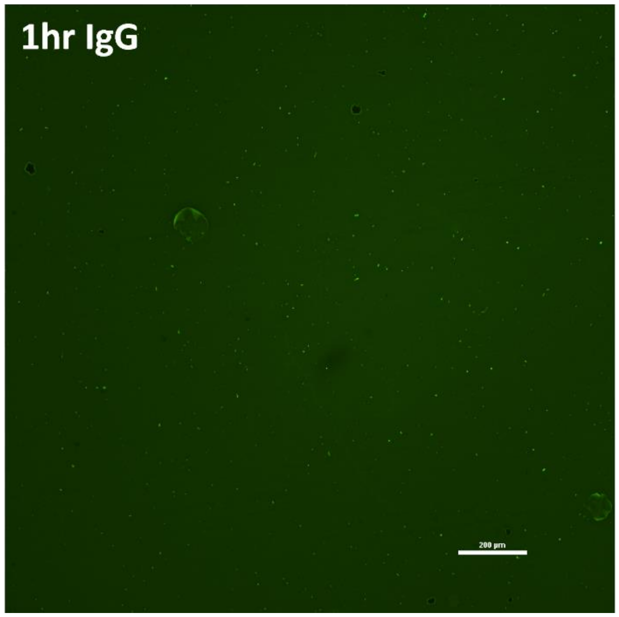

Figure 3.5: Confirmation of IgG coating after 1hr using FITC staining. Sulfo-SANPAH-activated polyacrylamide gels are coated with human IgG for 1hr and stained with anti-human IgG, FITC secondary antibody to visualize. Gels were imaged under 10x magnification. n = 3 polyacrylamide gels. Scale bar = 200 µm.

Both glycemic conditions demonstrated an increase in the percentage of frustrated phagocytes at higher substrate stiffness (**Figure 3.6C**). However, hyperglycemic conditions promoted enhanced mechanosensitivity to substrate stiffness for percentage of frustrated phagocytes compared to normoglycemic conditions ranging from 6.54 ± 1.03% to 11.66 ± 1.20% in normoglycemic conditions and 6.60 ± 2.60% to 22.62 ± 3.38% in hyperglycemic conditions. Hyperglycemic conditions also promoted a substantially significant increase in frustrated phagocytes at 274 kPa ($p < 0.0001$). A logarithmic relationship could be identified between substrate stiffness and the percentage of cells experiencing frustrated phagocytosis (**Figure 3.6D**).

To further conclude the role of glycemic condition on substrate stiffness-mediated mechanosensitivity in phagocytic function, glucose inhibitor, 2-deoxy-glucose (2-DG), was added to sample media and the percentage of frustrated phagocytes was quantified for all conditions (**Figure 3.6E**). Interestingly, inhibiting the ability of macrophages to uptake glucose removed substrate stiffness-mediated trends across both glycemic conditions with the percentage of frustrated phagocytes being analogous across all samples. These results demonstrated that glucose has a critical role in macrophage mechanotransduction leading to frustrated phagocytosis. A blind review was conducted to confirm these findings (**Figure 3.8**).

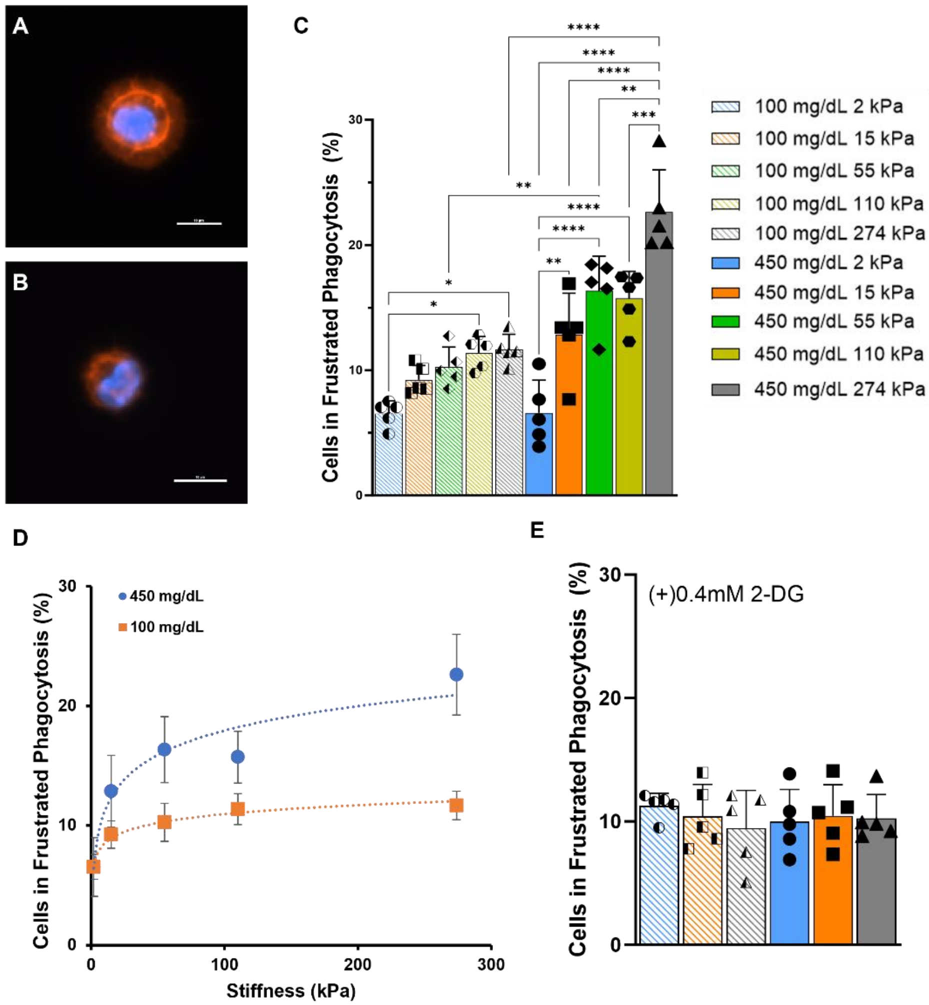

Figure 3.6: Hyperglycemic conditions enhance mechanosensitivity to substrate stiffness of macrophages experiencing frustrated phagocytosis. Macrophages were seeded on IgG-coated polyacrylamide for 1 hr, stained for actin (TRITC), and analyzed for the percentage of macrophages undergoing frustrated phagocytosis. **A.** Positive cell for frustrated phagocytosis. **B.** Negative cells for frustrated phagocytosis. **C.** Comparison of the percentage of cells experiencing frustrated phagocytosis by glucose condition and substrate stiffness. **D.** Trend of substrate stiffness vs cells undergoing frustrated phagocytosis for hyperglycemic and normoglycemic conditions. **E.** Addition of glucose inhibitor (0.4mM 2-deoxy-glucose) on cells experiencing frustrated phagocytosis on 2, 15, and 274 kPa. n = 5 biological replicates were conducted for all samples. n = 5 technical replicates conducted for each biological replicate. Statistical analysis was conducted using ANOVA and Tukey tests, where $p < 0.05$ indicated statistical significance. *$p < 0.05$; **$p < 0.005$; ***$p < 0.0005$; ****$p < 0.0001$. Scale bar: 10 μm

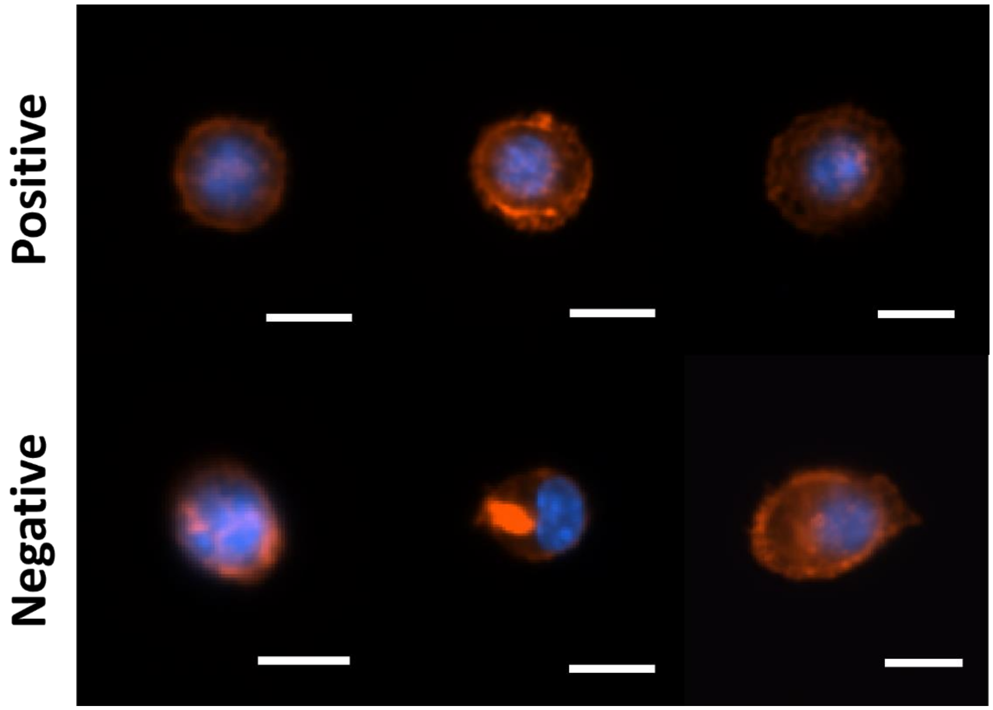

Figure 3.7: Range of macrophages labeled positive and negative for Fc-mediated phagocytosis. Macrophages are seeded onto IgG-coated polyacrylamide gels and incubated for 1 hr before fixing and staining for F-actin (TRITC) and nucleus (DAPI). Macrophages experiencing Fc-mediated phagocytosis of the polyacrylamide gel were identified by actin filament extension symmetrically radial from the nucleus and were labeled positive. Cells with no actin extension occurred, actin extended to one side of the nucleus, or multi-nucleic were labeled negative. Scale bar = 10 µm.

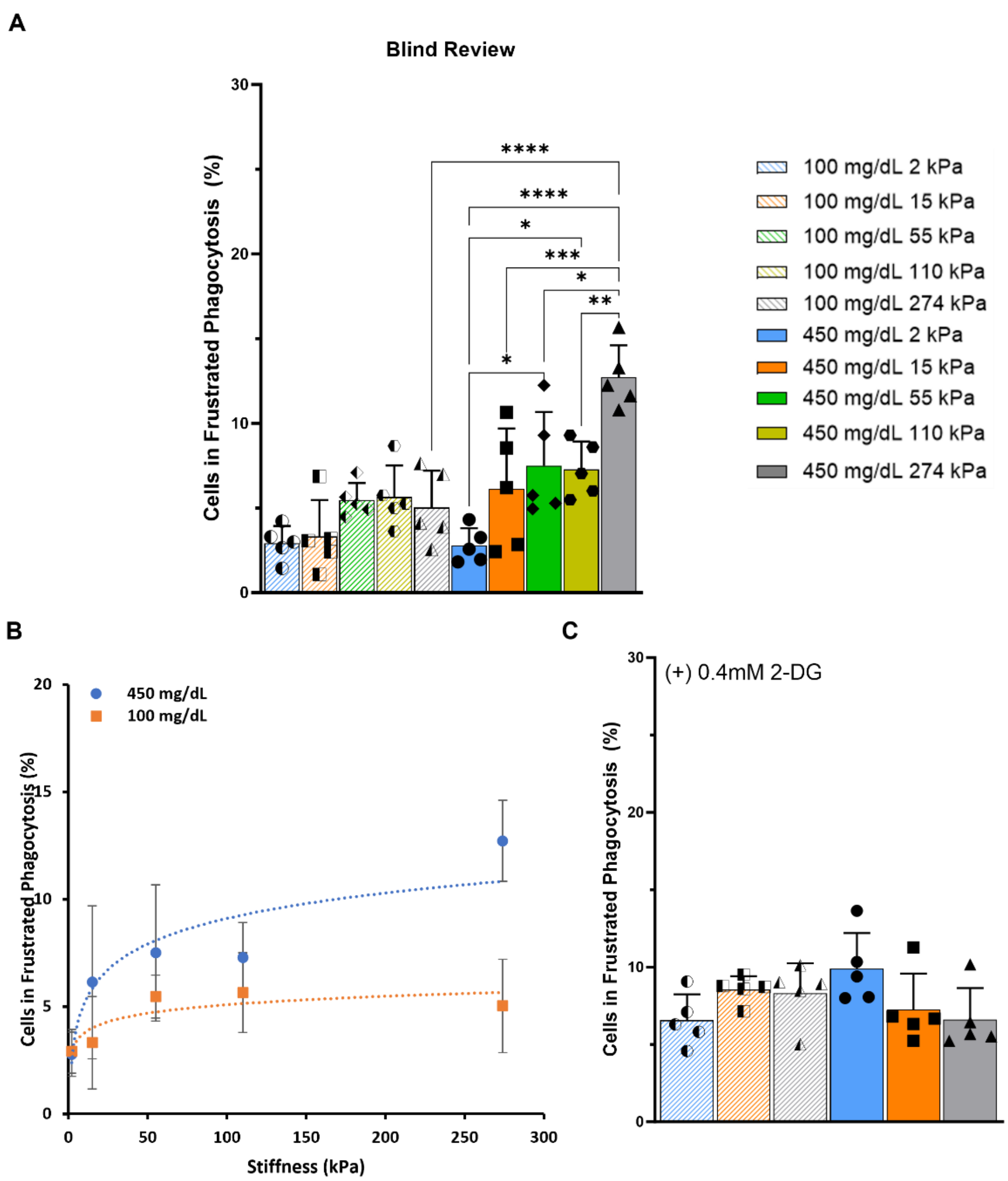

Figure 3.8: Blind review: Hyperglycemic conditions enhance mechanosensitivity to substrate stiffness of macrophages experiencing frustrated phagocytosis. A. Blind comparison of the percentage of cells experiencing frustrated phagocytosis by glucose condition and substrate stiffness. **B.** Trend of substrate stiffness vs cells undergoing frustrated phagocytosis for hyperglycemic and normoglycemic conditions. **C.** Addition of glucose inhibitor (0.4mM 2-deoxyglucose) on cells experiencing frustrated phagocytosis on 2, 15, and 274 kPa. n = 5 biological replicates were conducted for all samples. n = 5 technical replicates conducted for each biological replicate. Statistical analysis was conducted using ANOVA and Tukey tests, where $p < 0.05$ indicated statistical significance. *$p < 0.05$; **$p < 0.005$; ***$p < 0.0005$; ****$p < 0.0001$.

3.4. Discussion

Herein we report that there is a synergistic relationship between glucose metabolism and substrate stiffness-mediated mechanosensitivity in function induced mouse-derived macrophages: RAW264.7 and J774 macrophages. To explore the relationship between glycemic condition and substrate stiffness-mediated mechanosensitivity of unstimulated macrophages, we first assessed cellular morphology through cell area and circularity. Macrophage cell area and circularity was evaluated across all conditions, including normoglycemic and hyperglycemic environments, along with different substrate stiffness levels (2, 15, and 274 kPa). These assessments were conducted at both the 1hr and 18hr adherence time points. Similar to published work in our lab with human-derived macrophages under hyperglycemic conditions, substrate stiffness induced significant growth in cell area starting at 1hr and more significantly at 18hr of adhesion.[8] Unlike what was observed in hyperglycemic conditions, under normoglycemic conditions, we did not observe the same mechanosensitive trend at the 1hr adherence stage. Though, normoglycemic conditioned macrophages were significantly rounder in circularity than hyperglycemic conditions, by the 18hr timepoint, substrate stiffness-mediated mechanosensitivity occurred independent of glycemic condition. In addition to cell growth expansion as substrate stiffness increased, the circularity of the macrophages decreased significantly as well as 18hr of adhesion. Stiffer substrates encouraged the macrophages to spread more irregularly rather than just expanding in size. This response can be attributed to macrophages adhering to stiffer substrates more effectively than on soft substrates leading to more pronounced spreading of the macrophages. This phenomenon was demonstrated in both RAW264.7 and J774 macrophages supports findings by Blakney et al.[80], Patel et al.[81], Irwin et al.[83], Sridharan et al.[162], and Escolano et al.[79], conducted in hyperglycemic conditions.

Morphological changes are a key characteristic that can be used to indicate the polarization state of macrophages. While anti-inflammatory, M2, macrophages maintain a slender, spindle-like shape, pro-inflammatory macrophages appear rounder in shape. Literature also shows that by inducing a morphology change through confinement to a M2-like shape, macrophages upregulate arginase-1, an anti-inflammatory marker, compared to unconfined macrophages.[77] Due to this, it was important to assess if these substrate stiffness-mediated morphology changes displayed at 18hr resulted in changes to similar phenotype changes. The phenotype of the macrophages was evaluated using immunofluorescent imaging staining for CD86, a pro-inflammatory surface marker, CD206, an anti-inflammatory surface marker, and CD80, a co-stimulatory factor upregulated in pro-inflammatory macrophages at 18hr. As macrophages on soft (2 kPa) substrates demonstrated rounder morphology independent of glycemic condition, cells could be expected to display more pro-inflammatory characteristics.[80] Interestingly, macrophage phenotype remained comparable unrelated to stiffness and glycemic concentrations. This contrasts findings from Blakney et al. in unstimulated macrophages under hyperglycemic conditions. However, phenotype was inferred through gene expression analysis internally while our study evaluated surface marker changes, which may require a longer period of time to manifest. Though from our findings, it can be concluded that glycemic condition does not impact the characteristics in unstimulated macrophages experiencing substrate stiffness-mediated mechanosensitivity.

Transitioning to focal adhesion-based functionality of unstimulated macrophages, a critical function of macrophages is phagocytosis. This process allows macrophages to remove pathogens from the body and is a key aspect of FBR. This is an actin mediated process where the cytoskeleton of the macrophage extends out to consume the object. However, this process is hindered when macrophages engage with objects > 5 μm, as with implanted tissue-engineered therapies such as encapsulated islet therapy, in which case macrophages undergo a frustrated state as the object is too larger to be enveloped. This state can be investigated *in vitro* through opsonizing the substrate with human IgG inducing Fc-mediated phagocytosis and can be visualized through actin extension in a symmetrically radial fashion from the nucleus.[163,164] Fc-mediated phagocytosis impacted by substrate stiffness and increases in macrophages cultured on stiffer substrates supporting conclusions by Rougerie et al.[163] and Beningo et al.[164] However, glycemic condition played an important role in the stiffness-mediated mechanosensitivity. Reduced glucose impaired the response macrophages held to substrate stiffness in reference to phagocytosis. Inhibiting glucose uptake through the use of 2-DG resulted in the removal of substrate-stiffness mediated mechanosensitivity in its entirety, demonstrating an equivalent percentage of cells experiencing frustrated phagocytosis across all substrate stiffnesses and glycemic conditions. Extracellular glucose is needed for macrophages to effectively function as macrophage phagocytosis is fueled through glycolysis. The inhibition of glycolysis through 2-DG has been shown to impair the ability of macrophages to phagocytose particles compared to non-inhibited control.[172–174] Our findings show that not only does glycolysis play a significant effect on macrophage phagocytosis, but also impacts macrophage response to substrate stiffness.

Though not a frustrated phagocytosis model, Pavlou et al. demonstrated that sustained hyperglycemic conditions inhibit phagocytic activity by bone-marrow-derived macrophages (BMDMs) to ingest bioparticles.[175] This study used bacterial-based bioparticles that fluoresce upon ingestion by phagocytes from the acidic environment and compared fluorescent intensity across BMDMs from normal mice and induced-diabetic mice as well as under normoglycemic and hyperglycemic conditions. BMDMs from induced-diabetic mice also demonstrated significantly impaired phagocytosis compared to healthy and post-treated mice. This contrast in our findings may be due to changes in macrophage origin and experimental design. Our study uses RAW264.7 macrophages, a monocyte-derived cell line, to assess frustrated phagocytosis to implanted materials. Monocyte-derived macrophages play a significant role in the foreign body response compared to tissue-resident and bone-marrow-derived macrophages and can display different characteristics.[3,176,177] Also, the study described above investigated bacterial phagocytosis, a different mechanism than Fc-mediated phagocytosis investigated in our study. While both processes result in the formation and extension of pseudopodia to engulf the object, these types of phagocytosis have two different receptors for initiation, pattern recognition receptors for bacterial phagocytosis[178] and Fc receptors for Fc-mediated phagocytosis,[161] which could be causing conflicting findings. Overall, this work identified that glycolysis has a role in cytoskeletal-mediated functionality in macrophages while being independent of morphology and phenotype characteristics after 18hr unstimulated.

3.5. Conclusion

In this chapter, we successfully established a connection between glycemic condition and substrate stiffness-mediated mechanosensitivity, specifically in macrophage functionality regarding Fc-mediated phagocytosis. While it is evident that morphology and adherence remain independent of glycemic condition and predominately influenced by substrate stiffness, the connection in Fc-mediated phagocytosis deserves further investigation. Our results garner more questions for future studies into internalized mechanistic connections between focal adhesion and glucose metabolism pathways. Src and Syk have been identified as critical proteins in Fc-mediated phagocytosis and could explain what is leading to our findings internally. Moreover, these discoveries may shed light on a novel connection between glucose metabolism and mechanosensing in macrophage functionality.

Chapter 4: Glycemic Condition Enhance the Mechanosensitivity of Proinflammatory Macrophages[2]

[2]Adapted from Johnson C. D., Fischer D., Smith I. M., Aranda – Espinoza H., and Fisher J. P. (2023). Hyperglycemic Conditions Enhance the Mechanosensitivity of Proinflammatory RAW264.7 Macrophages. *Tissue Engineering Part A*, *29*(5-6), 172-184. https://doi.org/10.1089/ten.tea.2022.0.151

4.1. Introduction

Macrophages are innate immune cells and primary contributors to the foreign body response to tissue-engineered therapies.[86] As phagocytes and antigen-presenting cells, macrophages secrete degrading enzymes, chemokines, and pro-inflammatory cytokines, like tumor necrosis factor (TNF-α) and interleukin-6 (IL-6), to protect the body from the invader. Due to this functionality, macrophages can hinder the effectiveness of tissue-engineered therapies, leading to immune rejection. One tissue-engineered therapy of interest is encapsulated islet transplantation (EIT). EIT is a tissue-engineered therapy that targets exogenous insulin dependence and regulates glucose levels in Type 1 diabetic patients.[1] This therapy consists of encapsulated whole donor islets in a semipermeable polymeric membrane, specifically the insulin-secreting β cells from islets. The capsule protects the cells from leukocytes while promoting islet function and viability. While researchers have seen success in diabetic animal models, EIT therapies are not a commercially relevant, long-term solution for insulin dependence due to rejection by the patient’s immune system, which results in continued reliance on exogenous insulin.[140] Macrophages remain at the EIT site for the entire duration of the response, promoting intercellular signal cascades, which result in complete encapsulation of the transplant with fibrous tissue, named pericapsular fibrotic overgrowth (PFO).[5] PFO blocks the implanted islets from receiving oxygen, glucose, and nutrients, leading to loss of function and apoptosis. Altering the biochemical and mechanical characteristics of the capsule biomaterial may promote better viability for EIT.

Capsules can range in stiffness based on material and composition. However, the most common material used for EIT, alginate, can vary in stiffness from 1 – 100 kPa.[15] Though the role of mechanotransduction on the immune function of macrophages and other leukocytes is still being elucidated, recent studies have shown that macrophages are mechanosensitive. Substrate stiffness has been demonstrated to affect macrophage characteristics and function.[8,9] Our lab has shown that substrate stiffness alters macrophage cell area, proliferation, actin organization, and migration speed when cultured on polyacrylamide gels with Young's moduli ranging from 1 – 280 kPa.[8] This was comparable to the findings of Blakney et al.[80], who found that substrate stiffness caused changes in gene expression of proinflammatory cytokines, TNF-α, IL-1β, and IL-6, by macrophages stimulated with lipopolysaccharide (LPS) when cultured on 130 – 840 kPa poly(ethylene glycol) hydrogels. Furthermore, Escolano et al. found upregulated NLRP3 inflammasome formation, a multiprotein complex responsible for the final processing of IL-1β, and upregulated IL-1β and IL-6 secretion on 0.2 kPa polyacrylamide gels, compared to stiffer 33.1 kPa gels when stimulated with LPS and nigericin.[79] Though we can reasonably conclude that macrophages are mechanosensitive, we do not have a clear picture of the impact of glucose concentration on this phenomenon.

Dysregulation of glucose maintenance in diabetic patients causes blood glucose to vary from normoglycemic (70-120 mg/dL) to hypoglycemic (<70 mg/dL) or hyperglycemic (>120 mg/dL) conditions. It is understood that glucose dysregulation results in impaired immune function. Moreover, glucose metabolism plays an essential role in the function of macrophages.[10,179] Long-term hyperglycemia has been demonstrated to promote increased TNF-α and IL-1β secretion.[175] The metabolic pathway begins with the uptake of extracellular glucose surrounding the cell through the cell's glucose transporter, GLUT1, in the case of macrophages.[13] Increased glucose uptake due to GLUT1 overexpression resulted in increased reactive oxygen species (ROS) production and pro-inflammatory phenotype in macrophages.[13] The glucose is then broken down through glycolysis by various enzymes to form two molecules of ATP and pyruvate.[180] Lactate, a product of glycolysis, is produced by reducing pyruvate. Lactate is secreted in high amounts by innate immune cells after inflammatory stimulation and has been linked to hindering proinflammatory cytokine secretion.[181,182] Furthermore, literature has demonstrated that inhibiting glycolysis using 2-deoxyglucose prevented macrophage activation *in vitro* and reduced inflammation *in vivo*.[174,183]

These findings suggest a potential synergistic relationship between glucose metabolism and mechanosensitivity that profoundly influences macrophage function.

However, it is critical to establish how glycemic condition impacts the macrophage mechanosensitivity in response to EIT biomaterials. Elucidating the role of mechanosensitivity in macrophage function in varied glycemic conditions can better inform EIT capsule design. This chapter explores the relationship between glucose metabolism and mechanosensitivity and assesses its impact on macrophage function. Using a 2D polyacrylamide gel model of 3-order magnitude in stiffness, we cultured unstimulated and LPS-stimulated RAW264.7 macrophages under normoglycemic (100 mg/dL) conditions and hyperglycemic (450 mg/dL) conditions on 2, 15, and 274 kPa polyacrylamide gels. Macrophages were cultured on the model for up to 3 days, and key aspects of glycolysis and LPS-stimulated mechanistic pathways were assessed. For glycolysis, samples were assayed for glucose uptake, lactate secretion, and gene expression of GLUT1 and the glycolysis enzyme GAPDH. Macrophages were also evaluated for TNF-α, IL-6, and IL-10 cytokine secretion and gene expression of toll-like receptor 4 (TLR4), a receptor for LPS stimulation, TNF-α, IL-6, and IL-10 (**Figure 4.1**). This work provides critical evidence that hyperglycemic conditions significantly enhance the substrate stiffness-mediated mechanosensitivity in proinflammatory macrophages.

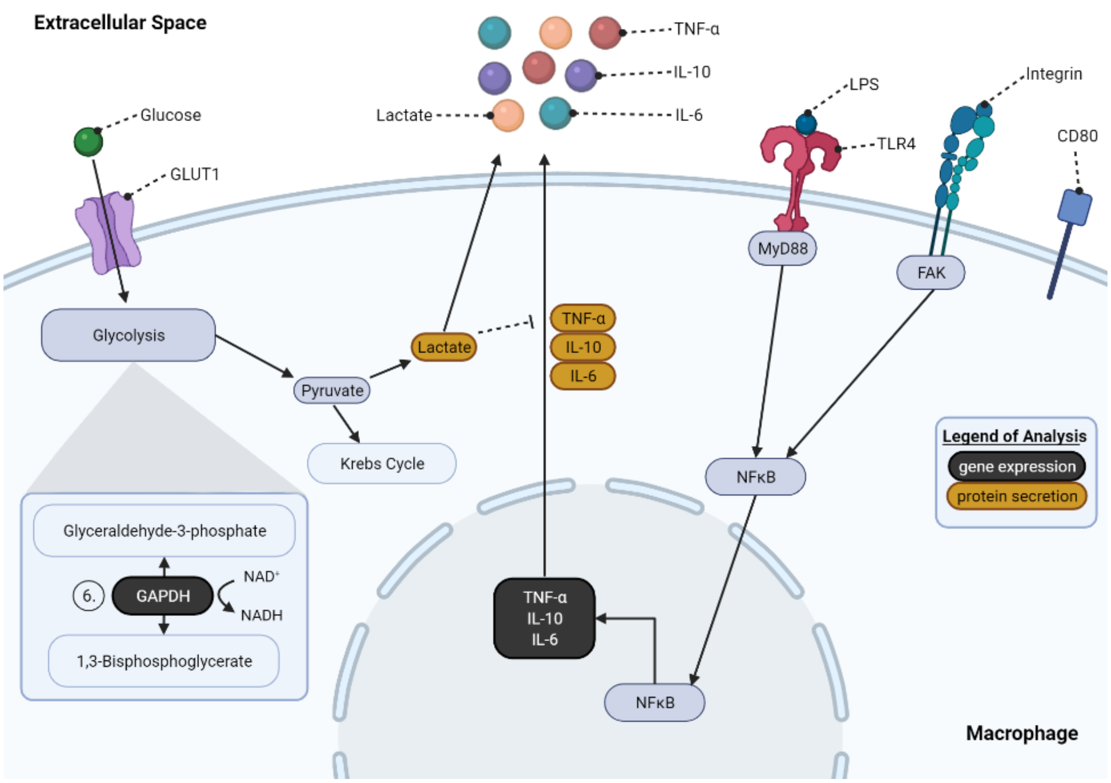

Figure 4.1: General overview of glycolysis, LPS/TLR4, and focal adhesion kinase (FAK) signaling pathways in macrophages relevant to the cellular experimentation conducted in this study. On the left side, glucose enters the cell through glucose transporter 1 (GLUT1).[180] Once glucose uptake occurs, glucose undergoes glycolysis to break down the molecule into pyruvate and ATP. Pyruvate can later undergo lactic acid fermentation to form lactate which is secreted from the macrophage. On the center-right side, lipopolysaccharide (LPS) binds with TLR4 through LBP, MD-2, and CD14 (not shown) to form a complex leading to MyD88 (myeloid differentiation primary response gene 88) dependent signal cascade.[78] Activation of MyD88 signals the activation and translocation of NFκB into the nucleus to activate the cytokine genes, TNF-α, IL-6, and IL-10. These cytokines are later secreted out of the cell. Under LPS stimulation, macrophages polarize to an inflammatory M1-like phenotype that can be signified by the surface marker CD80.[184] Furthermore, macrophages sense the mechanical properties, stiffness, of the ECM through the FAK pathway which also leads to NFκB activation and translocation into the nucleus similar to MyD88 dependent signaling.[73,185] This figure was illustrated using BioRender.

4.2. Methods

4.2.1. Cell Culture

Unstimulated RAW264.7 macrophages (ATCC, Manassas, VA, USA) were cultured separately on tissue-culture polystyrene based on glucose conditions before experimentation. Macrophages cultured under hyperglycemic conditions were cultured in 450 mg/dL Dulbecco's Modified Eagle's Media (DMEM) (ATCC, Manassas, VA, USA). In contrast, cells in normoglycemic conditions were cultured in 100 mg/dL DMEM (Thermo Fisher Scientific, Waltham, MA, USA). 10% Fetal bovine serum (FBS) was added to all culture media. Cells were seeded onto polyacrylamide gels of 2, 15, or 274 kPa in a 6-well dish and allowed to adhere for 16 – 18 hours at 37°C, 5% CO_2. After, gels with adhered cells were transferred into a new well with fresh media based on the condition to begin each study (**Figure 4.2**). Unstimulated adherence media samples were stored at -80°C until assayed.

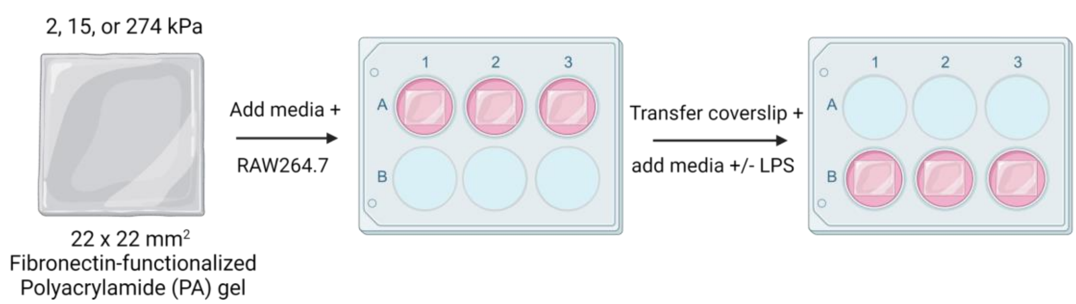

Figure 4.2: Schematic of the experimental setup. Polyacrylamide gels (PA), 2, 15, or 274 kPa, are synthesized on sulfo-SANPAH activated 22 mm x 22 mm glass coverslips. PA gels are transferred into a 6-well plate. RAW264.7 macrophages are seeded with hyperglycemic or normoglycemic media to adhere overnight at 37°C. Samples are transferred to the new well with media +/- LPS stimulation for time studies.

4.2.2. Polyacrylamide Synthesis Characterization

Polyacrylamide gels were synthesized according to previously established methods.[8,169] Concentrations for each stiffness were as follows: 2 kPa – 3% acryl and 0.1% bis, 15 kPa – 8% acryl and 0.2% bis, 274 kPa – 15% acryl and 1.2% bis (Bio-Rad Laboratories, Hercules, CA, USA). Ammonium persulfate (APS) (Thermo) and N, N, N', N' – tetramethylethylenediamine (TEMED) (Bio-Rad Laboratories, Hercules, CA, USA) were added to the acrylamide mixture. Gel substrates about 80 µm thick were synthesized by dispensing 30 µL of polyacrylamide on amine-activated glass coverslips (22 x 22 mm, Fisher Scientific, Pittsburg, PA, USA) sandwiching between a sterilized glass slide. Gels were cured at room temperature for 30 mins and then pried from the glass slide using a sterile razor blade. Gels were coated with 0.1 mg/mL human fibronectin (Sigma-Aldrich, St. Louis, MO, USA) after activating with 0.5 mg/mL sulfo-SANPAH (Sigma-Aldrich, St. Louis, MO, USA) according to previously published methodology.[169] Gels were sterilized by exposure to ultraviolet light for 15 mins and rinsed with sterile phosphate-buffered saline (Thermo Fisher Scientific, Waltham, MA, USA) before cells were seeded for experimentation. To validate the stiffness of each gel, bulk polyacrylamide was synthesized using the same formulations previously outlined. Gels were sectioned into cylindrical columns using a 2:1 ratio of height to diameter as outlined by the ASTM standard for compressive testing of hydrogels.[170,171] Bulk compression tests on the Instron confirmed Young's modulus of each gel (**Table 1.1**).

4.2.3. Cytokine Secretion Quantification

First, 10^5 RAW264.7 macrophages were seeded onto each fibronectin-coated gel to adhere for 16 – 18 hours at 37°C, 5% CO_2. After macrophages were transferred into a new well, 3 mL of hyperglycemic or normoglycemic media, based on the original glycemic condition used for culture, was added to each well. For stimulated samples, 0.5 µg/mL salmonella typhosa lipopolysaccharide (LPS) (Sigma-Aldrich, St. Louis, MO, USA) was included in the media. Samples were incubated at 37°C, 5% CO_2, for 3 days. Supernatants were collected from each sample after each day and stored at -80°C until assayed. TNF-α, IL-10, and IL-6 were quantified using sandwich ELISAs (TNF-α and IL-6: Peprotech Inc., East Windsor, NJ, USA; IL-10: Thermo Fisher Scientific, Waltham, MA, USA) with protocols from their respective kits. Three biological replicates were conducted for each sample.

4.2.4. Proliferation of Unstimulated RAW264.7 Macrophages

10^5 RAW264.7 macrophages were seeded onto 2 and 274 kPa fibronectin-coated gels under hyperglycemic and normoglycemic conditions to adhere for 16 – 18 hours at 37°C, 5% CO_2. Gels with adhered macrophages are then transferred into a new well imaged at timepoints 0, 24, and 48 hours. Five technical replicates were imaged for each biological sample. Three biological samples were conducted.

4.2.5. Real-Time Quantitative PCR

To quantify gene expression, 2 x 10^5 macrophages were seeded on each gel and adhered for 16 – 18 hrs. Adhered cells were transferred into a new well to begin experimentation. Fresh media was added based on glycemic condition, and cells were stimulated with 0.5 μg/mL LPS for 4 hours at 37°C, 5% CO_2. Macrophages were harvested for gene expression analysis using StemPro™ Accutase™ cell dissociation reagent (Thermo Fisher Scientific, Waltham, MA, USA) for 30 mins at room temperature. Cells were collected into pools by sample (n = 6 gels for each sample; ~1.2 x 10^6 cells total), and cell pellets were generated via centrifugation at 1000 RPM for 10 mins. The supernatant was aspirated, and TRI_{ZOL} and chloroform reagents were added to the remaining pellet to begin RNA isolation. RNA was extracted using RNeasy Plus Mini Kit (Qiagen) according to the manufacturer's instructions. RNA concentration and purity were quantified using Nanodrop 2000 (Thermo Fisher Scientific, Waltham, MA, USA). Subsequently, using a high-capacity cDNA reverse transcriptase kit (Thermo Fisher Scientific, Waltham, MA, USA), RNA was reverse transcribed to cDNA. TaqMan probes and TaqMan™ Universal PCR Master Mix were added to the cDNA and loaded to a 384-well plate. TaqMan probes used are as follows: *TNF-α* – Mm00443258_m1, *IL-10* – Mm00439614_m1, *IL-6* – Mm00446190_m1, *TLR4* – Mm00445273_m1, *GLUT1* – Mm00441473_m1, *GAPDH* – Mm99999915_g1, and *18S ribosomal RNA* (*18srRNA*) – Mm03928990_g1 (Thermo Fisher Scientific, Waltham, MA, USA). PCR plates were run on a QuantStudio 7 Flex Real-Time qPCR system (Thermo Fisher Scientific, Waltham, MA, USA). 18srRNA was used as a reference gene, and all samples were normalized to 100 mg/dL 2 kPa for comparison. Samples were compared to each other using the fold change of gene expression calculated using the $2^{-\Delta\Delta CT}$ method. Three biological replicates were conducted for each sample.

4.2.6. Western blotting

Protein expression of TLR4 was examined using the same culture method as section 2.5, 2 x 10^5 macrophages were seeded on each gel and adhered for 16 – 18 hours. Adhered cells were transferred into a new well to begin experimentation. Fresh media was added based on glycemic condition, and cells were stimulated with 0.5 µg/mL LPS for 4 hours at 37°C, 5% CO_2. Protein isolation buffer (RIPA Buffer (ThermoFisher, Waltham, MA)), 1:100 protease inhibitor cocktail (Sigma Aldrich, St. Louis, MO), and 20µg/mL phenylmethylsulfonyl fluoride (PMSF) was added to inverted polyacrylamide gels in a 6 well plate and was incubated on ice for 5 mins. Following incubation cell lysate was scraped from gels using a cell scrapper and collected. Cell lysates were further incubated on ice for 1 hour, with rigorous vortexing every 15 mins, after which, the tubes were spun down at 1000xg for 5 mins and the protein solution lysate was collected. To analyze protein content, a BCA assay was run on the protein solution lysate in accordance with Pierce BCA Protein Assay Kit protocol (ThermoFisher, Waltham, MA). The loading weight of protein was extrapolated from absorbance readouts calibrated to a standard curve. Samples were diluted to a loading weight of 10µg. Diluted protein samples were incubated with 4x Laemmli buffer (Bio-Rad, Hercules, CA) and β-mercaptoethanol (Bio-Rad, Hercules, CA) for 10 minutes at 100°C. Following a brief microcentrifugation, protein solutions in Laemmli buffer were loaded into a precast Mini-PROTEAN TGX Gel (Bio-Rad, Hercules, CA) with a Precision Plus Dual Color ladder (Bio-Rad, Hercules, CA) in an empty well for reference. The gel was run at 120V for 1 hour using the Bio-Rad PowerPac HQ in a Tris/Glycine/SDS Buffer (Bio-Rad, Hercules, CA). Prior to membrane transfer in a Bio-Rad Trans-Blot Turbo Transfer System, supported Nitrocellulose Membrane (Bio-Rad, Hercules, CA) and two transfer spongers were pre-soaked in Trans-Blot Turbo Transfer Buffer (Bio-Rad, Hercules, CA) for 10 minutes. After transfer from TGX gel to membrane, the membrane was blocked in 1:1 PBS: Intercept Blocking Buffer (Li-Cor, Lincoln, NE) for 1 hour at RT. Membranes were subsequently incubated with 2μg/mL TLR4 polyclonal antibody (ThermoFisher, Waltham, MA) and 1:500 β-actin monoclonal antibody (BD, Franklin Lakes, NJ) for 16 – 18 hours at 4°C. The following day, the membrane was washed 3x with PBS with 0.1% Tween 20 (PBST) for 15 minutes each. The membrane was then treated with 1:10,000 Li-Cor IR-Dyes (Li-Cor, Lincoln, NE) in 1:1 PBST: Intercept Blocking Buffer for one hour at room temperature. The membrane was washed 3x with PBS for 15 minutes each. The membrane's fluorescent readout was captured with a Li-Cor Odyssey CLx (Li-Cor, Lincoln, NE) imager and analyzed using Li-Cor ImageStudio Version 5 software.

4.2.7. Immunofluorescence Imaging and Quantification

After culturing RAW264.7 macrophages for 3 days, samples were fixed with 4% PFA followed by 1X PBS washes before blocking with 4% BSA/PBS. The primary antibody (CD80), used to indicate the pro-inflammatory (M1) phenotype, was incubated for 16 – 18 hours at 4°C. Samples were then washed with 1X PBS. Secondary antibody (FITC) in 4% BSA/PBS was added to samples for 1hr incubation at room temperature in the dark. DAPI was used to counterstain the cell nucleus. ImageJ software was used to determine the fluorescence intensity of each cell. The average $CD80^+$ expression of each sample was quantified using the mean intensity of the FITC channel divided by the number of nuclei per image (**Equation 4.1**). Five technical replicates were done for each biological replicate. Three biological replicates were conducted for each sample.

$$\boldsymbol{Equation\ 4.1}: Average\ CD80^{+}\ Expression = \frac{FITC\ Mean\ Intensity\ (CD80)}{Number\ of\ Nuclei\ (DAPI)}$$

4.2.8. Glucose Uptake and Lactate Secretion

After 10^5 RAW264.7 macrophages adhered to fibronectin-activated polyacrylamide gels overnight and gels were transferred into a new well, fresh media was added based on glycemic condition. Stimulated cells were treated with 0.5 µg/mL LPS. Media samples were aliquoted each day for 3 days and stored at -20°C until analyzed. Glucose and lactate concentrations of samples are quantified using a YSI 2950D Biochemistry Analyzer (YSI, Yellow Springs, OH). The rate of glucose uptake and lactate secretion were determined by glucose and lactate concentration in the media over 3 days.

4.2.9. Statistical Analysis

Statistical tests were conducted using GraphPad Prism 9 (GraphPad, San Diego, CA). Normality was verified for data groups using Shapiro-Wilks tests with $n = 3$ biological replicates. For immunofluorescence imaging, $n = 5$ technical replicates were conducted, while $n = 3$ technical replicates were performed for all other assays. Once completed, data groups were analyzed using ANOVA and between pairs using Tukey tests. Statistical significance was indicated by $p < 0.05$.

4.3 Results

4.3.1. Macrophage Cytokine Secretion is Impacted by Substrate Stiffness and Glycemic Condition when Stimulated with LPS

To determine if there is a synergistic relationship between mechanosensitivity and glucose metabolism on macrophage function, we first investigated proinflammatory cytokine secretion. Seeding RAW264.7 macrophages, cultured under normoglycemic (100 mg/dL glucose) and hyperglycemic (450 mg/dL glucose) conditions, onto fibronectin-coated polyacrylamide gels of 2, 15, and 274 kPa, we examined cytokine secretion of TNF-α, IL-10, and IL-6 when LPS stimulated and unstimulated over 3 days.

Mechanosensitivity trends in TNF-α production changed based on glucose concentration and stimulation conditions. Under LPS stimulation, TNF-α production was inversely proportionate with stiffness, where increased stiffness significantly reduced production of TNF-α by the macrophages when under hyperglycemic conditions (450 mg/dL) after 3 days of stimulation (**Figure 4.3A**). Interestingly, this inverse proportionality was not present in the normoglycemic condition (100 mg/dL) when LPS stimulated. In fact, this linear trend was only demonstrated again in unstimulated 100 mg/dL conditions (**Figure 4.3B**). When TNF-α production was compared based on the glycemic condition under the same stiffness, LPS-stimulated macrophages on 2 kPa substrates held the most significant variance from normoglycemic to hyperglycemic condition at day 3 (**Figure 4.3C**). As substrate stiffness increased, the variance between TNF-α production of 450 mg/dL samples and 100 mg/dL samples became comparable. This phenomenon was only seen when cells were stimulated, with TNF-α production of unstimulated cells with comparable secretion between 450 mg/dL and 100 mg/dL across all stiffnesses (**Figure 4.4A**).

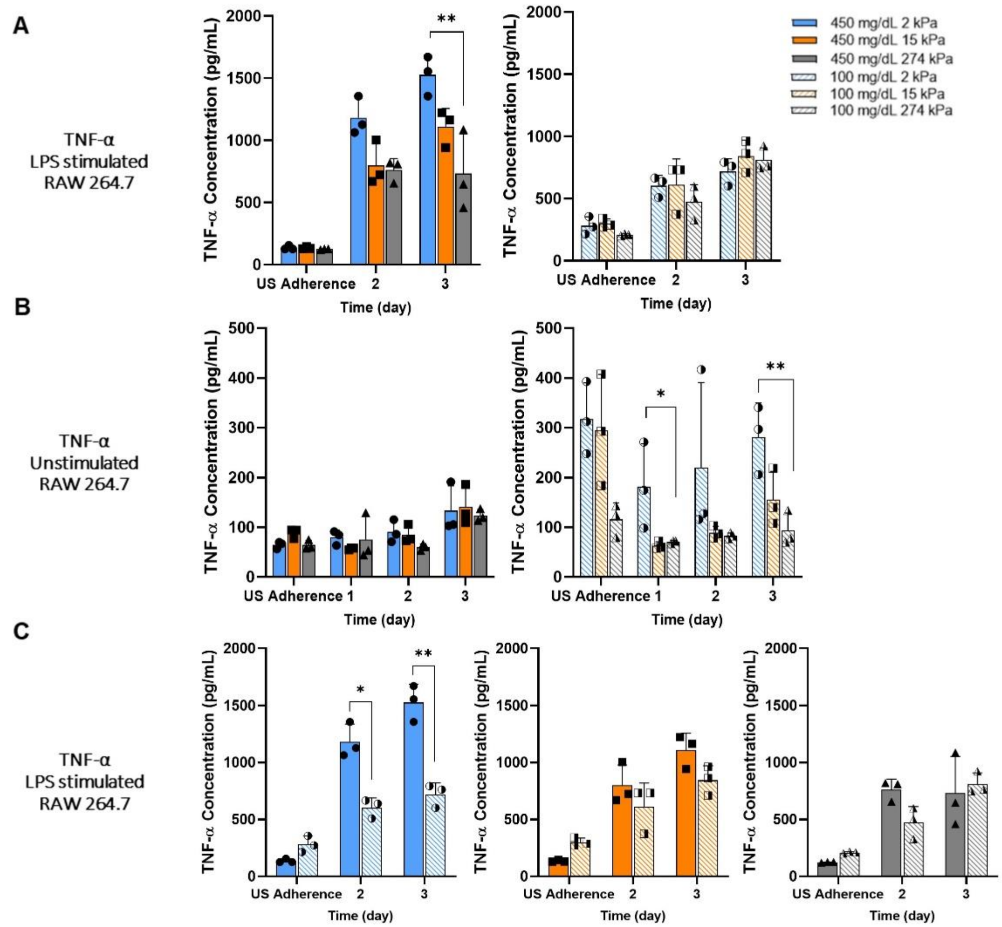

Figure 4.3: TNF-α production by macrophages were inversely proportionate to increased stiffness where mechanosensitive. A) TNF-α production by LPS stimulated RAW264.7 macrophages cultured on 2, 15, and 274 kPa PA gels under hyperglycemic (450 mg/dL) and normoglycemic (100 mg/dL) conditions. Under LPS stimulation, mechanosensitivity trends were present in hyperglycemic conditions only, while expression was comparable in normoglycemic conditions across all stiffnesses. **B)** TNF-α production by unstimulated RAW264.7 macrophages. When unstimulated, RAW264.7 macrophages experienced mechanosensitivity trends under normoglycemic conditions only. **C)** Comparison between 450 mg/dL and 100 mg/dL LPS stimulated samples cultured on the same stiffness. Variance between TNF-α production under 450 mg/dL and 100 mg/dL conditions increased under softer stiffness. n = 3

biological replicates were conducted for all samples. Statistical analysis was conducted using ANOVA and Tukey tests on post-transfer data. The overnight unstimulated adherence samples (US Adherence) were not included in analysis. Statistical significance was indicated by $p < 0.05$. *$p < 0.05$ and **$p < 0.005$.

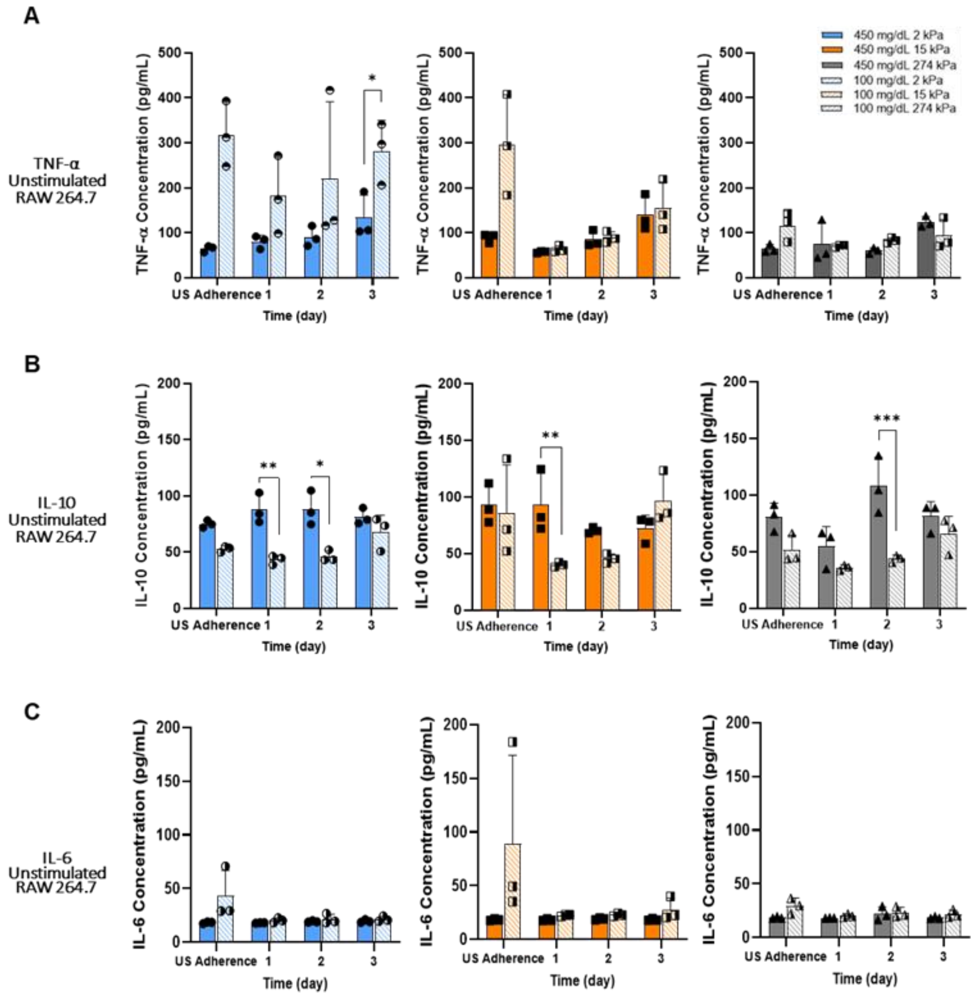

Figure 4.4: No noticeable glycemic and stiffness trends in TNF-α, IL-10, and IL-6 cytokine secretion by unstimulated macrophages. Glucose comparison of A) TNF-α, B) IL-10, and C) IL-6 cytokine production by unstimulated RAW264.7 macrophages cultured on either 2, 15, or 274 kPa PA gels under hyperglycemic (450 mg/dL) and normoglycemic (100 mg/dL) conditions. n = 3 biological replicates were conducted for all samples. Statistical analysis was conducted using ANOVA and Tukey tests. The overnight unstimulated adherence samples (US Adherence) were not included in analysis. Statistical significance was indicated by $p < 0.05$. *$p < 0.05$; **$p < 0.005$.

IL-10 displayed no mechanosensitivity trends under hyperglycemic or normoglycemic conditions. IL-10 production was also comparable across all stiffnesses for stimulated (**Figure 4.5A**) and unstimulated samples (**Figure 4.6A**). However, when evaluated by glycemic condition on the same stiffness, similar to TNF-α, 2 kPa samples under LPS stimulation held a significantly ($p < 0.0005$) higher upregulation than 15 kPa and 274 kPa (**Figure 4.5C**). While there is no distinctive trend in IL-10 production through comparing stiffness under the same glycemic condition, hyperglycemic conditions drastically increased IL-10 production by LPS-stimulated macrophages, but not in unstimulated macrophages (**Figure 4.4B and Figure 4.6A**).

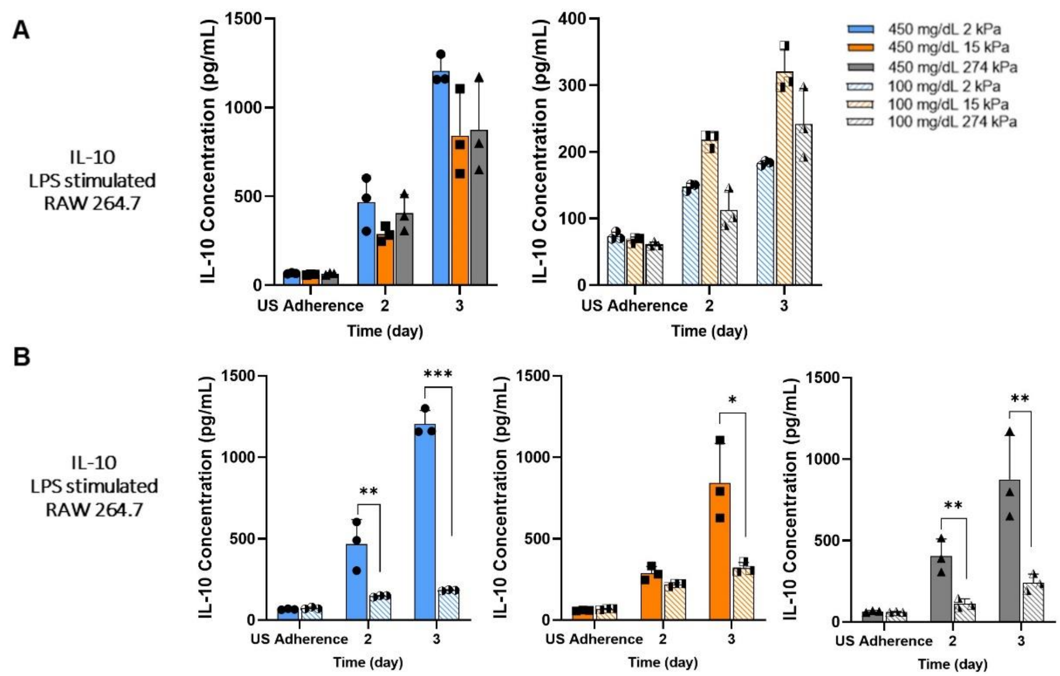

Figure 4.5: Hyperglycemia upregulated IL-10 secretion by proinflammatory macrophages most significantly on 2 kPa PA gels. A) IL-10 production by LPS stimulated RAW264.7 macrophages cultured on 2, 15, and 274 kPa PA gels under hyperglycemic (450 mg/dL) and normoglycemic (100

mg/dL) conditions. No significant mechanosensitivity trends present for IL-10 under either glucose conditions while LPS stimulated. **B)** Comparison between glycemic condition cultured on the same stiffness while LPS stimulated. Variance between expression held a biphasic trend from 2 kPa to 274 kPa PA gels but most significant on 2 kPa. n = 3 biological replicates were conducted for all samples. Statistical analysis conducted using ANOVA and Tukey tests on post transfer data. The overnight unstimulated adherence samples (US Adherence) were not included in analysis. Statistical significance was indicated by $p < 0.05$. *$p < 0.05$; **$p < 0.005$; ***$p < 0.0005$.

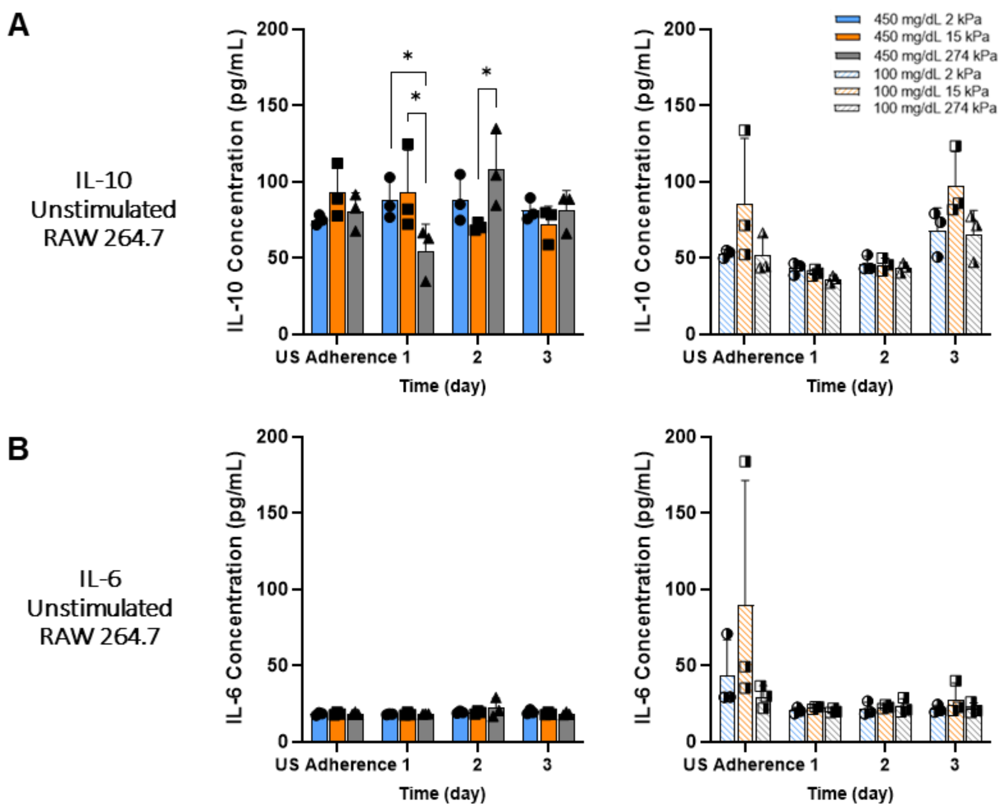

Figure 4.6: No noticeable mechanosensitivity trends in IL-10 and IL-6 cytokine secretion by unstimulated macrophages. Mechanosensitivity comparison of **A)** IL-10 and **B)** IL-6 cytokine secretion by unstimulated RAW264.7 macrophages cultured on 2, 15, and 274 kPa polyacrylamide gels under 450 mg/dL and 100 mg/dL glucose conditions. n = 3 biological replicates were conducted for all samples. Statistical analysis was conducted using ANOVA and Tukey tests. The overnight unstimulated adherence samples (US Adherence) were not included in analysis. Statistical significance was indicated by $p < 0.05$. *$p < 0.05$.

Furthermore, glucose metabolism affected the mechanosensitivity of the macrophages with IL-6 production. Mechanosensitivity differences in IL-6 production were only witnessed once stimulated under 450 mg/dL (**Figure 4.7A**). A biphasic trend was demonstrated as substrate stiffness increased in 450 mg/dL LPS samples, in which IL-6 secretion was reduced on 15 kPa, while 2 kPa and 274 kPa held comparable secretion levels. Hyperglycemic samples also had drastically higher IL-6 secretion than normoglycemic samples, with a similar biphasic trend as stiffness increased (**Figure 4.7B**). Unstimulated macrophages produced low levels of IL-6 across all stiffness and glycemic conditions (**Figure 4.4C and Figure 4.6B**). A proliferation study was conducted comparing macrophages cultured on 2 and 274 kPa gels under both glycemic conditions to confirm if cell number was the cause of these findings. While there was a slight increase in cell number based on glucose, this was not significant and would not account for our findings (**Figure 4.8**). These results suggest hyperglycemia influences macrophage mechanosensitivity to different substrate stiffnesses through cytokine production.

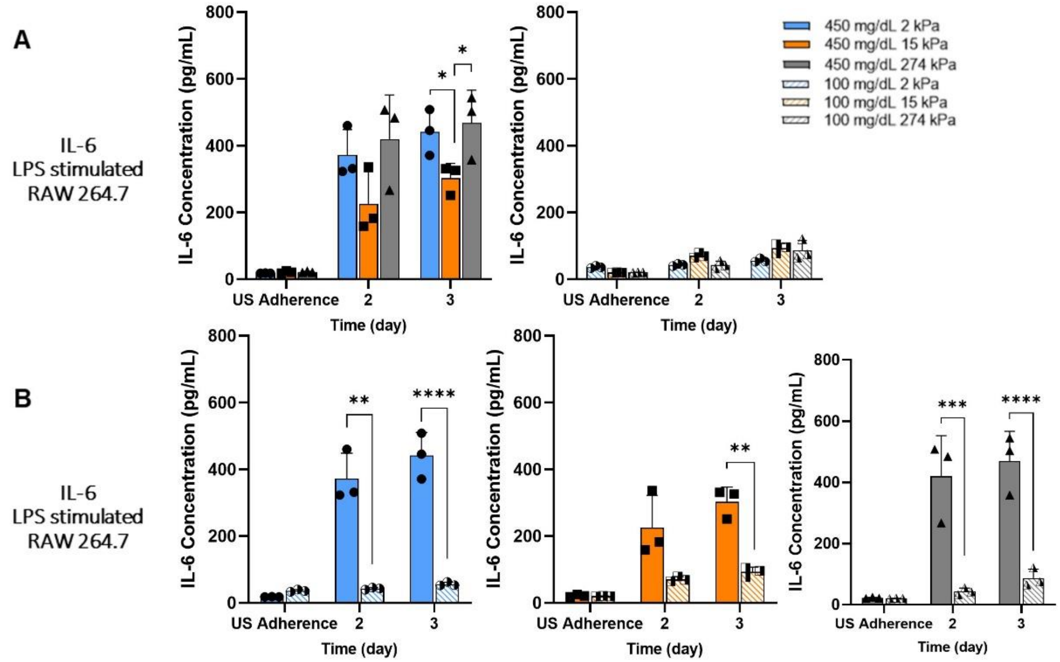

Figure 4.7: Hyperglycemia promoted bi-phasic mechanosensitivity trend in IL-6 secretion by LPS-stimulated macrophages. A) IL-6 secretion by LPS stimulated RAW264.7 macrophages cultured on 2, 15, and 274 kPa PA gels under hyperglycemic (450 mg/dL) and normoglycemic (100 mg/dL) conditions. Under LPS stimulation, IL-6 held a biphasic mechanosensitivity trend in hyperglycemic conditions only while expression was comparable in normoglycemic conditions across all stiffnesses. **B)** Comparison between 450 mg/dL and 100 mg/dL samples cultured on the same stiffness. Biphasic mechanosensitivity trend present in variance between secretion from 2 kPa to 274 kPa PA gels with reduced IL-6 secretion on 15 kPa PA gels. n = 3 biological replicates were conducted for all samples. Statistical analysis conducted using ANOVA and Tukey tests on post transfer data. The overnight unstimulated adherence samples (US Adherence) were not included in analysis. Statistical significance was indicated by $p < 0.05$. *$p < 0.05$; **$p < 0.005$; ***$p < 0.0005$; ****$p < 0.0001$.

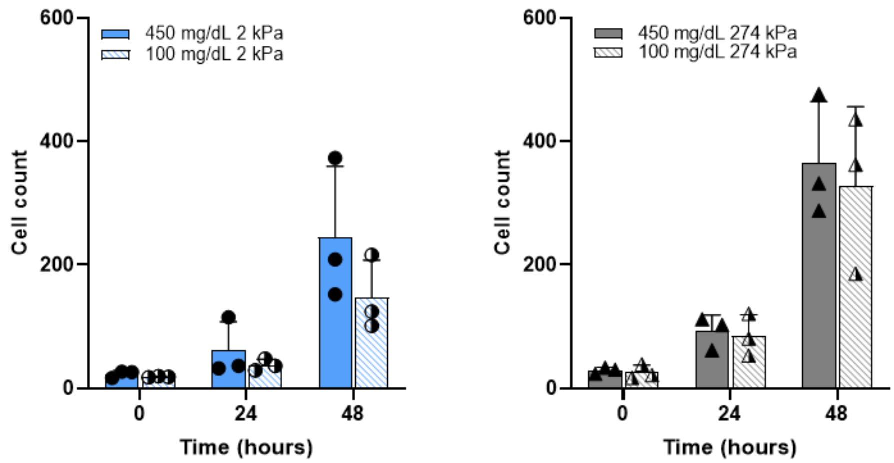

Figure 4.8: No significant differences between glycemic conditions on the proliferation of RAW264.7 macrophages. A comparison of the average cell count under hyperglycemic and normoglycemic conditions on 2 and 274 kPa gels. n = 3 biological replicates conducted for each sample.

4.3.2. Macrophage Phenotype Changes with Response to Substrate Stiffness and Glycemic Condition

To further investigate the effect of glycemic condition and substrate stiffness on macrophage function, we assess how macrophages polarized to their proinflammatory, M1 phenotype when stimulated using the CD80 surface marker. LPS stimulation promoted enhanced M1 polarization under both glycemic conditions as expected (**Supplementary Figure 4.9**). 450 mg/dL samples demonstrated comparable $CD80^+$ macrophages when stimulated across all stiffnesses (**Figure 4.10A**). LPS-stimulated 100 mg/dL macrophages, however, held a significant decline was seen in $CD80^+$ cells from 2 kPa to 274 kPa (**Figure 4.10B**). With these results, it can be suggested that glucose can alter the polarization of macrophages in response to substrate stiffness and LPS stimulation.

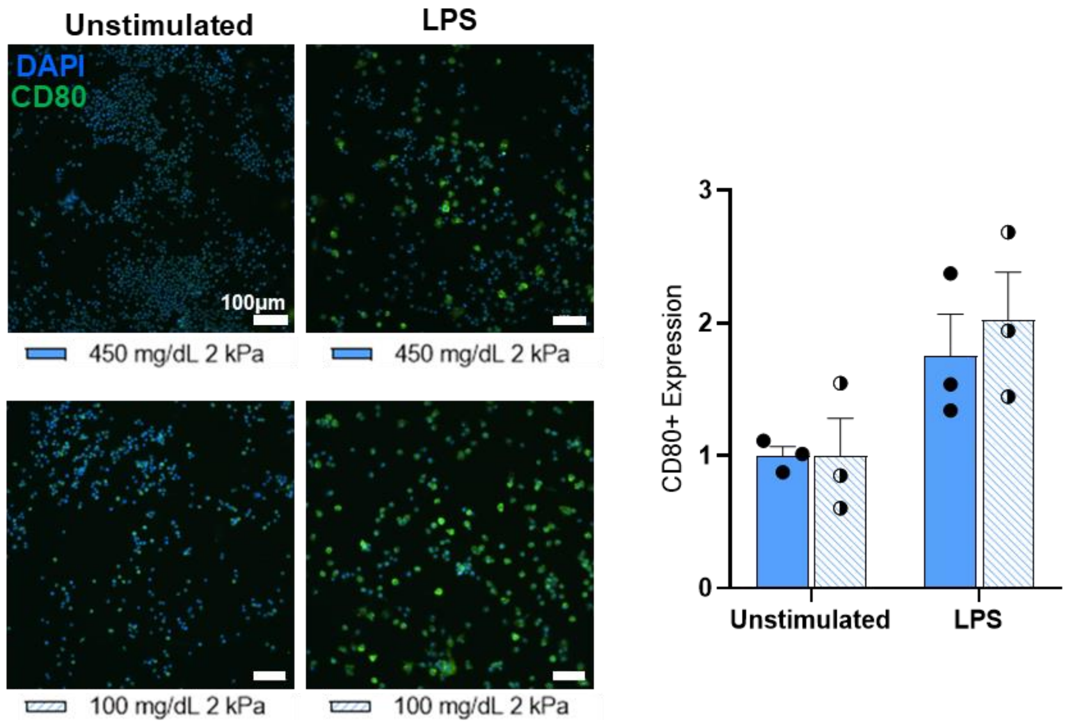

Figure 4.9: LPS upregulated CD80 expression. A verification of macrophage polarization comparing unstimulated RAW264.7 macrophages cultured on 2 kPa PA gels under normoglycemic (100 mg/dL) and hyperglycemic (450 mg/dL) conditions to LPS stimulated RAW264.7. Samples were fixed on day 3. n = 3 biological replicates and n = 5 technical replicates were conducted for all samples. Data normalized to unstimulated samples of their respective glucose condition.

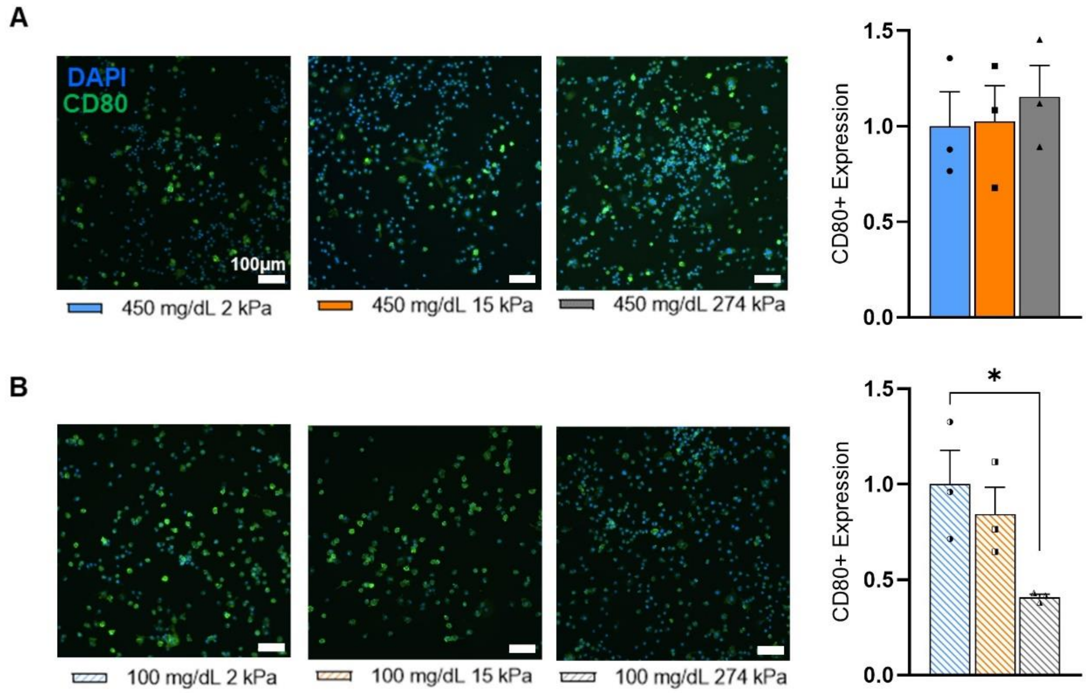

Figure 4.10: Glycemic condition altered phenotypic response to substrate stiffness by proinflammatory macrophages. A) Quantitative analysis of RAW264.7 macrophage polarization to M1 phenotype after LPS stimulation under hyperglycemic (450 mg/dL) conditions on 2, 15, and 274 kPa PA gels through CD80 surface marker. **B)** Quantification of M1 polarization under normoglycemic conditions. Average CD80+ expression decreased as stiffness increased when conditioned to normoglycemic (100 mg/dL) levels. n = 3 biological replicates were conducted for all samples. n = 5 technical replicates conducted for each biological replicate. FITC: CD80. Data normalized to 2 kPa samples for their respective glucose condition. Statistical analysis was conducted using ANOVA and Tukey tests, where $p < 0.05$ indicated statistical significance. *$p < 0.05$. Scale bar = 100µm

4.3.3. Hyperglycemic Conditions and Substrate Stiffness Altered Cytokine Gene Expression in the TLR4/LPS Signaling Pathway of LPS-Stimulated Macrophages

To continue our investigation of the effect of glycemic condition and substrate stiffness on proinflammatory markers, we examined the TLR4 signaling pathway (**Figure 4.1**). TLR4 held no changes in gene or protein expression based on glucose or stiffness (**Figure 4.11A**). Examining downstream, only IL-6 held similar trends in relative gene expression to protein secretion. No stiffness-influenced trends were demonstrated in TNF-α (**Figure 4.11B**). IL-6 held a significant upregulation in gene expression dependent on glycemic condition, with 450 mg/dL samples displaying significantly higher relative gene expression than 100 mg/dL, as seen in protein secretion data (**Figure 4.11C**). Mechanosensitivity trends were also similar to protein secretion, though not statistically significant. Glycemic condition and substrate stiffness did alter IL-10 gene expression (**Figure 4.11D**). Glucose affected IL-10 gene expression more than substrate stiffness, with significant upregulation in IL-10 expression between 100 mg/dL and 450 mg/dL on 15 kPa substrates, similar to protein secretion. These results suggest glycemic condition and substrate stiffness alter how macrophages process LPS, especially in IL-10 and IL-6 expression.

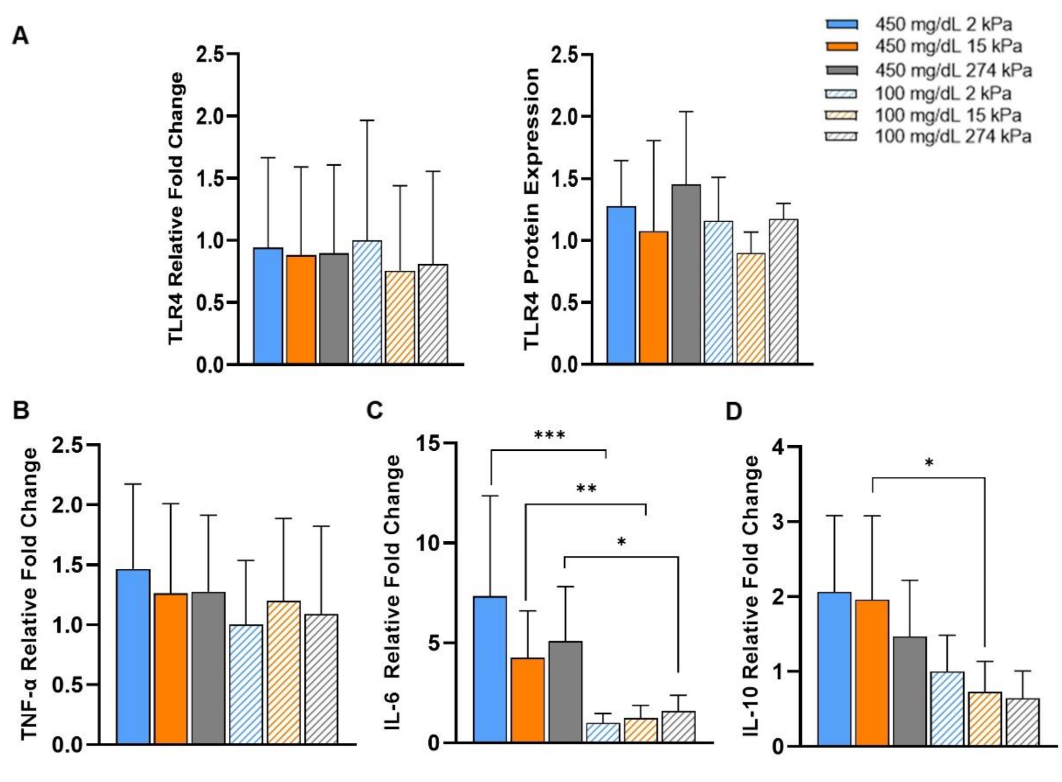

Figure 4.11: Hyperglycemia upregulated gene expression and mechanosensitivity downstream in TLR4/LPS signaling pathway of proinflammatory macrophages. Comparison of gene and protein expression of **A)** TLR4. Comparison of gene expression of **B)** TNF-α, **C)** IL-6, and **D)** IL-10 in LPS stimulated RAW264.7 macrophages cultured on 2, 15, and 274 kPa PA gels under hyperglycemic (450 mg/dL) and normoglycemic (100 mg/dL) conditions. n = 3 biological replicates were conducted for all samples. Statistical analysis was conducted using ANOVA and Tukey tests, where $p < 0.05$ indicated statistical significance. *$p < 0.05$; **$p < 0.005$; ***$p < 0.0005$.

4.3.4. Lactate Secretion Rates by LPS Stimulated Macrophages are Proportionate with Substrate Stiffness Increases in Hyperglycemic Conditions Only

Key aspects of the glycolysis pathway were investigated to determine the effect of substrate stiffness on the glucose metabolism under normoglycemic and hyperglycemic conditions. GLUT1 held no statistically significant changes in relative mean expression by glycemic condition or stiffness (**Figure 4.12A**). However, glucose uptake rates were significantly increased across all stiffnesses of 450 mg/dL compared to 100 mg/dL, in both LPS stimulated and unstimulated (**Figure 4.12B**). Moving downstream, GAPDH held no trends in gene expression based on glucose and stiffness (**Figure 4.12C**). Finally, lactate secretion increased with stiffness and glucose only when stimulated (**Figure 4.12D**). Under hyperglycemic conditions, lactate secretion rates trended upward with rising stiffness and significantly increased compared to normoglycemic samples. These results indicate that mechanosensitivity in glycolysis is occurring downstream in the signaling pathway but only in hyperglycemic proinflammatory macrophages.

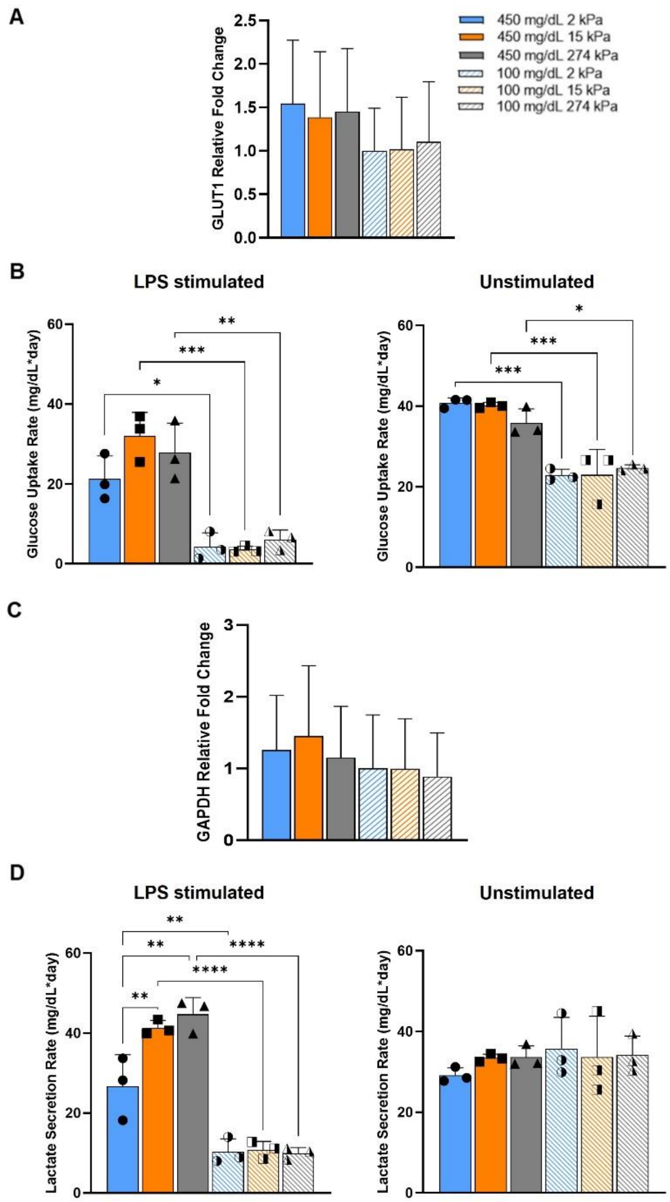

Figure 4.12: Hyperglycemia promoted mechanosensitivity in downstream glycolysis by LPS stimulated macrophages indicated by lactate secretion. Comparison of **A)** GLUT1 and **C)** GAPDH gene expression by LPS stimulated RAW264.7 macrophages after 4 hours of stimulation. **B)** Glucose uptake rate comparisons and **D)** lactate secretion rate comparisons of LPS stimulated and unstimulated (US) RAW264.7 macrophages cultured on 2, 15, and 274 kPa PA gels under hyperglycemic (450 mg/dL) and normoglycemic (100 mg/dL) conditions. Mechanosensitivity trends on demonstrated in lactate secretion. Lactate secretion by LPS stimulated macrophages was upregulated as stiffness increased. n = 3 biological replicates were conducted for all samples. Statistical analysis was conducted using ANOVA and Tukey tests, where $p < 0.05$ indicated statistical significance. **$p < 0.005$; ***$p < 0.0005$; ****$p < 0.0001$.

4.4. Discussion

In this chapter, we sought to determine the effects of glucose dysregulation on the mechanosensitivity seen in proinflammatory macrophage function. Using a 2D polyacrylamide model of 3-order magnitude stiffness to mimic 1 – 100 kPa EIT stiffness range, our results indicate that there is a synergistic effect between glycemic condition and substrate stiffness on proinflammatory macrophage function: hyperglycemic conditions enhance mechanosensitivity in proinflammatory macrophages. To the best of our knowledge, this study represents the first of its kind, establishing the relationship between glycemic condition and mechanosensitivity in macrophage function. As such, our comparisons are primarily limited to studies that have separately investigated the effects of glucose metabolism and substrate stiffness on macrophage function.

Though RAW264.7 cells were used in our study, hyperglycemic conditions triggered distinctive mechanosensitivity trends by substrate stiffness in cytokine secretion under LPS stimulation as seen in literature under various murine and human cell lines and murine primary cells. More specifically, TNF-α production was inversely proportionate with increased stiffness in hyperglycemic conditions; this aligns with previous findings by Patel et al.[81] and Escolano et al.[79] Similar to our study, Patel et al. used a smaller range of substrate stiffnesses (0.3-76.8 kPa) to demonstrate a reduction in TNF-α production, with increased stiffness in LPS-stimulated RAW264.7 and U937 macrophages compared to unstimulated macrophages.[81]

However, our study showed mechanosensitivity trends in unstimulated macrophages under normoglycemic conditions for TNF-α production, but not in hyperglycemic conditions similar to Patel et al.[81] Interestingly, the phenomenon only occurred for TNF-α secretion, while IL-10 and IL-6 secretion remained comparable when unstimulated. IL-10 did not show mechanosensitivity trends when compared under the same glycemic conditions for both unstimulated and LPS-stimulated macrophages. However, as glucose concentration changed from normoglycemic to hyperglycemic conditions on the same stiffness, IL-10 production on 2 kPa expressed the most significant increase in secretion when stimulated with reduced significance as stiffness increased. Moreover, hyperglycemia promoted mechanosensitivity in IL-6 secretion in LPS-stimulated macrophages, a trend not observed in normoglycemic conditions. In fact, macrophages did not display any significant secretion differences based on stiffness for any of the examined cytokines in normoglycemic conditions in the presence of LPS. Overall, this suggests that glycemic condition is a driving factor in mechanosensitive response to substrate stiffness for cytokine secretion by proinflammatory macrophages.

We further explored the TLR4/LPS signaling pathway for gene expression of the TNF-α, IL-6, and IL-10 as well as TLR4. The mean relative gene expression of the corresponding cytokines that were assessed mimicked mechanosensitivity and glucose trends highlighted in cytokine secretion. Our hyperglycemic TNF-α and IL-10 gene expression findings align with previous worked conducted by Chuang et al.[186] Interestingly, IL-6 gene expression was most distinctive by glycemic condition with a significant upregulation in expression in hyperglycemic conditions compared to normoglycemic conditions - further highlighting the synergy between glucose in mechanosensitivity and proinflammatory macrophage function. Contrary to Previtera et al.'s[187] findings, which indicated TLR4 upregulation in response to increased stiffness, our results did not mirror this observation. This may be attributed to differences in cell type, as their study utilized primary murine bone marrow macrophages. Nevertheless, our findings suggest that mechanosensitivity occurs downstream in the TLR4/LPS signaling pathway, and glycemic condition significantly affects this phenomenon.

Macrophage phenotype has been tied to cytokine secretion, with M1 macrophages secreting upregulated levels of TNF-α, IL-6, and IL-12, while M2 macrophages secrete more IL-4 and IL-10.[71] Okamato et al. found that stiff gels attenuated proinflammatory response by macrophages after stimulation.[188] Chen et. al. further illustrated this phenomena, displayed downregulated CD86, another M1 marker, expression as stiffness increased corresponding with an upregulated CD206, a M2 marker, expression in bone-marrow derived macrophages.[82] While we did observe this effect through quantifying immunofluorescence imaging, a distinctive difference emerged. The polarization of M1 macrophages was inversely proportionate to increased stiffness in normoglycemic conditions. Unexpectedly, no mechanosensitivity trends observed in hyperglycemic conditions, contradicting the expected outcome, where distinct mechanosensitivity trends in the hyperglycemic condition and insignificant stiffness effects in normoglycemic conditions would have matched both our cytokine results. This observation may be specific to the surface marker CD80, therefore other proinflammatory and anti-inflammatory surface markers should be evaluated to determine mechanosensitivity trends by substrate stiffness on macrophage phenotype. Regardless, these results provide valuable insights into the influence of glycemic condition on macrophage response to substrate stiffness.

Glucose is a critical mediator to immune function, reviewed in detail by O'Neill et al.[10] Further to this point, Gonzalez et al. displayed that hyperglycemic conditions induced proinflammatory cytokine production in primary human monocytes, upregulating IL-6 and TNF-α.[12] Freemerman et al. demonstrated a similar conclusion by overexpressing GLUT1 in RAW264.7 macrophages to increase glucose uptake. Due to this, it was important to determine if components of the glycolysis pathway are mechanosensitive. It was expected that hyperglycemic conditions caused an increase in GLUT1 expression. While our findings indicated that GLUT1 expression was influenced more by glycemic condition than substrate stiffness, the difference was not statistically significant. Similar results were observed for glucose uptake and GAPDH gene expression. Interestingly, lactate secretion in hyperglycemic LPS stimulated macrophages increased proportionately to stiffness opposite of TNF-α data under the same parameters. This demonstrates the role of lactate as an inhibitor of TNF-α secretion, elucidated by Ratter et al.[182] However, this trend was only displayed in hyperglycemic LPS-stimulated macrophages. These findings highlight mechanosensitivity in downstream glycolysis genes in stimulated macrophages that should be further studied.

While this study used a well-studied and characterized cell population and gel model, it is fair to note that this study is limited in the following ways. This study was conducted *in vitro* under static glycemic conditions which does not fully represent the fluctuation in glycemic conditions experienced by patients with diabetes. Furthermore, while this work could be compared to mechanobiology and glucose metabolism studies using various murine and human macrophage lines and primary bone marrow-derived macrophages, the phenomenon of periodically changing external glucose condition on stiffness-influenced function has not been investigated and could provide more insight to better mimic glycemic dysregulation for diabetics.

4.5. Conclusion

In this chapter, we successfully demonstrated that glycemic condition can influence mechanosensitivity to substrate stiffness in macrophage function. This work suggests hyperglycemic conditions enhance mechanosensitivity in proinflammatory macrophage function, specifically in downstream proinflammatory gene expression, cytokine secretion and lactate secretion. Additional studies can further elucidate this phenomenon to encompass the full range of macrophage functions.

Chapter 5: 3D Mechanosensitivity Model for Glycemic Condition - Stiffness-Mediated Mechanosensitivity Exploration in Pro-Inflammatory Macrophages

5.1. Introduction

Three-dimensional (3D) biomaterial models offer several advantages in mimicking the *in vivo* environment compared to traditional 2D cell culture systems. 3D models provide a more physiologically relevant context for cellular behavior for tissue-engineered applications.[189] One key advantage of 3D biomaterial models is the ability to replicate better the complex cell-extracellular matrix (ECM) interactions demonstrated *in vivo.* Various mechanical characteristics of the ECM are included in 3D biomaterial models to assess cellular function, including porosity, permeability, and substrate stiffness.[190]

3D mechanobiology models have become an important tool for analyzing and understanding the effect of mechanical forces on biological systems. Regarding the effect of substrate stiffness, while 3D models are moving into prominence, it should be noted that the vast majority of current mechanobiological literature has been attained using 2D elastic models. 3D models can provide more clarity on findings demonstrated in 2D studies. For example, Guo et al. determined that stiffer matrices caused cellular volume to decrease as cellular area expands as a result of water efflux in various cell populations.[191] Further to this, Bao et al. found this reduction in volume affects yes-associated protein (YAP) translocation to the nucleus of human mesenchymal stem cells.[192] YAP plays a crucial role in mechanotransduction, regulating multiple signal pathways leading to cell proliferation, differentiation, gene expression, and inflammation.[193–195]

During foreign body response (FBR) to implant tissue-engineered constructs, monocyte-derived macrophages migrate through the ECM and adhere to the surface of the biomaterial. While this interaction occurs, macrophages still engage with the mechanical properties of the ECM. This material-cell-ECM interplay should be investigated as we seek to understand macrophage functionality by mimicking FBR *in vitro*. The need to better understand substrate stiffness-mediated mechanotransduction and further the relationship that external glucose conditions have on this phenomenon in 3D for macrophages is crucial to confirming findings from 2D studies in earlier work.[196]

Gelatin methacrylate (GelMA) is a widely used biomaterial for 3D biomaterial models due to its close relationship with the ECM. GelMA is synthesized by incorporating methacrylate groups onto the amine-containing side groups of gelatin. The resulting methacrylated gelatin is photopolymerized into a biocompatible hydrogel for various tissue-engineered applications. GelMA can be used as an ECM phantom because it originates from denatured collagen, the most abundant protein in the body. Casting GelMA to well-established 2D polyacrylamide models would be advantageous to mimic macrophage function to implanted materials *in vitro*. This type of 3D model maintains the ability to vary the stiffness of the polyacrylamide to assess substrate stiffness-mediated mechanosensitivity while establishing the material-cell-ECM relationship seen during FBR.[197]

In this chapter, we establish a 3D mechanosensitivity biomaterial model to assess the role of glycemic condition on substrate stiffness-mediated mechanosensitivity in pro-inflammatory macrophages. This model 3D aims to mimic the acute inflammation phase of the foreign response to implanted biomaterial by macrophages. The model adds a GelMA (10% w/v) top layer to represent the ECM to polyacrylamide gels of varying substrate stiffness to represent an implanted biomaterial such as capsules for islet encapsulation therapy. The model is characterized for thickness, stiffness, and cell viability before functional experiments were completed to investigate the immuno-metabolic relationship with substrate stiffness-mediated mechanosensitivity in pro-inflammatory macrophages.

5.2. Methods

5.2.1. Polyacrylamide Synthesis and Characterization

Polyacrylamide gels were synthesized according to previously established methods.[8,169] Concentrations for each stiffness were as follows: 2 kPa – 3% acryl and 0.1% bis, 15 kPa – 8% acryl and 0.2% bis, 274 kPa – 15% acryl and 1.2% bis (Bio-Rad laboratories, Hercules, CA, USA).[196] Ammonium persulfate (APS) (Thermo Fisher Scientific, Waltham, MA, USA) and N, N, N', N' – tetramethylethylenediamine (TEMED) (Bio-Rad Laboratories, Hercules, CA, USA) were added to the acrylamide mixture. Gel substrates about 80 µm thick were synthesized by dispensing 30 µL of polyacrylamide on amine-activated glass coverslips (22 x 22 mm, Fisher Scientific, Pittsburg, PA, USA) and sandwiching between a sterilized glass slide. Gels were cured at room temperature for 30 mins and then pried from the glass slide using a sterile razor blade. Gels were coated with 0.1 mg/mL human fibronectin (Sigma-Aldrich, St. Louis, MO, USA) after activating with 0.5 mg/mL sulfo-SANPAH (Sigma-Aldrich, St. Louis, MO, USA) according to previously published methodology.[169] Gels were sterilized by exposure to ultraviolet light for 15 mins and rinsed with sterile phosphate-buffered saline (1X PBS) (Thermo Fisher Scientific, Waltham, MA, USA) before cells were seeded for experimentation.

5.2.2. Gelatin Methacrylate (GelMA) Synthesis

12g of Type A gelatin power (Sigma-Aldrich, St. Louis, MO, USA) was dissolved into 120 mL of 1X PBS in a beaker covered with aluminum foil for 30 mins at 50°C at 400 rpm using hot plate and magnetic stirrer. With stirring speed increased to 1200 rpm, 6.96 mL methacrylate anhydride (Sigma-Aldrich, St. Louis, MO, USA) was loaded to a 10 mL plastic syringe and added into vigorously stirring beaker dropwise, using springe needle and springe pump at rate of 1500 µL/min. The reaction was vigorously stirred for 1 hour at 50°C. Then, the solution was pipetted in 50 mL centrifuge tubes and was centrifuged at 1000g for 5 mins. The supernatant was collected in a separate beaker and diluted 1:1 with 1X PBS and stirred at 400 rpm at 50°C for 5 mins to ensure the solution is homogenous. This solution was placed into dialysis bags (Ward's Science, Rochester, NY, USA) dialyzed with Milli-Q water for a week, with daily refresh of water. After a week, GelMA solution is neutralized to pH of 7.3-7.5 using 1M and 0.1M NaOH. The GelMA solution was then transferred into 50mL falcon tubes and frozen at -80°C. It was placed in the lyophilized for at least 72 hours. The lyophilized GelMA is stored at room temperature util the further use.

To prepare the photocrosslinkable GelMA solution, the lyophilized GelMA was dissolved with 1X PBS (10 % w/v) in 50mL falcon tube, at 50°C in the oven, while getting vortex every 10 mins to ensure its dissolution. Tube with GelMA solution was completely covered with aluminum foil, then Lithium phenyl-2,4,6-trimethylbenzoylphosphinate (LAP) solution (Sigma-Aldrich, St. Louis, MO, USA) was added to GelMA to achieve final 0.1 % w/v while the solution is still warm. Gently vortex to ensure homogenous solution. The GelMA was then pipetted onto polyacrylamide gel (with or without cells) and then crosslinked in a UV chamber for 5 mins. Experimental design for the 3D model is depicted in **Figure 5.1**.

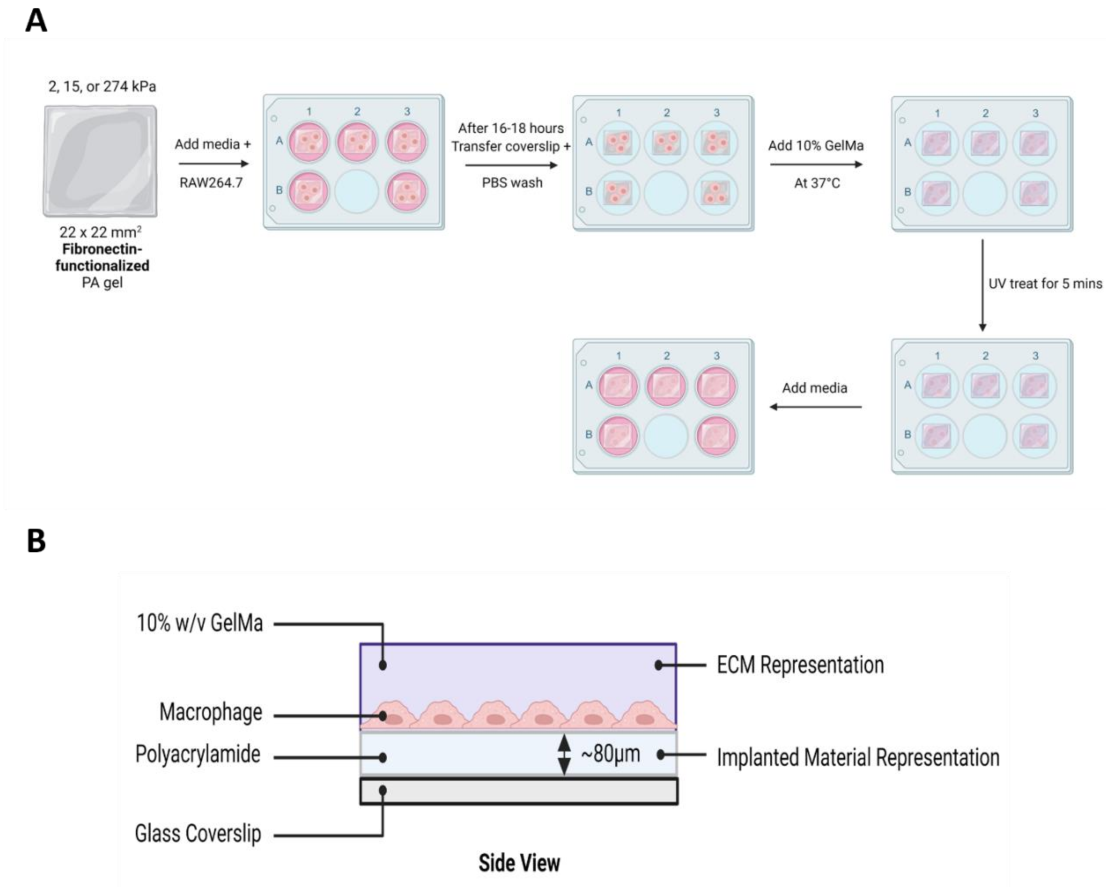

Figure 5.1: Experimental design of 3D mechanosensitivity model. A. Fibronectin-coated polyacrylamide gels are added to 6-well non-treated polystyrene plates. Cells are added with their respective media and left to adhere for 16-18hrs at 37°C, 5% CO_2. Samples are then washed with 1X PBS and transferred to new wells. 10% gelatin methacrylate (GelMA) is prepared with photo-initiator LAP and added to samples. Samples are UV-treated for 5 mins to cure the GelMA layer. Media is then added to begin cellular studies. **B.** Side view of the 3D mechanosensitivity model. Macrophages are sandwiched between both material layers where the polyacrylamide (bottom) layer represents an implanted material while the GelMA (top) layer represents the ECM. As the implanted material representative, the stiffness of the polyacrylamide layer will vary throughout experimentation while the GelMA layer will remain consistent.

5.2.3. GelMA Thickness Characterization

Lyophilized GelMA is dissolved with 1X PBS to a 10% w/v concentration as described previously. Alcian blue (1 mg/mL) is added to the 1X PBS to pigment the gel to a blue hue to distinguish the GelMA on the model. GelMA is casted onto polyacrylamide gels at 200 μL and 300 μL volume and crosslinked for 5 mins in the UV chamber. The 3D mechanosensitivity model was then added to a glass slide and positioned perpendicular to the nosepiece of the microscope to image under 2X magnification. Five images were acquired for each gel and five replicates for each condition. The thickness of the GelMA layer was measured using ImageJ.

5.2.4. GelMA Young's Modulus Characterization

To validate the stiffness of the GelMA (10% w/v), bulk GelMA was cured in a PDMS mold shown. After 5 min UV treatment, bulk cylindrical GelMA columns of a 2:1 height to diameter ratio, as outlined by the ASTM standard for compressive testing of hydrogels, were removed from the mold to undergo bulk compression tests on the Instron.[170,171] Young's modulus was calculated using a stress vs strain curve for each gel.

5.2.5. Cell Culture

RAW264.7 and J774.1 macrophages (ATCC, Manassas, VA, USA) were cultured separately based on cell line and glucose conditions. Macrophages cultured under hyperglycemic conditions were cultured in 450 mg/dL Dulbecco's Modified Eagle's Media (DMEM) (ATCC, Manassas, VA, USA). In contrast, cells in normoglycemic conditions were cultured in 100 mg/dL DMEM (Thermo Fisher Scientific, Waltham, MA, USA). 10% Fetal bovine serum (FBS) was added to all culture media. Cells were seeded onto polyacrylamide gels in a 6-well dish and allowed to adhere overnight at 37°C, 5% CO_2. After the overnight culture, gels with adhered cells were transferred into a new well with fresh media based on the condition to begin each study.

5.2.6. Cell Viability

10^5 RAW264.7 macrophages were added to 15 kPa polyacrylamide gels and left to adhere overnight at 37°C, 5% CO_2 under hyperglycemic conditions. Samples are casted with either 200 µL or 300 µL of GelMA (10% w/v) with 5 mins of UV-treatment and compared to a 5 min UV-treated 2D control. Cells were stained using the LIVE/DEAD kit (Invitrogen; Carlsbad, CA, USA) occurring to the manufacturer's protocol. Briefly, after 5 mins of UV-treatment, a 1X PBS solution with live stain calcein AM (1:2000; FITC) and dead stain ethidium homodimer (1:500; Cy5) for 30 mins at room temperature covered from light. Samples were then rinsed with 1X PBS before imaging. Cell viability was calculated according to **Equation 5.1**. Images were analyzed using ImageJ. Five images were obtained for each biological replicate. Five biological replicates were conducted for each condition.

$$\boldsymbol{Equation\ 5.1}: Cell\ Viability = \frac{Number\ of\ Live\ Cells}{Number\ of\ Live\ Cells + Number\ of\ Dead\ Cells} * 100$$

5.2.7. Cytokine and Nitrite Secretion Quantification

First, 10^5 macrophages (RAW264.7 or J774.1) were seeded onto each fibronectin-coated polyacrylamide gels to adhere overnight at 37°C, 5% CO_2. Gels are transferred to new wells and GelMA (10% w/v) is casted onto cell-covered polyacrylamide gels.

After UV-treatment, 3 mL of hyperglycemic or normoglycemic media, based on the original glycemic condition used for culture, with 0.5 µg/mL salmonella typhosa lipopolysaccharide (LPS) (Sigma-Aldrich, St. Louis, MO, USA) are added to wells. Samples were incubated at 37°C, 5% CO_2, for 3 days. Supernatants were collected from each sample after each day and stored at -80°C until assayed. TNF-α, IL-10, IL-6, and nitrite secretion were quantified using sandwich ELISAs and Griess Assay (TNF-α, IL-6, and IL-10: Peprotech Inc., East Windsor, NJ, USA; Nitrite: Thermo Fisher Scientific, Waltham, MA, USA) with protocols from their respective kits.

5.2.8. Statistical Analysis

Statistical tests were conducted using GraphPad Prism 9 (GraphPad, San Diego, CA). Normality was verified for data groups using Shapiro-Wilks tests with $n = 5$ biological replicates. For imaging, $n = 5$ technical replicates were conducted for each biological replicate. Once completed, data groups were analyzed using ANOVA and between pairs using Tukey tests. Statistical significance was indicated by $p < 0.05$.

5.3. Results

5.3.1. GelMA top layer successfully able to be casted onto polyacrylamide gel to form 3D mechanosensitivity model.

To establish a 3D mechanosensitivity model to better mimic the *in vivo* environment of an implanted material, GelMA (10% w/v) of 200 µL and 300 µL volume was pipetted onto polyacrylamide gel and cured using UV for 5 mins. The model transferred onto a glass slide and positioned perpendicular to the nosepiece of the microscope to confirm the GelMA top layer did not slide off the polyacrylamide gel, introducing shear to the model, and the thickness of the layer could be visualized (**Figure 5.2A**) and measured (**Figure 5.2B**). As expected, there was a significant increase in thickness between 200 µL and 300 µL: 329.60 ± 96.52 µm^2 to 540.90 ± 78.00 µm^2. In addition, the Young's modulus of bulk GelMA (10% w/v) was calculated by measuring the stress and strain of the material through compression tests (**Figure 5.2C**). 10% GelMA cured for 5 mins under UV resulted in a modulus of 34.65 ± 1.86 kPa, similar to calculated values in literature under similar conditions.

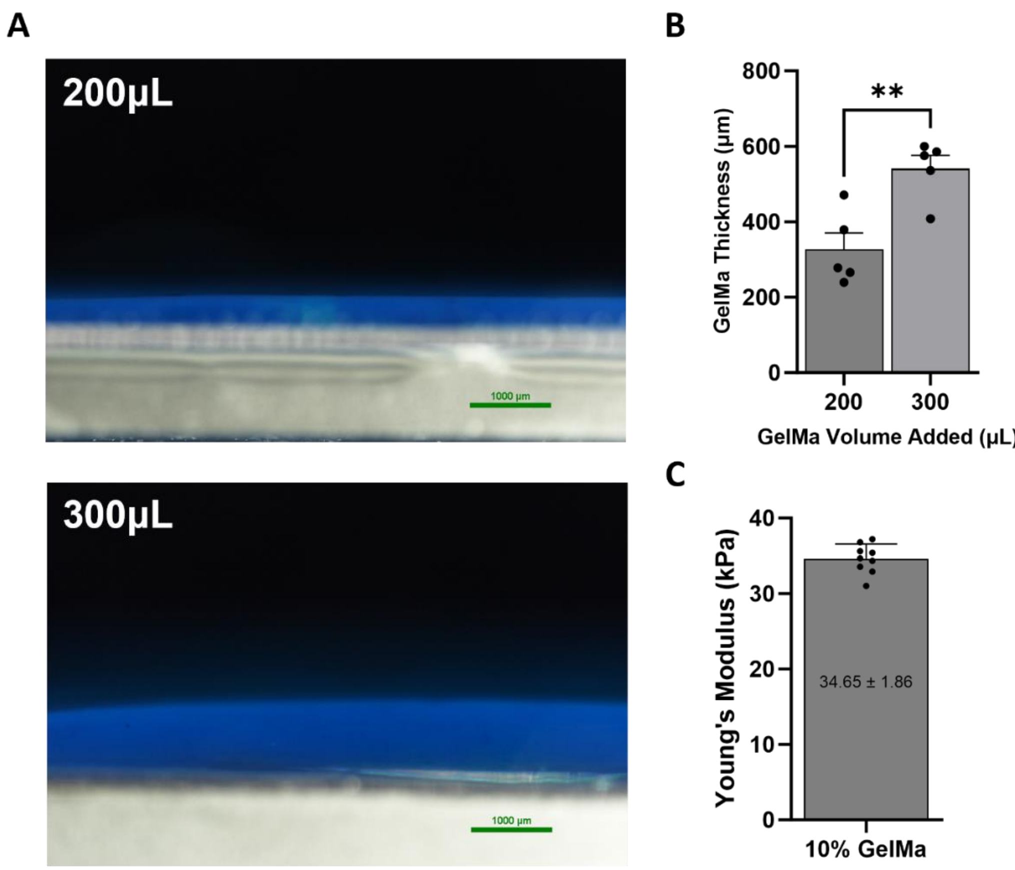

Figure 5.2: Mechanical characterization of the 10% GelMA top layer. A. Images of the thickness of the GelMA layer, represented in blue, cured onto polyacrylamide under brightview at 2X

magnification. **B.** Thickness quantification of GelMA layer. **C.** Stiffness (Young's Modulus) quantification of 10% GelMA. n = 5 experimental replicates with n = 5 technical replicates for images per experimental replicate were conducted for thickness measurements and n = 9 experimental replicates were conducted for compression tests. The thickness of the GelMA top layer was measured using ImageJ. Statistical analysis was conducted using student t test, where $p < 0.05$ indicated statistical significance. Scale bar: 1000 μm

5.3.2. Addition of 10% GelMA top layer maintained a cellular viability of over 70% after casting.

The cellular viability of the 3D mechanosensitivity model was assessed to determine is the cells remained viable after GelMA was casted onto the cell-covered polyacrylamide layer. RAW264.7 macrophages were seeded onto polyacrylamide gels and cultured overnight. GelMA (10% w/v) solution of 200 μL and 300 μL volume were pipetted onto cell-covered polyacrylamide and cured under UV for 5 mins before stained for cell viability and compared to a 2D control (**Figure 5.3**). The 200 μL casting volume resulted in a significant reduction in cellular viability of the macrophages compared to the 2D control. However, the casted GelMA layer of both volumes maintained a viability of above 70% with 200 μL samples maintaining a 72.48 ± 14.58% cellular viability while 300 μL resulted in a 78.91 ± 16.78% viability. Due to the significant reduction in viability in 200 μL samples, 300 μL casting volume will be used moving forward with the model.

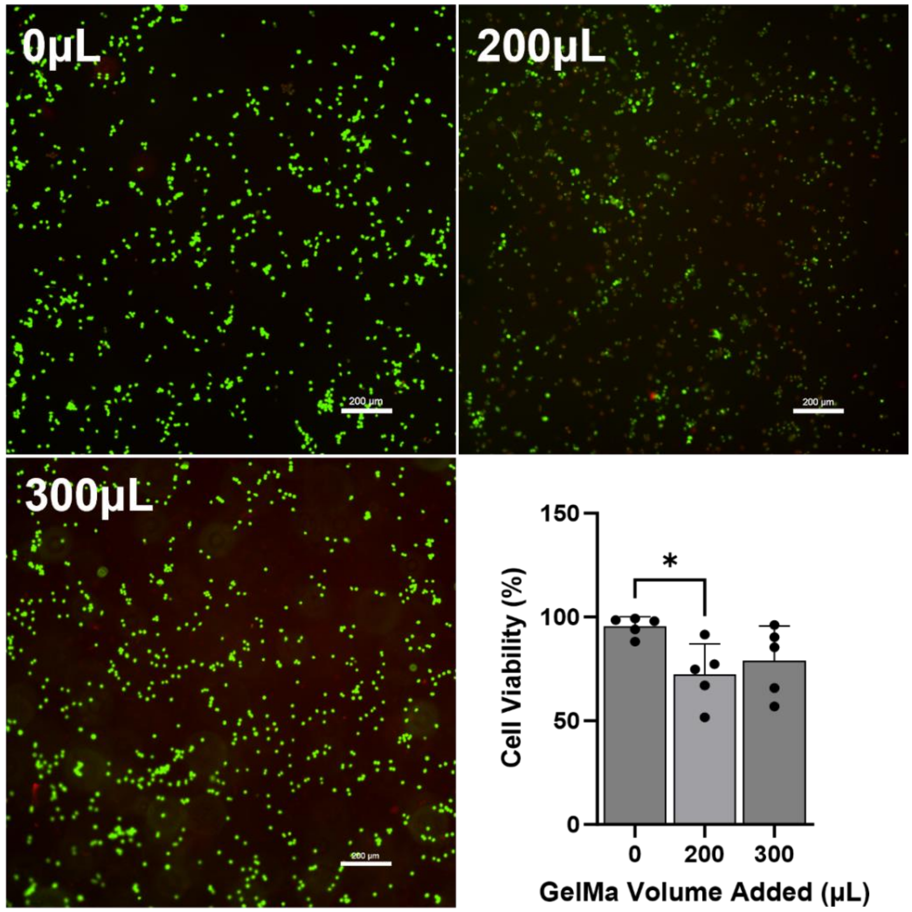

Figure 5.3: >70% cell viability of macrophages in 3D mechanosensitivity model after 10% GelMA casting. Various volumes of 10% GelMA were cast onto cell-laden polyacrylamide gels, and cell viability was quantified using 5 mins of UV treatment. *n* = 5 biological replicates with *n* = 5 technical replicates for images per biological replicate were conducted. Cell viability of samples was quantified using ImageJ. Statistical analysis was conducted using ANOVA and Tukey tests, where $p < 0.05$ indicated statistical significance. *$p < 0.05$. Scale bar: 200 μm

5.3.3. Hyperglycemic conditions promoted enhanced cytokine production and mechanosensitivity to substrate stiffness of macrophages in 3D environment.

To evaluate the addition of this material on the mechanosensitivity of macrophages and the relationship demonstrated between glycemic condition and substrate stiffness-mediated mechanosensitivity in pro-inflammatory functionality under 2D conditions, macrophages were seeded onto polyacrylamide gels of 2, 15, and 274 kPa to adhere overnight before casting GelMA top layer to establish the 3D mechanosensitivity model. After the model is constructed, macrophages are stimulated with LPS for three days before cytokine productions is quantified and assessed across substrate stiffness and glycemic condition. Hyperglycemic conditions promoted both elevated cytokine and nitrite secretion while also enhancing substrate stiffness-mediated mechanosensitivity overall in RAW264.7 macrophages. While TNF-α were averages were higher in hyperglycemic conditions compared to normoglycemic conditions and softer (2 kPa) substrates compared to stiffer (274 kPa), there are no significant differences between TNF-α production across all parameters (**Figure 5.4A**). However, significant stiffness-mediated mechanosensitivity effects were demonstrated in IL-6 (**Figure 5.4B**) and IL-10 production (**Figure 5.4C**) in LPS-stimulated RAW264.7 macrophages at day 3. Hyperglycemic conditions also promoted a drastic increase in IL-6, IL-10, and nitrite production on softer substrates (**Figure 5.4D**).

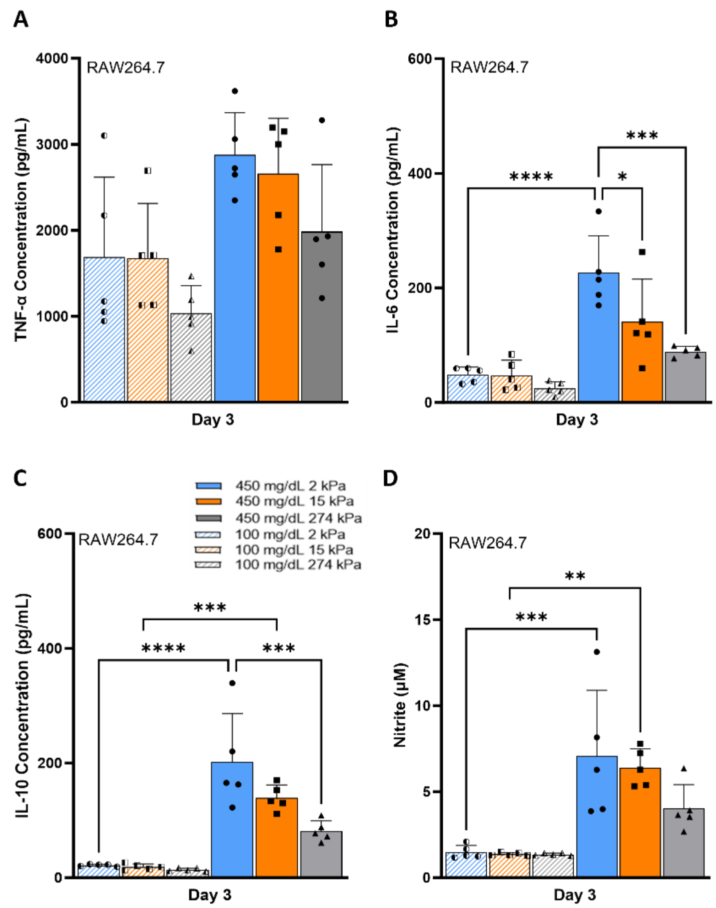

Figure 5.4: Hyperglycemic conditions promoted mechanosensitivity changes as well as increased cytokine and ROS production by LPS-stimulated RAW264.7 macrophages. A. TNF-α, **B.** IL-6, **C.** IL-10, and **D.** nitrite quantification of LPS-stimulated RAW264.7 macrophages after 3 days of culture under hyperglycemic and normoglycemic conditions on either 2, 15, or 274 kPa polyacrylamide gels. n = 5 biological replicates were conducted for all samples. Statistical analysis was conducted using ANOVA and Tukey tests. Statistical significance was indicated by $p < 0.05$. *$p < 0.05$; **$p < 0.005$; ***$p < 0.0005$; and ****$p < 0.0001$.

To confirm the relationship between glycemic condition and substrate stiffness in macrophage functionality, this experiment was replicated using a secondary murine macrophage cell line: J774 cells. Contrasting RAW264.7 macrophages, LPS-stimulated J774 macrophages produced prominent substrate stiffness-mediated mechanosensitivity changes in hyperglycemic conditions with macrophages cultured on 274 kPa substrates producing a significant reduction in TNF-α expression than macrophages exposed to 2 kPa substrates (**Figure 5.5A**). Macrophages cultured on soft (2 kPa) substrates under hyperglycemic conditions also produced drastically higher TNF-α than normoglycemic conditions. IL-6 production resulted in stiffness-driven mechanosensitivity trends in hyperglycemic conditions while also significant increases in production compared to macrophages in normoglycemic conditions on the same substrate stiffness (**Figure 5.5B**). While LPS-stimulated J774 macrophages demonstrated significant changes in IL-10 secretion based on stiffness and glycemic conditions, expression was significantly reduced compared to RAW264.7 macrophages (**Figure 5.5C**). Also, nitrite secretion remained equivalent across all sample parameters (**Figure 5.5D**) and was similar to secretion from LPS-stimulated RAW264.7 macrophages in normoglycemic condition.

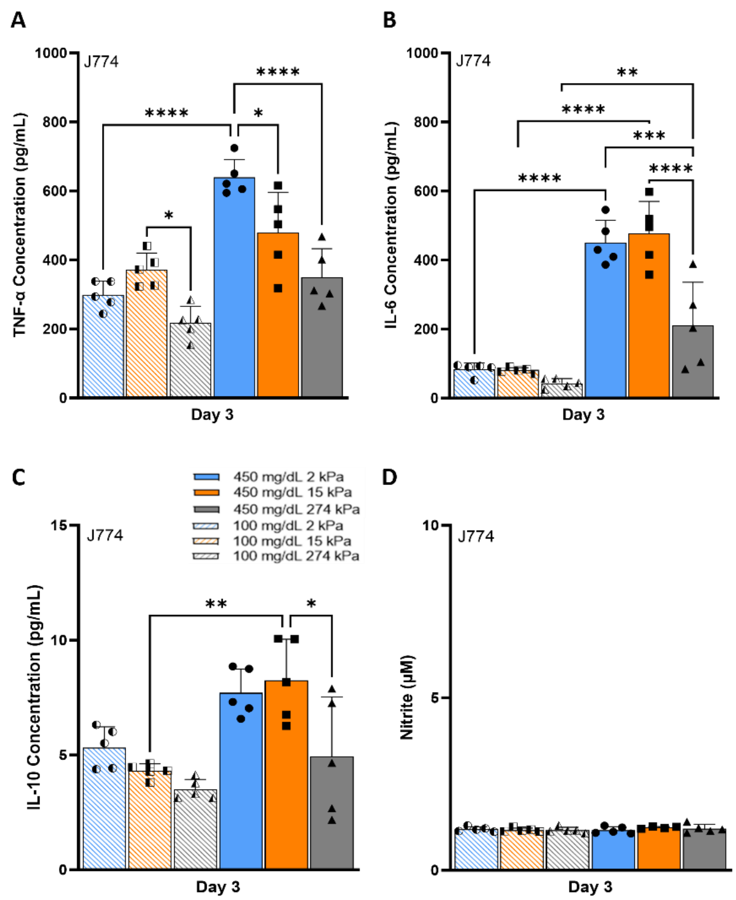

Figure 5.5: Similar to RAW264.7 macrophages, hyperglycemic conditions promoted mechanosensitivity changes as well as increased cytokine and ROS production by LPS-stimulated J774 macrophages. A. TNF-α, **B.** IL-6, **C.** IL-10, and **D.** nitrite quantification of LPS-stimulated J774 macrophages after 3 days of culture under hyperglycemic and normoglycemic conditions on either 2, 15, or 274 kPa polyacrylamide gels. n = 5 biological replicates were conducted for all samples. Statistical analysis was conducted using ANOVA and Tukey tests. Statistical significance was indicated by $p < 0.05$. *$p < 0.05$; **$p < 0.005$; ***$p < 0.0005$; and ****$p < 0.0001$.

5.4. Discussion

Herein, we have established a 3D mechanosensitivity model designed to evaluate the role of substrate stiffness on macrophage functionality and further on the effect of glycemic condition on this mechanosensitivity. This model serves as a biomimetic approach for assessing the acute inflammation stage of foreign body response to tissue-engineered therapies for diabetics, such as encapsulated islet therapy. Polyacrylamide and gelatin methacrylate (GelMA) were used in this mechanobiological study.[8,79,186,187,198] Polyacrylamide is a well-established material in mechanobiology due to the ability to readily change the stiffness of the material without changing the chemical composition of the material, an advantageous characteristic to consistently control one parameter for investigation. GelMA is widely used for tissue-engineered models and scaffold design.[199] This versatile material is mechanically tunable with efficient biocompatibility allow the material to be an effect representative for ECM.[200]

First, the ability to create a stable model with the addition of GelMA onto the 2D polyacrylamide model was confirmed. GelMA (10% w/v) solution of 200 μL and 300 μL volume was coated onto the acellular polyacrylamide while ensuring solution remained on the surface of the polyacrylamide without spillover onto the well. This approach not only confirmed the consistent thickness of the GelMA layer with minimal variability but also ensured ease of transfer without compromising the model's integrity. Samples were added to a UV chamber for 5 mins to cure the GelMA layer. The thickness of the GelMA layer was measured to confirm the success of maintaining the integrity of the model. As expected, there was a significant increase in thickness based on increasing the volume of GelMA casted. The stiffness of the GelMA layer was quantified through compression tests of bulk GelMA. GelMA (10% w/v) cured for UV treated for 5 mins maintained a Young’s modulus of ~34 kPa which is within the range of what has been reported in literature.[201] In regards to physiology, this modulus is within the range of the subcutaneous cavity. [99,100] This is appropriate for our study as a location of interest for encapsulated islet transplantation (EIT) is the subcutaneous space. [33,34]

Next, cellular viability was evaluated to confirm the additional GelMA layer and casting method was not detrimental to the cells. Macrophages were added to the polyacrylamide and left to adhere overnight. GelMA (10% w/v) solution was added to cell-coated gels and cured for 5 mins under UV. From LIVE/DEAD fluorescent analysis, cells within the 3D model maintained a viability of >70%. The 300 μL volume of GelMA resulted in a statistically insignificant change in viability. Due to this, 300 μL volume was used as experimentation proceeded to assess pro-inflammatory macrophage functionality. Moving forward, we will test this model to mimic macrophages engaging with a material-based therapy, such as EIT, for foreign body response within patients experiencing glycemic dysregulation.

Investigating the effect of glycemic condition on the stiffness-mediated mechanosensitivity of pro-inflammatory macrophage functionality using this model validates findings from previous studies in our lab under a 2D polyacrylamide model.[196] In both macrophage populations, RAW264.7 and J774, hyperglycemic conditions promoted cytokine secretion and enhanced substrate stiffness-mediated mechanosensitivity effects compared to normoglycemic conditions. There was also a reduction in production with increased substrate stiffness where mechanosensitive effects applied supporting findings of Patel et al.[81] and Irwin et al.[83] Normoglycemic conditions generally resulted in subtle change in production based on substrate stiffness demonstrated in 2D environments as well.[196] While there were several similarities between RAW264.7 and J774 macrophages, some distinctions emerged. J774 macrophages did not produce much nitrite and was consistent across stiffness and glycemic condition where RAW264.7 cells only demonstrated this in normoglycemic conditions with hyperglycemic conditions resulting in a significant reduction from increased substrate stiffness. Also, J774 macrophages produced significantly less IL-10 than RAW264.7 macrophages though the general trend was the consist. Macrophages produced significantly less IL-10 at higher stiffnesses in hyperglycemic conditions. Overall, this study affirms external glucose levels are a significant factor in substrate stiffness-mediated mechanosensitivity in macrophage function in 3D environments.

It is important to acknowledge some limitations with this model. The synthesis of GelMA can be relatively time-consuming, often spanning up to two weeks. Also, GelMA layer has a finite lifespan and can begin to degrade over time, with complete degradation occurring within 2-4 weeks.[202,203] The Young's modulus capacity is limited with a range of 1-200 kPa, which may restrict its applicability in use-cases requiring larger stiffness.[201,204,205] Furthermore, while biocompatible, GelMA has been shown to reduce metabolic activity in fibroblasts.[206] These factors should be taken into consideration when applying this model for other mechanobiological investigations.

5.5. Conclusion

In this study, we have successfully constructed a 3D mechanosensitivity model to further evaluate the effect of substrate stiffness and on macrophage function. This multi-material sandwiched approach allowed the ability to assess multiple stiffnesses on cellular function without introducing shear stress to the cells. The model maintains macrophages viability >70% after curing from UV treatment. While evaluating this model, we sought to apply it to confirming the relationship between glycemic condition and substrate stiffness on macrophage mechanosensitivity demonstrated in 2D previously from our lab for tissue-engineered therapy design to treat diabetes and its various complications. Within this 3D model, LPS-stimulated RAW264.7 macrophages produced greater levels of cytokine and ROS production in hyperglycemic conditions than normoglycemic condition. Lower substrate stiffness (2 kPa) produced significantly higher in IL-6, IL-10, and ROS secretion, specifically nitrite. These findings were also confirmed in J774 macrophages. It should be noted that this study only varied the stiffness in the polyacrylamide bottom layer, to mimic an implant, while the GelMA, ECM representative, top layer remained consistent in stiffness across all conditions. This model can be expanded to vary the physiological stiffness of other areas in the body with GelMA by manipulating the concentration and UV treatment time during gelation. GelMA has a limited range of tens of kPA. Future work with this model will consist of continuing pro-inflammatory studies in macrophages, assessing phenotype, internal protein, gene, and ROS expression, as well as macrophage phagocytosis to characterize aspects of macrophage functionality in response to glycemic condition and substrate stiffness. These investigations aim bridge the gap in knowledge between immunometabolism and immuno-mechanobiology in macrophages.

Chapter 6: Summary and Future Directions

6.1. Summary

Throughout this dissertation, we investigated the effect of external glucose concentrations on substrate stiffness-mediated mechanosensitivity in macrophages. This work modeled FBR's initiation and acute inflammation stages to biomaterial implantation for diabetics, such as with encapsulated islet transplantation. Macrophages were cultured in their respective media conditions, hyperglycemic (450 mg/dL) and normoglycemic (100 mg/dL), as subpopulations before all experimentation. These findings will provide valuable knowledge in mechanobiology, immunometabolism, and tissue engineering concerning scaffold design for patients with diabetes.

In Chapter 3, we explored the role of glycemic condition on focal adhesion through morphology changes, phenotype, and Fc-mediated phagocytosis. Substrate stiffness-mediated morphology changes occurred independently of glycemic condition for extended periods. At 1hr of adherence, macrophages begin to show changes in cellular area based on stiffness under hyperglycemic conditions only. However, as macrophages adhered for more extended periods, morphology is dictated by substrate stiffness independent of glycemic condition. Stiffer substrates drove significant cellular growth as well as reduced circularity. This outcome did not lead to phenotypic changes in the macrophages, as cells remained consistent across both parameters in CD86, CD206, and CD80 expression. Evaluating adhesion-based functionality in macrophages through Fc-mediated phagocytosis demonstrated external glucose levels dictate the extent of substrate stiffness-mediated mechanosensitivity. Hyperglycemic conditions promoted a drastic increase in the percentage of frustrated phagocytes from soft (2 kPa) to stiff (274 kPa) substrates compared to normoglycemic conditions. By inhibiting glycolysis using 2-DG, substrate stiffness-mediated mechanosensitivity dissipated entirely in the percentage of frustrated phagocytosis. The work in this chapter demonstrated glycemic conditions held a crucial role in the functional response of unstimulated macrophages to substrate stiffness.

In Chapter 4, we assessed glucose and stiffness parameters on the functionality of unstimulated and pro-inflammatory macrophages on 2D substrates., evaluating pro-inflammatory cytokine gene expression and protein secretion and aspects of the glycolysis pathway to tie glucose metabolism to TLR4/LPS and FAK pathways. Our work determined that hyperglycemic conditions significantly enhance substrate stiffness-mediated mechanosensitivity in pro-inflammatory macrophage function, especially TNF-α and IL-6 secretion. Normoglycemic conditions resulted in reduced inflammation than hyperglycemic conditions and comparable cytokine secretion across all substrate stiffnesses. Lactate secretion in hyperglycemic LPS stimulated macrophages increased proportionately to stiffness opposite of TNF-α data under the same parameters, demonstrating the role of lactate as an inhibitor of TNF-α secretion. However, this trend was only displayed in hyperglycemic LPS-stimulated macrophages. These findings highlight mechanosensitivity in downstream glycolysis genes in stimulated macrophages that should be further studied.

In Chapter 5, we constructed a 3D mechanosensitivity model to expound on findings from Chapter 4 by mimicking the material-cell-ECM interplay seen when macrophages respond to implanted biomaterials during FBR. GelMA was cast onto the 2D polyacrylamide model used in Chapters 3 and 4. This GelMA top layer represented the ECM remaining within the range of stiffness as the subcutaneous space (~34 kPa). The polyacrylamide layer represented a biomaterial implant and varied in stiffness (2 – 274 kPa). Macrophages cultured using this model maintained a cellular viability of >70% after UV treatment compared to cells cultured using the 2D polyacrylamide model. When evaluating the effect of external glucose levels on substrate stiffness-mediated mechanosensitivity in pro-inflammatory macrophages, TNF-α, IL-6, IL-10, and nitrite secretion were significantly upregulated in hyperglycemic conditions. Lower substrate stiffness (2 kPa) produced substantially higher IL-6, IL-10, and nitrite. These findings were also confirmed in J774 macrophages. Overall, this work signifies that the glycemic condition is critical in mechanotransduction regarding substrate stiffness. As most mechanobiology studies are conducted in hyperglycemic conditions, it can be concluded that this is a vital parameter to note regarding cellular function in mechanobiology work. In reg

6.2. Future Directions

Future studies in unstimulated focal adhesion work is evaluating the internalized mechanistic connections between focal adhesion and glucose metabolism pathways.

Src and Syk have been identified as critical proteins in Fc-mediated phagocytosis and could explain what is leading to our findings internally. Moreover, these discoveries may shed light on a novel connection between glucose metabolism and mechanosensing in macrophage functionality.

A Seahorse assay could assess the relationship between immunometabolism and stiffness-driven mechanotransduction on macrophages. A Seahorse assay measures extracellular flux to measure metabolic activity in cells through changes in oxygen consumption rate (OCR) and extracellular acidification rate (ECAR).[207,208] ECAR represents the rate of glycolysis and lactate production, while OCR reflects the rate of mitochondrial respiration and oxidative phosphorylation.[209] These pathways are crucial for determining macrophage phenotype and function.[210] Pro-inflammatory (M1) macrophages exhibit increased glycolysis, while anti-inflammatory (M2) macrophages rely more on oxidative phosphorylation.[211] Due to the specialized microplates used for this assay, adapting and optimizing a model to utilize the assay for mechanobiology studies effectively is imperative.

Lastly, macrophage functionality can be assessed in later stages of FBR seen in chronic inflammation associated with FBGC formation, myofibroblast recruitment, anti-inflammation, and in vivo studies. This later stage FBGC formation from macrophages guides pericapsular fibrotic overgrowth, secluding EIT from nutrients. Moreover, an *in vivo* mouse model can be used to assess substrate stiffness-mediated mechanosensitivity in diabetic mice again normal mice to evaluate the extent of FBR.

For future EIT efficacy studies, the effect of substrate stiffness on islet viability and functionality can be investigated to strengthen the use of substrate stiffness in EIT capsule design. These studies can give us a comprehensive understanding of foreign body response in diabetics in relation to mechanobiology.

Bibliography

1. Vaithilingam V, Bal S and Tuch BE. Encapsulated Islet Transplantation: Where Do We Stand? Rev Diabet Stud 2017;14(1):51–78; doi: 10.1900/RDS.2017.14.51.
2. Foster GA and García AJ. Bio-Synthetic Materials for Immunomodulation of Islet Transplants. Adv Drug Deliv Rev 2017;114.
3. Anderson JM, Rodriguez A and Chang DT. Foreign Body Reaction to Biomaterials. Semin Immunol 2008;20(2):86–100; doi: 10.1016/j.smim.2007.11.004.
4. Ward WK. A Review of the Foreign-Body Response to Subcutaneously-Implanted Devices: The Role of Macrophages and Cytokines in Biofouling and Fibrosis. 2008.
5. Vaithilingam V, Evans MDM, Lewy DM, et al. Co-Encapsulation and Co-Transplantation of Mesenchymal Stem Cells Reduces Pericapsular Fibrosis and Improves Encapsulated Islet Survival and Function When Allografted. Sci Rep 2017;7(1); doi: 10.1038/s41598-017-10359-1.
6. Wu S, Wang L, Fang Y, et al. Advances in Encapsulation and Delivery Strategies for Islet Transplantation. Adv Healthc Mater 2021;10(20):2100965; doi: 10.1002/ADHM.202100965.
7. Markov PA, Khramova DS, Shumikhin K V., et al. Mechanical Properties of the Pectin Hydrogels and Inflammation Response to Their Subcutaneous Implantation. J Biomed Mater Res Part A 2019;107(9):2088–2098; doi: 10.1002/jbm.a.36721.
8. Adlerz KM, Aranda-Espinoza H and Hayenga HN. Substrate Elasticity Regulates the Behavior of Human Monocyte-Derived Macrophages. Eur Biophys J 2016;45(4):301–309; doi: 10.1007/s00249-015-1096-8.
9. Mennens SFB, van den Dries K and Cambi A. Role for Mechanotransduction in Macrophage and Dendritic Cell Immunobiology. In: Results and Problems in Cell Differentiation Springer Verlag; 2017; pp. 209–242; doi: 10.1007/978-3-319-54090-0_9.
10. O’Neill LAJJ, Kishton RJ and Rathmell J. A Guide to Immunometabolism for Immunologists. Nat Rev Immunol 2016 169 2016;16(9):553–565; doi: 10.1038/nri.2016.70.
11. Viola A, Munari F, Sánchez-Rodríguez R, et al. The Metabolic Signature of Macrophage Responses. Front Immunol 2019;10(JULY):1462; doi: 10.3389/FIMMU.2019.01462.
12. Gonzalez Y, Herrera MT, Soldevila G, et al. High Glucose Concentrations Induce TNF-α Production through the down-Regulation of CD33 in Primary Human Monocytes. BMC Immunol 2012;13(1):19; doi: 10.1186/1471-2172-13-19.
13. Freemerman AJ, Johnson AR, Sacks GN, et al. Metabolic Reprogramming of Macrophages: Glucose Transporter 1 (GLUT1)-Mediated Glucose Metabolism Drives a Proinflammatory Phenotype. 2014;289(11); doi: 10.1074/JBC.M113.522037.
14. Enck K, Tamburrini R, Deborah C, et al. Effect of Alginate Matrix Engineered

to Mimic the Pancreatic Microenvironment on Encapsulated Islet Function. 2021;118(3); doi: 10.1002/BIT.27641.
15. Richardson T, Barner S, Candiello J, et al. Capsule Stiffness Regulates the Efficiency of Pancreatic Differentiation of Human Embryonic Stem Cells. Acta Biomater 2016;35:153–165.
16. Chan E-S, Lim T-K, Voo W-P, et al. Effect of Formulation of Alginate Beads on Their Mechanical Behavior and Stiffness. Particuology 2011;9(3):228–234; doi: 10.1016/j.partic.2010.12.002.
17. International Diabetes Federation (IDF). IDF Diabetes Atlas 9th Edition 2019. 9th ed. Diabetes Atlas; 2019.
18. Chatterjee S, Khunti K and Davies MJ. Type 2 Diabetes. Lancet 2017;389(10085):2239–2251; doi: 10.1016/S0140-6736(17)30058-2.
19. Headen DM, Woodward KB, Coronel MM, et al. Local Immunomodulation with Fas Ligand-Engineered Biomaterials Achieves Allogeneic Islet Graft Acceptance. Nat Mater 2018;17(8):732–739; doi: 10.1038/s41563-018-0099-0.
20. Guariguata L, Whiting DR, Hambleton I, et al. Global Estimates of Diabetes Prevalence for 2013 and Projections for 2035. Diabetes Res Clin Pract 2014;103(2):137–149; doi: 10.1016/J.DIABRES.2013.11.002.
21. Herman WH. The Global Burden of Diabetes: An Overview. In: Diabetes Mellitus in Developing Countries and Underserved Communities Springer International Publishing: Cham; 2017; pp. 1–5; doi: 10.1007/978-3-319-41559-8_1.
22. American Diabetes Association AD. Economic Costs of Diabetes in the U.S. in 2017. Diabetes Care 2018;dci180007; doi: 10.2337/dci18-0007.
23. Beran D, Lazo-Porras M, Mba CM, et al. A Global Perspective on the Issue of Access to Insulin. Diabetol 2021 645 2021;64(5):954–962; doi: 10.1007/S00125-020-05375-2.
24. Darrabie MD, Kendall WF and Opara EC. Characteristics of Poly-L-Ornithine-Coated Alginate Microcapsules. Biomaterials 2005;26(34):6846–6852; doi: 10.1016/J.BIOMATERIALS.2005.05.009.
25. Shorten PR, McMahon CD and Soboleva TK. Insulin Transport within Skeletal Muscle Transverse Tubule Networks. Biophys J 2007;93(9):3001; doi: 10.1529/BIOPHYSJ.107.107888.
26. Krombach F, Münzing S, Allmeling AM, et al. Cell Size of Alveolar Macrophages: An Interspecies Comparison. Environ Health Perspect 1997;105(Suppl 5):1261; doi: 10.1289/EHP.97105S51261.
27. Yeow N, Tabor RF and Garnier G. Mapping the Distribution of Specific Antibody Interaction Forces on Individual Red Blood Cells. Sci Reports 2017 71 2017;7(1):1–7; doi: 10.1038/srep41956.
28. Tasnim H, Fricke GM, Byrum JR, et al. Quantitative Measurement of Naïve T Cell Association with Dendritic Cells, FRCs, and Blood Vessels in Lymph Nodes. Front Immunol 2018;9(JUL):1571; doi: 10.3389/FIMMU.2018.01571/BIBTEX.
29. Liu W, Flanders JA, Wang LH, et al. A Safe, Fibrosis-Mitigating, and Scalable Encapsulation Device Supports Long-Term Function of Insulin-Producing Cells. Small 2022;18(8):2104899; doi: 10.1002/SMLL.202104899.

30. Citro A, Moser PT, Dugnani E, et al. Biofabrication of a Vascularized Islet Organ for Type 1 Diabetes. Biomaterials 2019;199:40–51; doi: 10.1016/J.BIOMATERIALS.2019.01.035.
31. Tuch BE, Keogh GW, Williams LJ, et al. Safety and Viability of Microencapsulated Human Islets Transplanted into Diabetic Humans. Diabetes Care 2009;32(10):1887–1889; doi: 10.2337/DC09-0744.
32. G B, P M, G L, et al. Long-Term Metabolic and Immunological Follow-up of Nonimmunosuppressed Patients with Type 1 Diabetes Treated with Microencapsulated Islet Allografts: Four Cases. Diabetes Care 2011;34(11):2406–2409; doi: 10.2337/DC11-0731.
33. Mesmaeker I De, Robert T, Suenens KG, et al. Increase Functional β-Cell Mass in Subcutaneous Alginate Capsules With Porcine Prenatal Islet Cells but Loss With Human Adult Islet Cells. Diabetes 2018;67(12):2640–2649; doi: 10.2337/DB18-0709.
34. M F, R C, T P, et al. Subcutaneous Xenotransplantation of Bovine Pancreatic Islets. Biomaterials 2005;26(28):5640–5647; doi: 10.1016/J.BIOMATERIALS.2005.02.019.
35. Schaschkow A, Sigrist S, Mura C, et al. Glycaemic Control in Diabetic Rats Treated with Islet Transplantation Using Plasma Combined with Hydroxypropylmethyl Cellulose Hydrogel. Acta Biomater 2020;102:259–272; doi: 10.1016/j.actbio.2019.11.047.
36. Zhang M, Du H, Guan Y, et al. Study on the Effect of PDA-PLGA Scaffold Loaded With Islet Cells for Skeletal Muscle Transplantation in the Treatment of Diabetes. Front Bioeng Biotechnol 2022;10:927348–927348; doi: 10.3389/FBIOE.2022.927348.
37. Buder B, Alexander M, Krishnan R, et al. Encapsulated Islet Transplantation: Strategies and Clinical Trials. Immune Netw 2013;13(6):235–9; doi: 10.4110/in.2013.13.6.235.
38. Weaver JD, Headen DM, Hunckler MD, et al. Design of a Vascularized Synthetic Poly(Ethylene Glycol) Macroencapsulation Device for Islet Transplantation. Biomaterials 2018;172:54–65; doi: 10.1016/J.BIOMATERIALS.2018.04.047.
39. Chen T, Yuan J, Duncanson S, et al. Alginate Encapsulant Incorporating CXCL12 Supports Long-Term Allo- and Xenoislet Transplantation Without Systemic Immune Suppression. Am J Transplant 2015;15(3):618–627; doi: 10.1111/AJT.13049.
40. MJ K, HS P, JW K, et al. Suppression of Fibrotic Reactions of Chitosan-Alginate Microcapsules Containing Porcine Islets by Dexamethasone Surface Coating. Endocrinol Metab (Seoul, Korea) 2021;36(1):146–156; doi: 10.3803/ENM.2021.879.
41. Abuid NJ, Gattás-Asfura KM, Schofield EA, et al. Layer-by-Layer Cerium Oxide Nanoparticle Coating for Antioxidant Protection of Encapsulated Beta Cells. Adv Healthc Mater 2019;8(12):1801493; doi: 10.1002/adhm.201801493.
42. Laporte C, Tubbs E, Pierron M, et al. Improved Human Islets' Viability and Functionality with Mesenchymal Stem Cells and Arg-Gly-Asp Tripeptides Supplementation of Alginate Micro-Encapsulated Islets in Vitro. Biochem

Biophys Res Commun 2020;528(4):650–657; doi: 10.1016/j.bbrc.2020.05.107.
43. Maruyama K, Nemoto E and Yamada S. Mechanical Regulation of Macrophage Function - Cyclic Tensile Force Inhibits NLRP3 Inflammasome-Dependent IL-1β Secretion in Murine Macrophages. Inflamm Regen 2019;39(1); doi: 10.1186/s41232-019-0092-2.
44. Baranov M V., Kumar M, Sacanna S, et al. Modulation of Immune Responses by Particle Size and Shape. Front Immunol 2021;11:3854; doi: 10.3389/FIMMU.2020.607945/BIBTEX.
45. Chaudhuri O, Cooper-White J, Janmey PA, et al. Effects of Extracellular Matrix Viscoelasticity on Cellular Behaviour. Nature 2020;584(7822):535–546; doi: 10.1038/s41586-020-2612-2.
46. Lim CT, Bershadsky A and Sheetz MP. Mechanobiology. J R Soc Interface 2010;7(Suppl 3):S291; doi: 10.1098/RSIF.2010.0150.FOCUS.
47. Witkowska-Zimny M, Walenko K, Wrobel E, et al. Effect of Substrate Stiffness on the Osteogenic Differentiation of Bone Marrow Stem Cells and Bone-Derived Cells. Cell Biol Int 2013;37(6):608–616; doi: 10.1002/CBIN.10078.
48. Manzoni EFM, Arcuri S, Brevini TAL, et al. Matrix Stiffness Boosts Pancreatic Differentiation via the YAP/TAZ Mechanotransduction Mediated Pathway. Int J Heal Anim Sci Food Saf 2018;5(1s); doi: 10.13130/2283-3927/10002.
49. Razinia Z, Castagnino P, Xu T, et al. Stiffness-Dependent Motility and Proliferation Uncoupled by Deletion of CD44. Sci Reports 2017 71 2017;7(1):1–10; doi: 10.1038/s41598-017-16486-z.
50. Shen K, Kenche H, Zhao H, et al. The Role of Extracellular Matrix Stiffness in Regulating Cytoskeletal Remodeling via Vinculin in Synthetic Smooth Muscle Cells. Biochem Biophys Res Commun 2019;508(1):302; doi: 10.1016/J.BBRC.2018.11.142.
51. O'Connor RS, Hao X, Shen K, et al. Substrate Rigidity Regulates Human T Cell Activation and Proliferation. J Immunol 2012;189(3):1330 LP – 1339; doi: 10.4049/jimmunol.1102757.
52. Klopfleisch R and Jung F. The Pathology of the Foreign Body Reaction against Biomaterials. J Biomed Mater Res - Part A 2017;105(3):927–940; doi: 10.1002/jbm.a.35958.
53. Hirsh SL, McKenzie DR, Nosworthy NJ, et al. The Vroman Effect: Competitive Protein Exchange with Dynamic Multilayer Protein Aggregates. Colloids Surfaces B Biointerfaces 2013;103:395–404; doi: 10.1016/J.COLSURFB.2012.10.039.
54. Visalakshan RM, Macgregor MN, Sasidharan S, et al. Biomaterial Surface Hydrophobicity-Mediated Serum Protein Adsorption and Immune Responses. ACS Appl Mater Interfaces 2019;11(31):27615–27623; doi: 10.1021/acsami.9b09900.
55. Jenney CR and Anderson JM. Adsorbed Serum Proteins Responsible for Surface Dependent Human Macrophage Behavior. J Biomed Mater Res 2000;49(4):435–447; doi: 10.1002/(SICI)1097-4636(20000315)49:4<435::AID-JBM2>3.0.CO;2-Y.

56. Zhang L, Cao Z, Bai T, et al. Zwitterionic Hydrogels Implanted in Mice Resist the Foreign-Body Reaction. Nat Biotechnol 2013;31(6):553–556; doi: 10.1038/nbt.2580.
57. Murakami D, Kobayashi S and Tanaka M. Interfacial Structures and Fibrinogen Adsorption at Blood-Compatible Polymer/Water Interfaces. 2016;2; doi: 10.1021/acsbiomaterials.6b00415.
58. Llopis-Hernández V, Rico P, Ballester-Beltrán J, et al. Role of Surface Chemistry in Protein Remodeling at the Cell-Material Interface. Chin W-C. ed. PLoS One 2011;6(5):e19610; doi: 10.1371/journal.pone.0019610.
59. Toromanov G, Gugutkov D, Gustavsson J, et al. Dynamic Behavior of Vitronectin at the Cell-Material Interface. ACS Biomater Sci Eng 2015;1(10):927–934; doi: 10.1021/ACSBIOMATERIALS.5B00147/ASSET/IMAGES/LARGE/AB-2015-00147F_0009.JPEG.
60. Shen M, Garcia I, Maier R V., et al. Effects of Adsorbed Proteins and Surface Chemistry on Foreign Body Giant Cell Formation, Tumor Necrosis Factor Alpha Release and Procoagulant Activity of Monocytes. J Biomed Mater Res A 2004;70(4):533–541; doi: 10.1002/JBM.A.30069.
61. McNally AK, Jones JA, MacEwan SR, et al. Vitronectin Is a Critical Protein Adhesion Substrate for IL-4-induced Foreign Body Giant Cell Formation. J Biomed Mater Res Part A 2008;86A(2):535–543; doi: 10.1002/jbm.a.31658.
62. Balabiyev A, Podolnikova NP, Kilbourne JA, et al. Fibrin Polymer on the Surface of Biomaterial Implants Drives the Foreign Body Reaction. Biomaterials 2021;277; doi: 10.1016/J.BIOMATERIALS.2021.121087.
63. Ridiandries A, Tan JTM and Bursill CA. The Role of Chemokines in Wound Healing. Int J Mol Sci 2018;19(10); doi: 10.3390/ijms19103217.
64. Wilgus TA. Alerting the Body to Tissue Injury: The Role of Alarmins and DAMPs in Cutaneous Wound Healing. Curr Pathobiol Rep 2018;6(1):55–60; doi: 10.1007/s40139-018-0162-1.
65. de Oliveira S, Reyes-Aldasoro CC, Candel S, et al. Cxcl8 (IL-8) Mediates Neutrophil Recruitment and Behavior in the Zebrafish Inflammatory Response. J Immunol 2013;190(8):4349–4359; doi: 10.4049/jimmunol.1203266.
66. Sremac M, Lei J, Penson MFE, et al. Preliminary Studies of the Impact of CXCL12 on the Foreign Body Reaction to Pancreatic Islets Microencapsulated in Alginate in Nonhuman Primates Pancreas and Islet Transplantation. Transplant Direct 2019;5(447); doi: 10.1097/TXD.0000000000000890.
67. Kaneko N, Kurata M, Yamamoto T, et al. The Role of Interleukin-1 in General Pathology. Inflamm Regen 2019;39(1):1–16; doi: 10.1186/s41232-019-0101-5.
68. Harada A, Sekido N, Akahoshi T, et al. Essential Involvement of Interleukin-8 (IL-8) in Acute Inflammation. In: Journal of Leukocyte Biology Federation of American Societies for Experimental Biology; 1994; pp. 559–564; doi: 10.1002/jlb.56.5.559.
69. MacLauchlan S, Skokos EA, Meznarich N, et al. Macrophage Fusion, Giant Cell Formation, and the Foreign Body Response Require Matrix Metalloproteinase 9. J Leukoc Biol 2009;85(4):617–626; doi: 10.1189/JLB.1008588.

70. Jhunjhunwala S, Aresta-DaSilva S, Tang K, et al. Neutrophil Responses to Sterile Implant Materials. Palaniyar N. ed. 2015;10(9):e0137550.
71. Mosser DM and Edwards JP. Exploring the Full Spectrum of Macrophage Activation. Nat Rev Immunol 2008;8(12):958–69; doi: 10.1038/nri2448.
72. Cheng B, Wan W, Huang G, et al. Nanoscale Integrin Cluster Dynamics Controls Cellular Mechanosensing via FAKY397 Phosphorylation. Sci Adv 2020;6(10); doi: 10.1126/SCIADV.AAX1909/SUPPL_FILE/AAX1909_SM.PDF.
73. Zhao X and Guan J-L. Focal Adhesion Kinase and Its Signaling Pathways in Cell Migration and Angiogenesis. Adv Drug Deliv Rev 2011;63(8):610–615; doi: 10.1016/j.addr.2010.11.001.
74. Gruber E, Heyward C, Cameron J, et al. Toll-like Receptor Signaling in Macrophages Is Regulated by Extracellular Substrate Stiffness and Rho-Associated Coiled-Coil Kinase (ROCK1/2). Int Immunol 2018;30(6):267–278; doi: 10.1093/intimm/dxy027.
75. Hsieh JY, Keating MT, Smith TD, et al. Matrix Crosslinking Enhances Macrophage Adhesion, Migration, and Inflammatory Activation. APL Bioeng 2019;3:16103; doi: 10.1063/1.5067301.
76. Martinez FO and Gordon S. The M1 and M2 Paradigm of Macrophage Activation: Time for Reassessment. F1000Prime Rep 2014;6:13; doi: 10.12703/P6-13.
77. McWhorter FY, Davis CT and Liu WF. Physical and Mechanical Regulation of Macrophage Phenotype and Function. Cell Mol Life Sci 2015;72(7):1303–16; doi: 10.1007/s00018-014-1796-8.
78. Lu YC, Yeh WC and Ohashi PS. LPS/TLR4 Signal Transduction Pathway. Cytokine 2008;42(2):145–151; doi: 10.1016/J.CYTO.2008.01.006.
79. Escolano J-C, Taubenberger A V, Abuhattum S, et al. Compliant Substrates Enhance Macrophage Cytokine Release and NLRP3 Inflammasome Formation During Their Pro-Inflammatory Response. Front Cell Dev Biol 2021;9; doi: 10.3389/fcell.2021.639815.
80. Blakney AK, Swartzlander MD and Bryant SJ. The Effects of Substrate Stiffness on the in Vitro Activation of Macrophages and in Vivo Host Response to Poly(Ethylene Glycol)-Based Hydrogels. J Biomed Mater Res A 2012;100(6):1375–86; doi: 10.1002/jbm.a.34104.
81. Patel NR, Bole M, Chen C, et al. Cell Elasticity Determines Macrophage Function. PLoS One 2012;7(9):e41024; doi: 10.1371/journal.pone.0041024.
82. Chen M, Zhang Y, Zhou P, et al. Substrate Stiffness Modulates Bone Marrow-Derived Macrophage Polarization through NF-KB Signaling Pathway. Bioact Mater 2020;5(4):880–890; doi: 10.1016/j.bioactmat.2020.05.004.
83. Irwin EF, Saha K, Rosenbluth M, et al. Modulus-Dependent Macrophage Adhesion and Behavior. J Biomater Sci Polym Edn 2008;19(10):1363–1382.
84. Busscher HJ, van der Mei HC, Subbiahdoss G, et al. Biomaterial-Associated Infection: Locating the Finish Line in the Race for the Surface. Sci Transl Med 2012;4(153); doi: 10.1126/scitranslmed.3004528.
85. Scott EA, Stano A, Gillard M, et al. Dendritic Cell Activation and T Cell Priming with Adjuvant- and Antigen-Loaded Oxidation-Sensitive

Polymersomes. Biomaterials 2012;33(26):6211–6219; doi: 10.1016/j.biomaterials.2012.04.060.
86. Sheikh Z, Brooks PJ, Barzilay O, et al. Macrophages, Foreign Body Giant Cells and Their Response to Implantable Biomaterials. Materials (Basel) 2015;8(9):5671–5701; doi: 10.3390/ma8095269.
87. Goswami R, Arya RK, Sharma S, et al. Mechanosensing by TRPV4 Mediates Stiffness-Induced Foreign Body Response and Giant Cell Formation. Sci Signal 2021;14(707); doi: 10.1126/SCISIGNAL.ABD4077/SUPPL_FILE/SCISIGNAL.ABD4077_SM.PDF.
88. Dutta B, Goswami R, Rahaman SO, et al. TRPV4 Plays a Role in Matrix Stiffness-Induced Macrophage Polarization. Front Immunol 2020;11; doi: 10.3389/fimmu.2020.570195.
89. Goswami R, Arya RK, Biswas D, et al. Transient Receptor Potential Vanilloid 4 Is Required for Foreign Body Response and Giant Cell Formation. Am J Pathol 2019;189(8):1505–1512; doi: 10.1016/J.AJPATH.2019.04.016.
90. Majd H, Scherer SS, Boo S, et al. Novel Micropatterns Mechanically Control Fibrotic Reactions at the Surface of Silicone Implants. Biomaterials 2015;54:136–147; doi: 10.1016/j.biomaterials.2015.03.027.
91. Hinz B. The Role of Myofibroblasts in Wound Healing. Curr Res Transl Med 2016;64(4):171–177; doi: 10.1016/J.RETRAM.2016.09.003.
92. Hesketh M, Sahin KB, West ZE, et al. Macrophage Phenotypes Regulate Scar Formation and Chronic Wound Healing. Int J Mol Sci 2017;18(7):1545; doi: 10.3390/ijms18071545.
93. Krzyszczyk P, Schloss R, Palmer A, et al. The Role of Macrophages in Acute and Chronic Wound Healing and Interventions to Promote Pro-Wound Healing Phenotypes. Front Physiol 2018;9(MAY):419; doi: 10.3389/fphys.2018.00419.
94. Roman B. Varying Ratios Of Collagen I And Iii For The Study Of Fibrotic Conditions In Tissue Engineering. Open Access Theses Diss 2019.
95. Ibrahim M, Bond J, Medina MA, et al. Characterization of the Foreign Body Response to Common Surgical Biomaterials in a Murine Model. Eur J Plast Surg 2017;40(5):383–392; doi: 10.1007/s00238-017-1308-9.
96. Alsebaey A, Allam N, Alswat K, et al. Normal Liver Stiffness: A Study in Living Donors with Normal Liver Histology. World J Hepatol 2015;7(8):1149; doi: 10.4254/WJH.V7.I8.1149.
97. Fung J, Lee CK, Chan M, et al. Defining Normal Liver Stiffness Range in a Normal Healthy Chinese Population without Liver Disease. PLoS One 2013;8(12):e85067; doi: 10.1371/journal.pone.0085067.
98. Johnson B, Campbell S and Campbell-Kyureghyan N. Characterizing the Material Properties of the Kidney and Liver in Unconfined Compression and Probing Protocols with Special Reference to Varying Strain Rate. Biomech 2021, Vol 1, Pages 264-280 2021;1(2):264–280; doi: 10.3390/BIOMECHANICS1020022.
99. Li C, Guan G, Reif R, et al. Determining Elastic Properties of Skin by Measuring Surface Waves from an Impulse Mechanical Stimulus Using Phase-Sensitive Optical Coherence Tomography. J R Soc Interface 2012;9(70):831–

841; doi: 10.1098/RSIF.2011.0583.
100. Feng X, Li G-Y, Ramier A, et al. In Vivo Stiffness Measurement of Epidermis, Dermis, and Hypodermis Using Broadband Rayleigh-Wave Optical Coherence Elastography. Acta Biomater 2022; doi: 10.1016/j.actbio.2022.04.030.
101. Strand BL, Coron AE and Skjak-Braek G. Current and Future Perspectives on Alginate Encapsulated Pancreatic Islet. Stem Cells Transl Med 2017;6(4):1053–1058; doi: 10.1002/sctm.16-0116.
102. Holdcraft RW, Gazda LS, Circle L, et al. Enhancement of in Vitro and in Vivo Function of Agarose-Encapsulated Porcine Islets by Changes in the Islet Microenvironment. Cell Transplant 2014;23(8):929–944; doi: 10.3727/096368913X667033/ASSET/IMAGES/LARGE/10.3727_096368913X667033-FIG2.JPEG.
103. Risbud M, Hardikar A and Bhonde R. Chitosan-Polyvinyl Pyrrolidone Hydrogels as Candidate for Islet Immunoisolation: In Vitro Biocompatibility Evaluation. 2000.
104. Yang KC, Qi Z, Wu CC, et al. The Cytoprotection of Chitosan Based Hydrogels in Xenogeneic Islet Transplantation: An in Vivo Study in Streptozotocin-Induced Diabetic Mouse. Biochem Biophys Res Commun 2010;393(4):818–823; doi: 10.1016/j.bbrc.2010.02.089.
105. Stabler CL, Giraldo JA, Berman DM, et al. Transplantation of PEGylated Islets Enhances Therapeutic Efficacy in a Diabetic Nonhuman Primate Model. Am J Transplant 2020;20(3):689–700; doi: 10.1111/ajt.15643.
106. Zondervan GJ, Hoppen HJ, Pennings AJ, et al. Design of a Polyurethane Membrane for the Encapsulation of Islets of Langerhans. Biomaterials 1992;13(3):136–144; doi: 10.1016/0142-9612(92)90061-R.
107. Kette F, Rojas-Canales D, Drogemuller C, et al. Modification of Polyurethane Scaffolds for Localised Immunosuppression of Subcutaneous Islet Transplantation. Transplantation 2018;102(Supplement 7):S77.
108. Handorf AM, Zhou Y, Halanski MA, et al. Tissue Stiffness Dictates Development, Homeostasis, and Disease Progression. http://dx.doi.org/101080/1547627820151019687 2015;11(1):1–15; doi: 10.1080/15476278.2015.1019687.
109. Darling EM, Topel M, Zauscher S, et al. Viscoelastic Properties of Human Mesenchymally-Derived Stem Cells and Primary Osteoblasts, Chondrocytes, and Adipocytes. J Biomech 2008;41(2):454; doi: 10.1016/J.JBIOMECH.2007.06.019.
110. Johnson CL, McGarry MDJ, Gharibans AA, et al. Local Mechanical Properties of White Matter Structures in the Human Brain. Neuroimage 2013;79:145; doi: 10.1016/J.NEUROIMAGE.2013.04.089.
111. Yin Z, Romano AJ, Manduca A, et al. Stiffness and beyond: What MR Elastography Can Tell Us about Brain Structure and Function under Physiologic and Pathologic Conditions. Top Magn Reson Imaging 2018;27(5):305; doi: 10.1097/RMR.0000000000000178.
112. Münch J and Abdelilah-Seyfried S. Sensing and Responding of Cardiomyocytes to Changes of Tissue Stiffness in the Diseased Heart. Front Cell Dev Biol 2021;9:403; doi: 10.3389/FCELL.2021.642840/BIBTEX.

113. Rho JY, Ashman RB and Turner CH. Young's Modulus of Trabecular and Cortical Bone Material: Ultrasonic and Microtensile Measurements. J Biomech 1993;26(2):111–119; doi: 10.1016/0021-9290(93)90042-D.
114. Boughton OR, Ma S, Zhao S, et al. Measuring Bone Stiffness Using Spherical Indentation. PLoS One 2018;13(7):e0200475; doi: 10.1371/JOURNAL.PONE.0200475.
115. Leiva O, Leon C, Kah Ng S, et al. The Role of Extracellular Matrix Stiffness in Megakaryocyte and Platelet Development and Function. Am J Hematol 2018;93(3):430–441; doi: 10.1002/ajh.25008.
116. Bayramoğlu Z, Öztürk M, Çalışkan E, et al. Normative Values of Thymus in Healthy Children; Stiffness by Shear Wave Elastography. Diagnostic Interv Radiol 2020;26(2):147; doi: 10.5152/DIR.2019.19344.
117. Ozturk M, Çalışkan E, Bayramoglu Z, et al. Normative Values of Pancreas Stiffness by Shear Wave Elastography in Healthy Children and Adolescents. J Med Ultrason (2001) 2020;47(4):583–589; doi: 10.1007/S10396-020-01039-1.
118. Matyash M, Despang F, Ikonomidou C, et al. Swelling and Mechanical Properties of Alginate Hydrogels with Respect to Promotion of Neural Growth. Tissue Eng Part C Methods 2014;20(5):401–411.
119. Normand V, Lootens DL, Amici E, et al. New Insight into Agarose Gel Mechanical Properties. Biomacromolecules 2000;1(4):730–738; doi: 10.1021/bm005583j.
120. Zhu T, Jiang J, Zhao J, et al. Regulating Preparation Of Functional Alginate-Chitosan Three-Dimensional Scaffold For Skin Tissue Engineering. Int J Nanomedicine 2019;14:8891; doi: 10.2147/IJN.S210329.
121. D'Angelo G, Elhussieny A, Faisal M, et al. Mechanical Behavior Optimization of Chitosan Extracted from Shrimp Shells as a Sustainable Material for Shopping Bags. J Funct Biomater 2018, Vol 9, Page 37 2018;9(2):37; doi: 10.3390/JFB9020037.
122. Tan S, Mettu S, Biviano MD, et al. Ultrasonic Synthesis of Stable Oil Filled Microcapsules Using Thiolated Chitosan and Their Characterization by AFM and Numerical Simulations. Soft Matter 2016;12(34):7212–7222; doi: 10.1039/C6SM01402J.
123. Whitehead AK, Barnett HH, Caldorera-Moore ME, et al. Poly (Ethylene Glycol) Hydrogel Elasticity Influences Human Mesenchymal Stem Cell Behavior. Regen Biomater 2018;5(3):167–175; doi: 10.1093/RB/RBY008.
124. Drira Z and Yadavalli VK. Nanomechanical Measurements of Polyethylene Glycol Hydrogels Using Atomic Force Microscopy. J Mech Behav Biomed Mater 2013;18:20–28; doi: 10.1016/J.JMBBM.2012.09.015.
125. Almany L and Seliktar D. Biosynthetic Hydrogel Scaffolds Made from Fibrinogen and Polyethylene Glycol for 3D Cell Cultures. Biomaterials 2005;26(15):2467–2477; doi: 10.1016/J.BIOMATERIALS.2004.06.047.
126. Calleros EL, Simonovsky FI, Garty S, et al. Crosslinked, Biodegradable Polyurethanes for Precision-Porous Biomaterials: Synthesis and Properties. J Appl Polym Sci 2020;137(25):48943; doi: 10.1002/APP.48943.
127. Laube T, Weisser J, Berger S, et al. In Situ Foamable, Degradable Polyurethane as Biomaterial for Soft Tissue Repair. Mater Sci Eng C

2017;78:163–174; doi: 10.1016/J.MSEC.2017.04.061.
128. Bochenek MA, Veiseh O, Vegas AJ, et al. Alginate Encapsulation as Long-Term Immune Protection of Allogeneic Pancreatic Islet Cells Transplanted into the Omental Bursa of Macaques. Nat Biomed Eng 2018;2(11):810–821; doi: 10.1038/s41551-018-0275-1.
129. Li L, Chen Y, Wang Y, et al. Effects of Concentration Variation on the Physical Properties of Alginate-Based Substrates and Cell Behavior in Culture. Int J Biol Macromol 2019;128:184–195; doi: 10.1016/J.IJBIOMAC.2019.01.123.
130. Basta G, Montanucci P, Luca G, et al. Long-Term Metabolic and Immunological Follow-Up of Nonimmunosuppressed Patients With Type 1 Diabetes Treated With Microencapsulated Islet Allografts. Diabetes Care 2011;34(11):2406–2409; doi: 10.2337/dc11-0731.
131. Paredes-Juarez GA, de Haan BJ, Faas MM, et al. A Technology Platform to Test the Efficacy of Purification of Alginate. Materials (Basel) 2014;7(3):2087–2103; doi: 10.3390/MA7032087.
132. Paredes-Juarez GA, De Haan BJ, Faas MM, et al. The Role of Pathogen-Associated Molecular Patterns in Inflammatory Responses against Alginate Based Microcapsules. J Control Release 2013;172(3):983–992; doi: 10.1016/J.JCONREL.2013.09.009.
133. Sondermeijer HP, Witkowski P, Woodland D, et al. Optimization of Alginate Purification Using Polyvinylidene Difluoride Membrane Filtration: Effects on Immunogenicity and Biocompatibility of Three-Dimensional Alginate Scaffolds. J Biomater Appl 2016;31(4):510–520; doi: 10.1177/0885328216645952.
134. Rezaa Mohammadi M, Rodrigez S, Cao R, et al. Immune Response to Subcutaneous Implants of Alginate Microcapsules. Mater Today Proc 2018;5(7):15580–15585; doi: 10.1016/J.MATPR.2018.04.166.
135. Gin H, Dupuy B, Baquey C, et al. Agarose Encapsulation of Islets of Langerhans: Reduced Toxicity in Vitro. J Microencapsul 1987;4(3):239–242; doi: 10.3109/02652048709021817.
136. Iwata H, Amemiya H, Matsuda T, et al. Microencapsulation of Langerhans Islets in Agarose Microbeads and Their Application for a Bioartificial Pancreas. J Bioact Compat Polym 1988;3(4):356–369; doi: 10.1177/088391158800300403.
137. Dumpala PR, Holdcraft RW, Martis PC, et al. Retention of Gene Expression in Porcine Islets after Agarose Encapsulation and Long-Term Culture. Biochem Biophys Res Commun 2016;476(4):580–585; doi: 10.1016/J.BBRC.2016.05.165.
138. Takemoto N, Konagaya S, Kuwabara R, et al. Coaggregates of Regulatory T Cells and Islet Cells Allow Long-Term Graft Survival in Liver Without Immunosuppression. Transplantation 2015;99(5):942–947; doi: 10.1097/TP.0000000000000579.
139. Narayanan J, Xiong J-Y and Liu X-Y. Determination of Agarose Gel Pore Size: Absorbance Measurements Vis a Vis Other Techniques. J Phys Conf Ser 2006;28:83–86; doi: 10.1088/1742-6596/28/1/017.

140. Yang HK, Ham D-SS, Park H-SS, et al. Long-Term Efficacy and Biocompatibility of Encapsulated Islet Transplantation With Chitosan-Coated Alginate Capsules in Mice and Canine Models of Diabetes. Transplantation 2016;100(2):334–343; doi: 10.1097/TP.0000000000000927.
141. Chen CL, Wang YM, Liu CF, et al. The Effect of Water-Soluble Chitosan on Macrophage Activation and the Attenuation of Mite Allergen-Induced Airway Inflammation. Biomaterials 2008;29(14):2173–2182; doi: 10.1016/J.BIOMATERIALS.2008.01.023.
142. Fullagar B, Rao W, Gilor C, et al. Nano-Encapsulation of Bilirubin in Pluronic F127–Chitosan Improves Uptake in β Cells and Increases Islet Viability and Function after Hypoxic Stress. Cell Transplant 2017;26(10):1703–1715; doi: 10.1177/0963689717735112.
143. Williams PA, Campbell KT, Gharaviram H, et al. Alginate-Chitosan Hydrogels Provide a Sustained Gradient of Sphingosine-1-Phosphate for Therapeutic Angiogenesis. Ann Biomed Eng 2017;45(4):1003–1014; doi: 10.1007/s10439-016-1768-2.
144. Bhujbal S V., Paredes-Juarez GA, Niclou SP, et al. Factors Influencing the Mechanical Stability of Alginate Beads Applicable for Immunoisolation of Mammalian Cells. J Mech Behav Biomed Mater 2014;37:196–208; doi: 10.1016/j.jmbbm.2014.05.020.
145. Villa C, Manzoli V, Abreu MM, et al. Effects of Composition of Alginate-Polyethylene Glycol Microcapsules and Transplant Site on Encapsulated Islet Graft Outcomes in Mice. Transplantation 2017;101(5):1025–1035; doi: 10.1097/tp.0000000000001454.
146. Weber LM, He J, Bradley B, et al. PEG-Based Hydrogels as an in Vitro Encapsulation Platform for Testing Controlled Beta-Cell Microenvironments. Acta Biomater 2006;2(1):1–8; doi: 10.1016/J.ACTBIO.2005.10.005.
147. Kizilel S, Scavone A, Liu X, et al. Encapsulation of Pancreatic Islets within Nano-Thin Functional Polyethylene Glycol Coatings for Enhanced Insulin Secretion. Tissue Eng Part A 2010;16(7):2217–2228; doi: 10.1089/TEN.TEA.2009.0640.
148. Coronel M, Weaver JD, Hunckler M, et al. Synthetic Immunomodulatory Biomaterials to Improve Islet Graft Survival. Transplantation 2018;102(Supplement 7):S230; doi: 10.1097/01.tp.0000542900.67611.3f.
149. Haque MR, Jeong J-H, Lee KW, et al. Effects of Transplanted Islets Nano-Encapsulated with Hyperbranched Polyethylene Glycol and Heparin on Microenvironment Reconstruction and Glucose Control. Bioconjug Chem 2018;29(9):2945–2953; doi: 10.1021/acs.bioconjchem.8b00364.
150. Weaver JD, Headen DM, Coronel MM, et al. Synthetic Poly(Ethylene Glycol)-based Microfluidic Islet Encapsulation Reduces Graft Volume for Delivery to Highly Vascularized and Retrievable Transplant Site. Am J Transplant 2019;19(5):1315–1327; doi: 10.1111/ajt.15168.
151. Abrego CJG, Dedroog L, Deschaume O, et al. Multiscale Characterization of the Mechanical Properties of Fibrin and Polyethylene Glycol (PEG) Hydrogels for Tissue Engineering Applications. Macromol Chem Phys 2022;223(1); doi: 10.1002/MACP.202100366.

152. Knobeloch T, Abadi SEM, Bruns J, et al. Injectable Polyethylene Glycol Hydrogel for Islet Encapsulation: An in Vitro and in Vivo Characterization . Biomed Phys Eng Express 2017;3(3):035022; doi: 10.1088/2057-1976/AA742B.
153. Ward RS., White KA., Wolcott CA., et al. Development of a Hybrid Artificial Pancreas with a Dense Polyurethane Membrane. ASAIO 1993;39(3):M261-7.
154. George S, Nair PD, Risbud M V., et al. Nonporous Polyurethane Membranes as Islet Immunoisolation Matrices - Biocompatibility Studies. J Biomater Appl 2002;16(4):327–340; doi: 10.1106/088532802024249.
155. Liu Q, Wang X, Chiu A, et al. A Zwitterionic Polyurethane Nanoporous Device with Low Foreign-Body Response for Islet Encapsulation. Adv Mater 2021;33(39):2102852; doi: 10.1002/ADMA.202102852.
156. Li J, Ma L, Chen G, et al. A High Water-Content and High Elastic Dual-Responsive Polyurethane Hydrogel for Drug Delivery. J Mater Chem B 2015;3(42):8401–8409; doi: 10.1039/C5TB01702E.
157. Petrini P, Farè S, Piva A, et al. Design, Synthesis and Properties of Polyurethane Hydrogels for Tissue Engineering. J Mater Sci Mater Med 2003 148 2003;14(8):683–686; doi: 10.1023/A:1024955531173.
158. Koo LY, Irvine DJ, Mayes AM, et al. Co-Regulation of Cell Adhesion by Nanoscale RGD Organization and Mechanical Stimulus. J Cell Sci 2002;115(Pt 7):1423–33.
159. Ruoslahti E. RGD AND OTHER RECOGNITION SEQUENCES FOR INTEGRINS. 1996.
160. Veiseh O, Doloff JC, Ma M, et al. Size- and Shape-Dependent Foreign Body Immune Response to Materials Implanted in Rodents and Non-Human Primates. Nat Mater 2015;14(6):643–651; doi: 10.1038/nmat4290.
161. Goodridge HS, Underhill DM and Touret N. Mechanisms of Fc Receptor and Dectin-1 Activation for Phagocytosis. Traffic 2012;13(8):1062–1071; doi: 10.1111/j.1600-0854.2012.01382.x.
162. Sridharan R, Cavanagh B, Cameron AR, et al. Material Stiffness Influences the Polarization State, Function and Migration Mode of Macrophages. Acta Biomater 2019;89:47–59; doi: 10.1016/J.ACTBIO.2019.02.048.
163. Rougerie P and Cox D. Spatio-Temporal Mapping of Mechanical Force Generated by Macrophages during FcγR-Dependent Phagocytosis Reveals Adaptation to Target Stiffness. bioRxiv 2020;2020.04.14.041335; doi: 10.1101/2020.04.14.041335.
164. Beningo KA and Wang YL. Fc-Receptor-Mediated Phagocytosis Is Regulated by Mechanical Properties of the Target. J Cell Sci 2002;115(Pt 4):849–856; doi: 10.1242/JCS.115.4.849.
165. Wang H, Fang G, Chen H, et al. Lysosome-Targeted Biosensor for the Super-Resolution Imaging of Lysosome – Mitochondrion Interaction. 2022;13(March):1–10; doi: 10.3389/fphar.2022.865173.
166. Gomes LC, Benedetto G Di and Scorrano L. During Autophagy Mitochondria Elongate, Are Spared from Degradation and Sustain Cell Viability. Nat Cell Biol 2011;13(5):589–598; doi: 10.1038/ncb2220.
167. Yu T, Robotham JL and Yoon Y. Increased Production of Reactive Oxygen

Species in Hyperglycemic Conditions Requires Dynamic Change of Mitochondrial Morphology. Proc Natl Acad Sci 2006;103(8):2653–2658; doi: 10.1073/pnas.0511154103.
168. Soto-Heredero G, Gómez de las Heras MM, Gabandé-Rodríguez E, et al. Glycolysis – a Key Player in the Inflammatory Response. FEBS J 2020;287(16):3350–3369; doi: 10.1111/febs.15327.
169. Stroka KM and Aranda-Espinoza H. Endothelial Cell Substrate Stiffness Influences Neutrophil Transmigration via Myosin Light Chain Kinase-Dependent Cell Contraction. Blood 2011;118(6):1632–1640; doi: 10.1182/blood-2010-11-321125.
170. International A. Standard Test Method for Compressive Properties Of Rigid Cellular Plastics. 2000;5–8.
171. International A. Designation : D695 − 15 Standard Test Method for Compressive Properties of Rigid Plastics. 2019;(July); doi: 10.1520/D0695-15.
172. Pavlou S, Wang L, Xu H, et al. Higher Phagocytic Activity of Thioglycollate-Elicited Peritoneal Macrophages Is Related to Metabolic Status of the Cells. J Inflamm 2017;14(1):4; doi: 10.1186/s12950-017-0151-x.
173. Venter G, Oerlemans FTJJ, Wijers M, et al. Glucose Controls Morphodynamics of LPS-Stimulated Macrophages. Singh PK. ed. PLoS One 2014;9(5):e96786; doi: 10.1371/journal.pone.0096786.
174. Michl J, Ohlbaum DJ and Silverstein SC. 2-Deoxyglucose Selectively Inhibits Fc and Complement Receptor-Mediated Phagocytosis in Mouse Peritoneal Macrophages. I. Description of the Inhibitory Effect. J Exp Med 1976;144(6):1465–1483; doi: 10.1084/JEM.144.6.1465.
175. Pavlou S, Lindsay J, Ingram R, et al. Sustained High Glucose Exposure Sensitizes Macrophage Responses to Cytokine Stimuli but Reduces Their Phagocytic Activity. BMC Immunol 2018;19(1); doi: 10.1186/s12865-018-0261-0.
176. Murray PJ and Wynn TA. Protective and Pathogenic Functions of Macrophage Subsets. Nat Rev Immunol 2011;11(11):723–737; doi: 10.1038/nri3073.
177. Saleh LS, Amer LD, Thompson BJ, et al. Mapping Macrophage Polarization and Origin during the Progression of the Foreign Body Response to a Poly(Ethylene Glycol) Hydrogel Implant. Adv Healthc Mater 2022;11(9):2102209; doi: 10.1002/adhm.202102209.
178. Sharma L, Feng J, Britto CJ, et al. Mechanisms of Epithelial Immunity Evasion by Respiratory Bacterial Pathogens. Front Immunol 2020;11(February):1–8; doi: 10.3389/fimmu.2020.00091.
179. Calder PC, Dimitriadis G and Newsholme P. Glucose Metabolism in Lymphoid and Inflammatory Cells and Tissues. Curr Opin Clin Nutr Metab Care 2007;10(4):531–540; doi: 10.1097/MCO.0b013e3281e72ad4.
180. Chandel NS. Glycolysis. Cold Spring Harb Perspect Biol 2021;13(5):a040535; doi: 10.1101/CSHPERSPECT.A040535.
181. Palsson-Mcdermott EM and O’Neill LAJ. The Warburg Effect Then and Now: From Cancer to Inflammatory Diseases. BioEssays 2013;35(11):965–973; doi: 10.1002/BIES.201300084.
182. Ratter JM, Rooijackers HMM, Hooiveld GJ, et al. In Vitro and in Vivo Effects

of Lactate on Metabolism and Cytokine Production of Human Primary PBMCs and Monocytes. Front Immunol 2018;9:2564; doi: 10.3389/FIMMU.2018.02564/BIBTEX.
183. Pelegrin P, Riteau N, Zanier ER, et al. 2-Deoxy-d-Glucose Treatment Decreases Anti-Inflammatory M2 Macrophage Polarization in Mice with Tumor and Allergic Airway Inflammation. Immunol 2017;8:637; doi: 10.3389/fimmu.2017.00637.
184. Bertani FR, Mozetic P, Fioramonti M, et al. Classification of M1/M2-Polarized Human Macrophages by Label-Free Hyperspectral Reflectance Confocal Microscopy and Multivariate Analysis. Sci Rep 2017;7(1):8965; doi: 10.1038/s41598-017-08121-8.
185. Li C, Liu Y, Li Y, et al. Collagen XV Promotes ER Stress-Induced Inflammation through Activating Integrin B1/FAK Signaling Pathway and M1 Macrophage Polarization in Adipose Tissue. Int J Mol Sci 2021;22(18):9997; doi: 10.3390/ijms22189997.
186. Chuang Y-C, Chang H-M, Li C-Y, et al. Reactive Oxygen Species and Inflammatory Responses of Macrophages to Substrates with Physiological Stiffness. ACS Appl Mater Interfaces 2020;12(43):48432–48441; doi: 10.1021/acsami.0c16638.
187. Previtera ML and Sengupta A. Substrate Stiffness Regulates Proinflammatory Mediator Production through TLR4 Activity in Macrophages. Tschumperlin DJ. ed. PLoS One 2015;10(12):e0145813; doi: 10.1371/journal.pone.0145813.
188. T O, Y T, E K, et al. Reduced Substrate Stiffness Promotes M2-like Macrophage Activation and Enhances Peroxisome Proliferator-Activated Receptor γ Expression. 2018;367(2):264–273.
189. Santos E, Hernández RM, Pedraz JL, et al. Novel Advances in the Design of Three-Dimensional Bio-Scaffolds to Control Cell Fate: Translation from 2D to 3D. Trends Biotechnol 2012;30(6):331–341; doi: 10.1016/J.TIBTECH.2012.03.005.
190. Saraswathibhatla A, Indana D and Chaudhuri O. Cell–Extracellular Matrix Mechanotransduction in 3D. Nat Rev Mol Cell Biol 2023;24(7):495–516; doi: 10.1038/s41580-023-00583-1.
191. Guo M, Pegoraro AF, Mao A, et al. Cell Volume Change through Water Efflux Impacts Cell Stiffness and Stem Cell Fate. Proc Natl Acad Sci 2017;114(41):E8618–E8627; doi: 10.1073/pnas.1705179114.
192. Bao M, Xie J, Katoele N, et al. Cellular Volume and Matrix Stiffness Direct Stem Cell Behavior in a 3D Microniche. ACS Appl Mater Interfaces 2019;11:1754–1759; doi: 10.1021/acsami.8b19396.
193. Dupont S, Morsut L, Aragona M, et al. Role of YAP/TAZ in Mechanotransduction. Nature 2011;474(7350):179–183; doi: 10.1038/nature10137.
194. Elosegui-Artola A, Andreu I, Beedle AEM, et al. Force Triggers YAP Nuclear Entry by Regulating Transport across Nuclear Pores. Cell 2017;171(6):1397-1410.e14; doi: 10.1016/j.cell.2017.10.008.
195. Meli VS, Atcha H, Veerasubramanian PK, et al. YAP-Mediated Mechanotransduction Tunes the Macrophage Inflammatory Response. Sci Adv

2020;6(49):eabb8471; doi: 10.1126/sciadv.abb8471.
196. Johnson CD, Fischer D, Smith IM, et al. Hyperglycemic Conditions Enhance the Mechanosensitivity of Proinflammatory RAW264.7 Macrophages. https://home.liebertpub.com/tea 2023; doi: 10.1089/TEN.TEA.2022.0151.
197. Johnson CD, Aranda-Espinoza H and Fisher JP. A Case for Material Stiffness as a Design Parameter in Encapsulated Islet Transplantation. https://home.liebertpub.com/teb 2023; doi: 10.1089/TEN.TEB.2022.0157.
198. Hind LE, Dembo M and Hammer DA. Macrophage Motility Is Driven by Frontal-Towing with a Force Magnitude Dependent on Substrate Stiffness. Integr Biol 2015;7(4):447–453; doi: 10.1039/C4IB00260A.
199. Bupphathong S, Quiroz C, Huang W, et al. Gelatin Methacrylate Hydrogel for Tissue Engineering Applications—A Review on Material Modifications. Pharmaceuticals 2022;15(2):171; doi: 10.3390/ph15020171.
200. Zhuang Z, Zhang Y, Sun S, et al. Control of Matrix Stiffness Using Methacrylate-Gelatin Hydrogels for a Macrophage-Mediated Inflammatory Response. ACS Biomater Sci Eng 2020;6(5):3091–3102; doi: 10.1021/ACSBIOMATERIALS.0C00295/SUPPL_FILE/AB0C00295_SI_001.PDF.
201. Wu Y, Xiang Y, Fang J, et al. The Influence of the Stiffness of GelMA Substrate on the Outgrowth of PC12 Cells. 2019;0(January):1–9.
202. Lin F-S, Lee J-J, Lee AK-X, et al. Calcium Silicate-Activated Gelatin Methacrylate Hydrogel for Accelerating Human Dermal Fibroblast Proliferation and Differentiation. Polymers (Basel) 2020;13(1):70; doi: 10.3390/polym13010070.
203. Heltmann-meyer S, Steiner D, Müller C, et al. Gelatin Methacryloyl Is a Slow Degrading Material Allowing Vascularization and Long-Term Use in Vivo OPEN ACCESS Gelatin Methacryloyl Is a Slow Degrading Material Allowing Vascularization and Long-Term Use in Vivo. Biomed Mater 2021;16(6); doi: 10.1088/1748-605X/acle9d.
204. Wang Z, Kumar H, Tian Z, et al. Visible Light Photoinitiation of Cell-Adhesive Gelatin Methacryloyl Hydrogels for Stereolithography 3D Bioprinting. ACS Appl Mater & Interfaces 2018;10(32):26859–26869; doi: 10.1021/acsami.8b06607.
205. Pashneh-Tala S, Owen R, Bahmaee H, et al. Synthesis, Characterization and 3D Micro-Structuring via 2-Photon Polymerization of Poly(Glycerol Sebacate)-Methacrylate–An Elastomeric Degradable Polymer. Front Phys 2018;6(May); doi: 10.3389/fphy.2018.00041.
206. Nichol JW, Koshy ST, Bae H, et al. Cell-Laden Microengineered Gelatin Methacrylate Hydrogels. Biomaterials 2010;31(21):5536–5544; doi: 10.1016/j.biomaterials.2010.03.064.
207. Stork BA, Dean A and York B. Methodology for Measuring Oxidative Capacity of Isolated Peroxisomes in the Seahorse Assay. J Biol Methods 2022;9(2):e160; doi: 10.14440/jbm.2022.374.
208. Kooragayala K, Gotoh N, Cogliati T, et al. Quantification of Oxygen Consumption in Retina Ex Vivo Demonstrates Limited Reserve Capacity of Photoreceptor Mitochondria. Invest Ophthalmol Vis Sci 2015;56(13):8428–

8436; doi: 10.1167/iovs.15-17901.
209. Germeys C, Vandoorne T, Bercier V, et al. Existing and Emerging Metabolomic Tools for ALS Research. Genes (Basel) 2019;10(12):1011; doi: 10.3390/genes10121011.
210. Obeidat YM, Cheng M, Catandi G, et al. Design of A Multi-Sensor Platform for Integrating Extracellular Acidification Rate with Multi-Metabolite Flux Measurement for Small Biological Samples. Biosens Bioelectron 2019;133:39–47; doi: 10.1016/j.bios.2019.02.069.
211. Van den Bossche J, Baardman J, Natasja, et al. Mitochondrial Dysfunction Prevents Repolarization of Inflammatory Macrophages. Cell Rep 2016;17(3):684–696; doi: 10.1016/j.celrep.2016.09.008.